MINISTÉRIO DA EDUCAÇÃO

UNIVERSIDADE FEDERAL DO RIO GRANDE DO SUL

ESCOLA DE ENGENHARIA

Programa de Pós-Graduação em Engenharia
de Minas, Metalúrgica e de Materiais
PPGEM

DESENVOLVIMENTO DE CRIOGÉIS DE CELULOSE/BIOCHAR

Lídia Kunz Lazzari

Tese para a obtenção do título de Doutor em Engenharia

Porto Alegre

2021

MINISTÉRIO DA EDUCAÇÃO

UNIVERSIDADE FEDERAL DO RIO GRANDE DO SUL

ESCOLA DE ENGENHARIA

Programa de Pós-Graduação em Engenharia
de Minas, Metalúrgica e de Materiais
PPGEM

DESENVOLVIMENTO DE CRIOGÉIS DE CELULOSE/BIOCHAR

Lídia Kunz Lazzari

Trabalho realizado no Departamento de Materiais da Escola de Engenharia da UFRGS, dentro do Programa de Pós-Graduação em Engenharia de Minas, Metalúrgica e de Materiais – PPGEM em colaboração como Laboratório de Materiais Poliméricos da Universidade de Caxias do Sul, como parte dos requisitos para a obtenção do título de doutor em Engenharia.

Área de concentração: Ciência dos Materiais

Porto Alegre
2021

Esta tese foi analisada e julgada adequada para a obtenção do Título de Doutor em Engenharia, na área de Ciência e Tecnologia dos Materiais, e aprovado em sua forma final pelo Orientador e pela Banca Examinadora designada pelo Programa de Pós-Graduação em Engenharia de Minas, Metalúrgica e de Materiais da Universidade Federal do Rio Grande do Sul.

Orientadora: Profª. Drª. Ruth Marlene Campomanes Santana
Co-orientador: Profº. Drº. Ademir José Zattera

Banca Examinadora:

_____

Profº Drº Paulo Roberto Wander

_____

Profº Drº Matheus Poletto

_____

Profº Drº Matheus V. G. Zimmermann

_____

Prof. Dr. Afonso Reguly
Coordenador do PPGEM

ARTIGOS PUBLICADOS EM PERIÓDICOS

Esta tese está baseada nos artigos a seguir:

ARTIGO I: Lazzari, Lídia K.; Perondi, Daniele ; Zattera, Ademir J. ; Santana, Ruth M. C. . Influence of the addition of carbon structures in cellulose cryogels. Journal of Porous Materials, v. 28, p. 279-288, 2021.

ARTIGO II: Lazzari, Lídia K.; Perondi, Daniele; Zampieri, Vitória B.; Zattera, Ademir J. ; Santana, Ruth M. C. . Cellulose/biochar aerogels with excellent mechanical and thermal insulation properties. Cellulose, v. 26, p. 9071-9083, 2019.

ARTIGO III: Lazzari, Lídia K.; Perondi, Daniele ; Zattera, Ademir J. ; Santana, Ruth M. C. . Cellulose/Biochar Cryogels: A Study of Adsorption Kinetics and Isotherms. Langmuir, v. 37, p. 3180-3188, 2021.

OUTROS ARTIGOS PUBLICADOS

PERIÓDICOS:

Lazzari, Lídia K.; Perondi, Daniele; Zattera, Ademir J.; Santana, Ruth M. C.. CO_2 adsorption by criogels produced from poultry litter wastes. Revista Polímeros: aceito em 28/12/2021.

Lazzari, Lídia K.; Zimmermann, Matheus V. G.; Perondi, Daniele; Zampieri, Vitória B.; Zattera, Ademir J.; Santana, Ruth M. C.. Production of carbon foams from rice husk. Materials Research, v.22 (suppl. 1), 2019.

CONGRESSOS:

Lazzari, Lídia K.; Perondi, Daniele; Zampieri, Vitória B.; Zattera, Ademir J. ; Santana, Ruth M. C. . Influência da adição de estruturas de carbono em aerogéis de celulose na resistência à compressão. In: 8º Congresso Brasileiro de Carbono, 2019, São Joao Del Rei. Anais do 8º Congresso Brasileiro de Carbono, 2019.

Lazzari, Lídia K.; Zampieri, Vitória B.; Zattera, Ademir J. ; Santana, Ruth M. C. .Criogéis de celulose Eucalyptus sp e resíduo para utilização como isolante térmico. In: 15º Congresso Brasileiro de Polímeros, 2019, Bento Gonçalves. Anais 15º Congresso Brasileiro de Polímeros, 2019.

Lazzari, Lídia K.; Zimmermann, Matheus V. G.; Perondi, Daniele; Zampieri, Vitória B.; Zattera, Ademir J.; Santana, Ruth M. C.. Aerogéis de carbono a partir de biomassa vegetal. In: 23º Congresso Brasileiro de Engenharia e Ciência dos Materiais, 2018, Foz do Iguaçu. ANAIS 23º Congresso Brasileiro de Engenharia e Ciência dos Materiais, 2018.

“Não é sobre chegar
No topo do mundo e saber que venceu
É sobre escalar e sentir que o caminho te fortaleceu”.

(Ana Vilela)

AGRADECIMENTOS

Em primeiro lugar quero agradecer por ter recebido o melhor presente da minha vida durante essa jornada, meu filho Vicente, que me inspirou a cada dia buscar o melhor como mãe, mulher e pesquisadora.

Aos meus pais Antoninho Lazzari e Nilce Kunz Lazzari e meu irmão Rafael Kunz Lazzari, que sempre me apoiaram e mantiveram um ambiente propício para minha criação e formação humana e social.

Ao Lucas Chaves Saldanha que sempre acreditou em mim, pelo incentivo e carinho, risadas e cumplicidade sempre. Pelo apoio constante e pela paciência em me ajudar, independente da distância e dos meios.

Aos professores Ruth M. C. Santana e Ademir J. Zattera e demais colegas, por terem compartilhado seus conhecimentos e por alguns se tornarem exemplos a se seguir.

Aos responsáveis técnicos dos laboratórios utilizados durante a elaboração deste trabalho.

A todos que direta ou indiretamente, por meios positivos ou negativos, me ajudaram a crescer pessoal e profissionalmente.

RESUMO

Os criogéis de celulose são materiais sólidos que apresentam baixa densidade, comparável a espumas de poliuretano e poliestireno expandido, e são muito estudados nas áreas de adsorção e isolamento térmico devido sua elevada porosidade (acima de 90%) e baixa condutividade térmica (próxima a do ar – 0,03 W m^{-1} K^{-1}). A utilização de estruturas de carbono, tais como o grafeno e nanotubos de carbono, em criogéis, cresce a cada ano, porém o alto custo e tecnologia na sintetização desses materiais torna-os custosos nos processos industriais. Visando a diminuição de custos, a substituição dessas estruturas pelo biochar, torna-se interessante visto que o mesmo pode ser produzido a partir de resíduos agrícolas. A utilização do biochar como reforço para criogéis de celulose trás propriedades interessantes para o mesmo, como o aumento da resistência mecânica e capacidade de adsorção (óleos, corantes,...). O presente trabalho teve como objetivo produzir criogéis de celulose/biochar e estudar estes materiais quanto a suas propriedades mecânicas, térmicas e de adsorção. Inicialmente foram comparados os criogéis de celulose/biochar com criogéis de celulose/nanoplaquetas de grafeno (GNP), para avaliar o comportamento das propriedades do biochar em relação as GNPs. Os criogéis foram produzidos a partir de uma suspensão de celulose com concentração de 1,5% (m/m) obtida em um moinho de pedras, e a esta foi adicionado o biochar em concentração de 0-100% (m/m) em relação a concentração de celulose. A suspensão de celulose/biochar foi congelada e liofilizada para a obtenção dos criogéis. Foram avaliadas as propriedades mecânicas, térmicas e de adsorção dos criogéis, sendo que no contexto geral, o biochar apresentou potencial para ser utilizado na substituição de estruturas de carbono comercialmente utilizadas, tal como as nanoplaquetas de grafeno. Na sequência do trabalho, foram avaliadas diferentes concentrações de celulose e biochar nos criogéis e avaliadas suas influências nas propriedades de condutividade térmica e capacidade de adsorção de óleos. Os criogéis de celulose/biochar, apresentaram porosidade acima de 90% e densidade aparente inferior a 0,035 g cm^{-3}, o que demostram que são materiais extremamente leves. A adição do biochar aos criogéis de celulose proporcionam um aumento de cerca de 60% na resistência a compressão do mesmo. A condutividade térmica dos criogéis foi de 0,021 a 0,026 W $m^{-1}K^{-1}$, a adição do biochar não apresentou influência significativa nesta propriedade. Porém os criogéis de celulose/biochar possuem capacidade para serem utilizados como isolantes térmicos devido sua condutividade térmica ser muito próxima a condutividade térmica do ar e também aos materiais utilizados comercialmente. Para a capacidade de adsorção, a adição de 5% de biochar (m/m em relação a celulose) ao criogel de celulose aumentou cerca de 76% a capacidade de adsorção de petróleo. No estudo da cinética e isoterma de adsorção os modelos que mais se ajustaram ao processo foram pseudossegunda ordem e Langmuir, respectivamente. Com isso, conclui-se que o processo de adsorção de petróleo pelo criogel de celulose ocorre em monocamada. No geral, a utilização do biochar como substituto de estruturas de carbono em criogéis de celulose, apresentou propriedades semelhantes aos produtos comerciais utilizados como adsorventes e isolantes térmicos mostrando-se adequados para estas aplicações.

Palavras-chave: celulose, biochar, criogel, adsorção, isolamento térmico.

ABSTRACT

Cellulose cryogels are solid materials that have low density, comparable to polyurethane and expanded polystyrene foams, and are widely studied in the areas of adsorption and thermal insulation due to their high porosity (above 90%) and low thermal conductivity (close to that of air – 0.03 W m^{-1} K^{-1}). The use of carbon structures, such as graphene and carbon nanotubes, in cryogels, grows every year, but the high cost and technology in synthesizing these materials make them costly in industrial processes. To reduce costs, the replacement of these structures by biochar becomes interesting since it can be produced from agricultural residues. The use of biochar as a reinforcement for cellulose cryogels brings interesting properties to it, such as increased mechanical strength and adsorption capacity. The present work aimed to produce cellulose/biochar cryogels and to study these materials in terms of their mechanical, thermal, and adsorption properties. Initially, cellulose/biochar cryogels were compared with cellulose/graphene nanoplatelet (GNP) cryogels to evaluate the behavior of biochar properties to GNPs. The cryogels were produced from a cellulose suspension with a concentration of 1.5% (m/m) obtained in a stone mill, and to this was added biochar in a concentration of 0-100% (m/m) to cellulose concentration. The cellulose/biochar suspension was frozen and lyophilized to obtain cryogels. The mechanical, thermal, and adsorption properties of cryogels were evaluated, and in the general context, biochar showed potential to be used in the replacement of commercially used carbon structures, such as graphene nanoplatelets. Following this work, different concentrations of cellulose and biochar in cryogels were evaluated and their influence on the properties of thermal conductivity and oil adsorption capacity was evaluated. Cellulose/biochar cryogels showed porosity above 90% and bulk density below 0.035 g cm^{-3}, which demonstrates that they are extremely light materials. The addition of biochar to cellulose cryogels provides an increase of about 60% in its compressive strength. The thermal conductivity of the cryogels ranged from 0.021 to 0.026 W $m^{-1}K^{-1}$, the addition of biochar had no significant influence on this property. However, cellulose/biochar cryogels are capable of being used as thermal insulators because their thermal conductivity is very close to the thermal conductivity of air and also to the materials used commercially. For the adsorption capacity, the addition of 5% biochar (w/w to cellulose) to the cellulose cryogel increased the oil adsorption capacity by about 76%. In the study of adsorption kinetics and isotherm, the models that best fit the process were pseudo second order and Langmuir, respectively. Thus, it is concluded that the process of adsorption of petroleum by the cellulose cryogel occurs in a monolayer. In general, the use of biochar as a substitute for carbon structures in cellulose cryogels presented properties similar to commercial products used as adsorbents and thermal insulators, proving to be suitable for these applications.

Keywords: cellulose, biochar, cryogel, adsorption, thermal insulation.

SUMÁRIO

LISTA DE FIGURAS

1 INTRODUÇÃO

Os aerogéis, sólidos porosos sintetizados por meio da via sol-gel (quando da utilização da liofilização para o processo de secagem, chamam-se criogéis), apresentam estruturas de rede tridimensionais em que seus poros são preenchidos por ar, tendo como principal aplicação, adsorção de corantes, óleos e solventes, e, também como isolante térmico devido sua baixa condutividade térmica. No primeiro caso os aerogéis de celulose apresentam elevada capacidade e rápida taxa de adsorção de óleo, matérias-primas e métodos de sintetização simples e baratos superando diversos outros aerogéis (XIANG et al., 2019; MI et al., 2018; HAN et al., 2016). Para a aplicação de isolamento térmico, as estruturas de carbono vem sendo utilizadas para aumentar as propriedades mecânicas do aerogel de celulose (entre 40 e 60% de aumento na resistência a compressão em relação aos aerogéis sem a adição de cargas), uma vez que essas partículas não afetam a condutividade térmica dos mesmos (LAZZARI et al., 2019; GE et al., 2018).

A utilização da celulose para a produção de aerogéis/criogéis torna-se interessante pois é uma fonte econômica, renovável, biodegradável e abundante no meio ambiente e, pode ser processada em larga escala utilizando métodos bem desenvolvidos pela indústria (NAKAGAITO; KONDO; TAKAGI, 2013; FISCHER et al., 2006).

Diversos autores reportaram pesquisas no desenvolvimento de aerogéis de celulose e formas alotrópicas de carbono, tais como: o óxido de grafeno (XIANG et al., 2019; MI et al., 2018; WAN; LI, 2016) e os nanotubos de carbono (CONG et al., 2018; HWANG; WOO; PARK, 2018) (como fonte de carbono) para diferentes aplicações. Entretanto, a grande quantidade de produtos químicos e geração de resíduos ácidos durante a síntese destes precursores, associado a complexas e caras tecnologias, além dos equipamentos envolvidos no preparo, restringem a sua produção em larga escala (MI et al., 2018; CONG et al., 2018; BI et al., 2013). A adição destes materiais agregam propriedades como hidrofobicidade e compressibilidade as propriedades dos aerogéis (XIANG et al., 2019; LI et al., 2014).

Devido seu baixo custo, não-toxicidade a humanos e abundância na natureza, a utilização de precursores orgânicos, como fonte de matéria-prima carbonosa vem recebendo crescente atenção na última década. Matérias-primas orgânicas, ao serem submetidas ao processo de pirólise, produzem um resíduo sólido carbonáceo (biochar) que possui elevado valor energético, além de ser um produto de valor agregado. A combinação de propriedades tais como, área superficial, volume de poros e estabilidade a longo prazo permite que este

material possa ser utilizado para muitos propósitos, tais como, tratamento de águas residuais, precursor de catalisadores, aditivos para digestão e compostagem anaeróbica, armazenamento de energia, além de reforço em aerogéis. Além disso, a inclusão deste biochar traz algumas vantagens, resistência à chama e impermeabilidade a água (ZHANG et al., 2019; WAN; LI, 2016; SKOUTERIS et al., 2015; BASU, 2010).

Considerando as propriedades mecânicas inferiores dos aerogéis de celulose e os caros precursores e tecnologias envolvidas no processo de produção de aerogéis de grafeno, são necessários estudos para a substituição de precursores mais eficientes para a melhoria destas propriedades. Como mencionado anteriormente, diversos autores apresentam pesquisas com adição de óxido de grafeno ou nanotubos de carbono aos aerogéis, porém não foram encontrados, na literatura, trabalhos que apresentem a adição de biochar em aerogéis. A celulose oriunda de *Pinus elliotti*, foi utilizada no presente trabalho como matéria prima para a produção dos criogéis e também do biochar, possibilitando desta forma agregar valor a esta biomassa.

2 OBJETIVOS

2.1 OBJETIVO GERAL

Avaliar as propriedades mecânicas, térmicas e de adsorção de criogéis de celulose/biochar.

2.2 OBJETIVOS ESPECÍFICOS

Os objetivos específicos deste trabalho são:

- Desenvolver criogéis de celulose/biochar e celulose/nanoplaquetas de grafeno e comparar suas propriedades mecânicas, físicas e térmicas e aplicações como adsorvente e isolante térmico.

- Avaliar a influência da concentração de biochar (0-100% m/m) nas propriedades mecânicas e térmicas dos criogéis de celulose.

- Avaliar a influência da concentração de biochar (0-20% m/m) na capacidade de adsorção de petróleo do criogel de celulose e realizar os estudos de cinética e isotermas de adsorção.

3 FUNDAMENTAÇÃO TEÓRICA

3.1 AEROGÉIS

Aerogel é uma terminologia geral utilizada para referenciar qualquer material preparado, normalmente, pelo processo sol-gel e um processo de secagem adequado no qual a estrutura tridimensional e a rede porosa são preservados (MALEKI, 2016; AEGERTER; LEVENTIS; KOEBEL, 2011; FRICKE, 1992).

O termo "aerogel[1]" foi introduzido por Steven Kistler em 1932. O pesquisador desenvolveu uma nova tecnologia para a secagem dos géis, a secagem supercrítica, que até então eram realizadas por evaporação. Nesta técnica, o líquido impregnado no gel foi evacuado após ser transformado em um fluido supercrítico. O pesquisador desenvolveu aerogéis a partir de diversos materiais como sílica e alumina, e com materiais mais diferenciados como óxidos de metais (tungstênio, ferro e níquel) e compostos orgânicos (celulose, albumina de ovo, gelatina, entre outros). Devido a estes estudos, Kistler percebeu o potencial de utilização dos aerogéis em aplicações como catalisadores, agentes espessantes, materiais isolantes ou repelentes de água quando eram hidrofóbicos (AEGERTER; LEVENTIS; KOEBEL, 2011).

As principais características apresentadas pelos aerogéis, segundo Maleki (2016) Hüsing e Schubert (1998) são: possuir massa específica extremamente baixa (0,003 – 0,5 $g.cm^{-3}$), o que gera a uma elevada porosidade (80 – 99,8%), e área de superfície interna elevada (500 – 1200 $m^2.g^{-1}$). A combinação dessas propriedades com a modificação da superfície e a capacidade de ser processado em diferentes morfologias e tamanhos, proporciona aos aerogéis inúmeras aplicações. Além de resultar em propriedades físicas interessantes, tais como: baixa condutividade térmica, baixa velocidade do som, índice de refração baixo combinado com alta transparência óptica (principalmente nos aerogéis de sílica), quando comparados com materiais comerciais como espumas de poliuretano (MALEKI, 2016).

3.1.1 Processo sol-gel

O desenvolvimento da ciência e tecnologia sol-gel, iniciada em meados do século XIX, é acompanhado por importantes aplicações práticas. Inúmeros estudos utilizando esta tecnologia foram relatados durante os anos para a preparação de materiais vítreos e cerâmicos

[1] Composto de um gel sólido microporoso em que a fase dispersa é um gás. Fonte: IUPAC. Disponível em: https://goldbook.iupac.org/html/A/A00173.html Acesso em jan. 2019.

em temperaturas consideravelmente baixas (DIMITRIEV; IVANOVA; IORDANOVA, 2008). O processo sol-gel envolve três etapas (Figura 3.1): solução, gelificação e secagem. Na primeira etapa ocorre a formação do sol[2], em seguida, estas partículas se unem através de interações eletrostáticas formando estruturas tridimensionais, atingindo o ponto de gelificação. A transição gel-aerogel pode ser realizada através de diferentes técnicas de secagem, tais como: secagem supercrítica, natural, por troca de solvente, superfície modificada, liofilização, entre outras (ESQUIVEL-CASTRO et al., 2018; HÜSING; SCHUBERT, 1998).

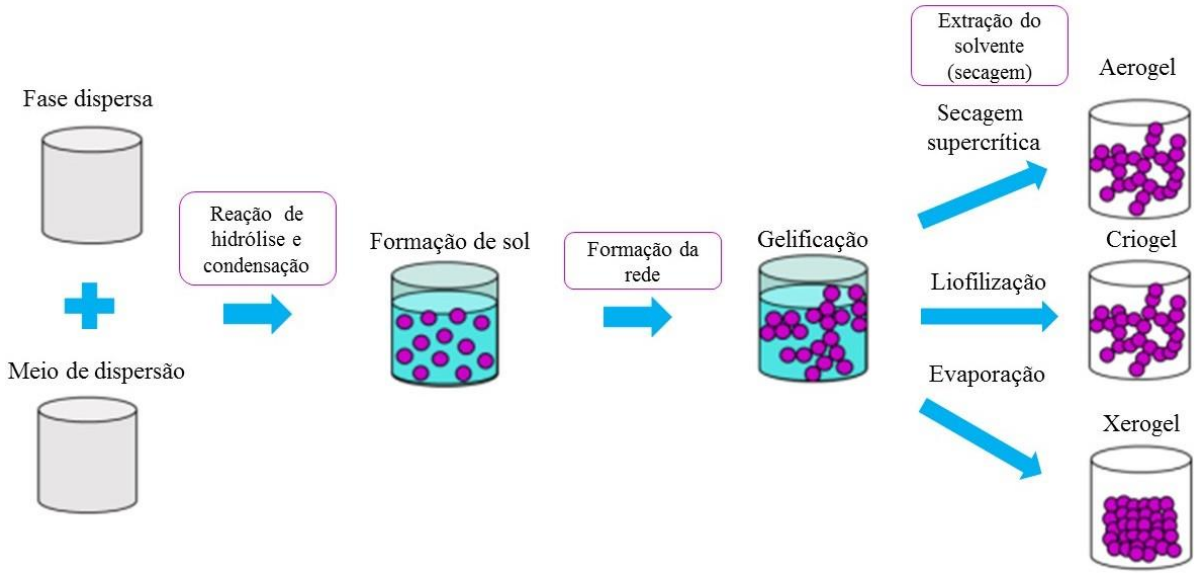

Figura 3. 1 - Processo sol-gel para síntese de aerogéis.
Fonte: adaptado de ESQUIVEL-CASTRO et al., 2018.

A principal característica dos aerogéis é a sua estrutura altamente porosa, que é alcançada sob condições controladas. Parâmetros químicos como o tipo de precursores e as condições de reação, influenciam diretamente a formação de redes na microestrutura resultante. Por sua vez, a microestrutura influencia as propriedades macroscópicas do sólido resultante. Nos aerogéis estas redes formadas podem ser preservadas praticamente inalteradas pelas técnicas de secagem bem desenvolvidas (HÜSING; SCHUBERT, 2002).

Os processos de secagem mais utilizados em pesquisas atualmente são a secagem supercrítica e a liofilização. No primeiro, o solvente é submetido ao seu estado supercrítico impossibilitando assim a formação da interface líquido/gás nos poros, o que evita tensões superficiais e a retração da rede tridimensional. Na liofilização, também chamada de

[2] Sol: partículas coloidais (fase dispersa) estão dispersas em um solvente (meio de dispersão) por reações de hidrólise e condensação. Fonte: (ESQUIVEL-CASTRO et al., 2018; HÜSING; SCHUBERT, 1998).

criosecagem, a substituição do solvente (geralmente água) é realizada através da sublimação do mesmo. Neste processo, o tamanho e distribuição dos poros estão relacionados diretamente com a velocidade de congelamento do gel e a formação dos cristais de gelo (GANESAN et al., 2016; DU et al., 2013; HÜSING; SCHUBERT, 1998).

O termo "aerogel", é comumente utilizado na literatura para referenciar todos os tipos de aerogéis, porém, alguns autores utilizam a nomenclatura de acordo com o processo utilizado, como por exemplo, "criogel" quando é utilizado a secagem por liofilização ou "xerogel" quando a secagem é por evaporação.

3.1.2 Materiais utilizados na produção de aerogéis

Desde sua introdução, em 1932, avanços tecnológicos na síntese dos aerogéis foram apresentados ao mundo científico, dentro dos quais, diferentes tipos de matérias-primas utilizadas em sua produção. Além da sílica (ZHAO; LI; ZHANG, 2018; FU et al., 2016; SUN et al., 2014), materiais orgânicos naturais como fibras naturais de celulose (LAZZARI et al., 2017; ZANINI et al., 2016; FU et al., 2016; NAKAGAITO; KONDO; TAKAGI, 2013), algodão (CHENG et al., 2017; BI et al., 2013), amido (CHANG; CHEN; JIAO, 2010) e argila (MADYAN; FAN, 2019); orgânicos sintéticos como álcool poli vinílico (JAVADI et al., 2013), polidimetilsiloxano (HU et al., 2014) e grafeno (CHEN et al., 2018a; MI et al., 2018; HU et al., 2013).

Os aerogéis de sílica (SiO_2), por exemplo, apresentam uma alta transparência que é próxima a do vidro, uma condutividade térmica correspondente as espumas de poliestireno ou de poliuretano, ou áreas de superfície específicas, que também são encontradas no carvão vegetal. Porém, estes aerogéis apresentam baixa resistência mecânica, baixa tenacidade e grande fragilidade, comparado as espumas comerciais, o que limitam sua aplicação em algumas áreas (FU et al., 2016; HÜSING; SCHUBERT, 1998). De forma a atenuar esses efeitos e melhorar suas propriedades, alguns materiais como celulose e grafeno foram estudados como reforço nos aerogéis de sílica (DERVIN et al., 2017; FU et al., 2016; FENG et al., 2016; DEMILECAMPS et al., 2015).

Os aerogéis de celulose, por serem produzidos a partir de fontes renováveis (plantas, madeira, algas e animais), podem ser considerados ambientalmente corretos e podem reduzir o custo de fabricação devido ao baixo custo da matéria-prima. A baixa densidade das fibras de celulose proporciona aos aerogéis de celulose alta porosidade (acima de 90%), além de resistência mecânica devido a estrutura tridimensional formada pelas fibras de celulose

(FENG et al., 2015; XIAO et al., 2015; INNERLOHINGER; WEBER; KRAFT, 2006).

Jiménez-Saelices et al. (2017) compararam aerogéis de celulose nanofibrilada (NFC) preparados por dois métodos de liofilização: por aspersão (SFD) e convencional (CFD). Diferenças nas estruturas foram percebidas a partir das micrografias onde os aerogéis preparados por CFD exibiram uma morfologia de folha 2D com macroporos, já os aerogéis obtidos por SFD produziram uma morfologia de estrutura nanoestruturada de fibrilas tridimensional, com tamanho de poro variando de poucas dezenas de nanômetros a alguns mícrons. A estrutura do aerogel CFD oferece uma resistência à compressão superior a estrutura do SFD, permitindo alcançar maior módulo de compressão. Porém, o resultado mais importante do estudo foi que os aerogéis SFD apresentaram uma condutividade térmica cerca de 50% menor (0,016 – 0,018 W m^{-1} K^{-1}) em relação aos aerogéis CFD (0,029 – 0,032 W m^{-1} K^{-1}).

Utilizando estruturas alotrópicas de carbono (carbono, grafite, grafeno, nanotubos de carbono, entre outros), foram produzidos diversos tipos de aerogéis, tais como:

- aerogéis de carbono: produzidos, inicialmente, a partir da carbonização de aerogéis de resorcinol-formaldeido (RF), apresentando elevada área superficial quando o sólido é ativado com dióxido de carbono (DU et al., 2013). Porém, aerogéis de carbono produzidos a partir de matérias primas orgânicas naturais (celulose, quitosana, amido, entre outros) exibem algumas vantagens por serem atóxicos, de baixo custo e abundantes na natureza (CHANG; CHEN; JIAO, 2010).

- aerogéis de nanotubos de carbono: utiliza-se nanotubos de carbono devido suas propriedades mecânicas, térmicas e elétricas. Devido a fragilidade desses aerogéis, pesquisadores utilizaram reforços como álcool poli vinílico (BRYNING et al., 2007) a fim de melhorar a resistência mecânica e estabilidade do material. Neste caso, os aerogéis suportaram 8000 vezes seu próprio peso, além de apresentarem-se altamente porosos. Estes aerogéis são muito estudados para aplicações em eletrodos porosos para baterias, células de combustíveis e supercapacitores, devido suas propriedades eletrônicas que são facilmente moduladas por pequenas variações estruturais (WANG; ELLSWORTH, 2009; EBBESEN et al., 1996).

- aerogéis de grafeno: o grafeno possui propriedades químicas e físicas semelhantes aos nanotubos. Wang e Ellsworth (2009) produziram o primeiro aerogel de grafeno, onde sintetizaram o grafeno a partir do óxido de grafite, através do método Hummers. Os autores mencionam que estes aerogéis são superiores aos aerogéis de carbono em aplicações como

sensores, dispositivos de armazenamento de energia, nanocompósitos de alto desempenho, entre outros.

3.1.3 Aplicações dos criogéis de celulose

3.1.3.1 Isolamento térmico

Isolantes térmicos são sólidos ou fluidos que apresentam baixa condutividade e elevada resistência térmica, utilizados como barreira a transferência de calor entre o sistema e o meio, de modo que a energia possa ser conservada. Suas aplicações vão de climatização (condicionamento de temperatura em um ambiente fechado); conservação, estocagem e processamento de alimentos; economia de energia, entre outros (CUCE et al., 2014a; CRUZ, 2009).

Materiais isolantes convencionais, tais como espumas de poliuretano e poliestireno expandido, são muito utilizados atualmente. O desenvolvimento de materiais de alto desempenho aliado a menores espessuras é uma necessidade para o mercado de isolamento (CUCE et al., 2014b; KOEBEL; RIGACCI; ACHARD, 2012).

A capacidade de isolamento de um material é medida de acordo com a condutividade térmica, ou seja, quanto menor for a condutividade térmica maior será a capacidade de isolamento. Em engenharia térmica, outras propriedades dos materiais isolantes são importantes, como a densidade aparente e a capacidade calorífica específica do isolante (SILVA, 2013).

Condutividade térmica de um material é definida como "a taxa de transferência de calor por meio de uma unidade de comprimento de um material por unidade de área por unidade de diferença de temperatura". Esta propriedade mostra a capacidade de um material de transferir calor, valores altos de condutividade térmica indicam que o material é bom condutor, enquanto que baixos valores de condutividade térmica indicam que o material é um bom isolante. Por exemplo, o diamante é um excelente condutor térmico pois sua condutividade térmica é de 2.300 W m^{-1} K^{-1}, já o ar é um bom isolante térmico pois sua condutividade térmica é de 0,026 W m^{-1} K^{-1}, ambas em temperatura ambiente (ÇENGEL; GHAJAR, 2012).

Recentes pesquisas trazem o desenvolvimento de novos materiais para serem utilizados em isolamentos térmicos. Tais como, os aerogéis de sílica (SILIGARDI et al., 2017), celulose (GUPTA et al., 2018; JIM; BERNARD; GROHENS, 2016) e

carbono/grafeno (FENG; ZHANG; FENG, 2012).

Os aerogéis são considerados materiais muito interessantes para isolamentos térmicos pois apresentam alto desempenho como resultado de sua condutividade térmica extremamente baixa. A condutividade térmica do aerogel inclui principalmente três etapas: condutividade térmica no estado sólido, condutividade térmica gasosa e condutividade térmica radiante. A condutividade térmica do estado sólido do aerogel é altamente dependente do fator de condutividade térmica do material sólido e da densidade do mesmo. Para o mesmo material sólido, a condutividade térmica do estado sólido do aerogel aumenta com o aumento da densidade (ZHU; LI, 2018). A condutividade térmica do gás é determinada principalmente pelo tamanho do poro do material poroso, quanto menor o tamanho do poro, menor a condutividade térmica gasosa. Portanto, a condutividade térmica dos aerogéis é determinada principalmente pelo fator de condutividade térmica do material sólido, densidade e tamanho do poro (GE et al., 2018a; CUCE et al., 2014a).

Ge et al. (2018) produziram aerogéis de carboximetilcelulose (CMC) e óxido de grafeno (OG) com concentração de 2,0% (m/m) de CMC e 0,1-5,0% (m/m base seca de CMC) de OG. Utilizando moldes de alumínio e vidro, os autores obtiveram aerogéis com estruturas isotrópicas e anisotrópicas, respectivamente. As estruturas diferem-se, pois, a condutividade térmica do alumínio (160 W m^{-1} K^{-1}) é superior à do vidro, portanto o gradiente de temperatura no molde é o mesmo em todas as direções. No caso do vidro, com condutividade térmica baixa (0,18 W m^{-1} K^{-1}), a taxa de transferência de calor é lenta, de modo que os cristais de gelo são formados do topo para dentro ao longo do gradiente de temperatura. A resistência à compressão do aerogel isotrópico alcançou de 5 à 14 vezes o aerogel anisotrópico. Os resultados mostraram que as propriedades mecânicas dos aerogéis aumentaram com o aumento do teor de OG, quando o teor de OG aumentou de 0 a 5% (m/m), a resistência à compressão dos aerogéis aumentou 62% e o módulo de Young foi 3,5 vezes superior ao do aerogel de CMC. Além disso, a condutividade térmica do aerogel isotrópico (0,0417 W m^{-1} K^{-1}) foi comparável à espuma de poliestireno (0,03 – 0,04 W m^{-1} K^{-1}). Os autores concluem que os aerogéis possuem potencial para substituir os materiais de isolamento térmico tradicionais.

Javadi et al. (2013) produziram aerogéis orgânicos híbridos compostos de álcool poli vinílico (PVA), nanofibras de celulose (CNFs) e nanopartículas de óxido de grafeno (GONSs) usando um processo de liofilização. Os aerogéis apresentaram densidade inferior a 0,035 g cm^{-3} e condutividade térmica de 0,045 W m^{-1} K^{-1}. Conforme conclusão dos autores estes

aerogéis orgânicos híbridos podem oferecer uma ampla gama de propriedades que os tornam uma alternativa econômica e ecologicamente correta para os materiais de isolamento térmico usados em indústrias de habitação, vestuário, aeroespacial e de aeronaves comerciais.

3.1.3.2 Adsorventes

A utilização de adsorventes é uma prática muito utilizada para a remoção do óleo em meios sólidos ou líquidos, este método facilita a transferência do líquido a uma fase semi-sólida tornando possível a retirada do óleo. Esse material deve apresentar elevada capacidade de adsorção de óleo, seletividade, reutilização, biodegradabilidade e baixo custo (NGUYEN et al., 2014).

A adsorção é um fenômeno superficial onde as moléculas do adsorvato (óleo) são atraídas para a superfície do adsorvente (sólido) sem sofrer alterações na sua composição química. É reconhecida como uma alternativa eficaz, promissora, acessível e amplamente utilizada na remoção de óleo em comparação com outras tecnologias devido à sua simplicidade e, geralmente, baixo custo de processamento (WAHI et al., 2013; FOO; HAMEED, 2010; QIU et al., 2009).

Com o objetivo de obter-se um sistema de adsorção ideal, ao explorar novos materiais adsorventes, é indispensável estabelecer a relaçao de equilíbrio mais apropriada para o sistema. A forma como os poluentes interagem com os materiais adsorventes, sao descritas através das relações de equilíbrio do sistema (isotermas de adsorção), sendo pontos críticos para a otimizaçao do mecanismo de adsorção, expressão das propriedades e capacidades superficiais dos adsorventes, além do planejameno efetivos dos sistemas de adsorção (FOO; HAMEED, 2010).

Além do estudo do equilíbrio, os aspectos termodinâmicos e cinéticos devem ser conhecidos para se obter mais detalhes do mecanismo e performance do processo de adsorção. A partir da análise cinética, é possível determinar o tempo de residência necessário para que o adsorvente atinja sua capacidade máxima de adsorção e, também, ser possível escalonar o sistema de adsorção (QIU et al., 2009).

A utilização de matérias-primas naturais, como a celulose, ou de resíduos industriais para a fabricação de adsorventes, para a remoção de poluentes da água, apresenta muitas características atraentes como sua contribuição na redução de custos para a eliminação de resíduos, contribuindo assim para a proteção ambiental (BHATNAGAR; SILLANPÄÄ, 2010).

Segundos estudos relatados na literatura, a principal aplicação dos aerogéis/criogéis de celulose é para a adsorção de petróleo e derivados (FENG et al., 2016; HAN et al., 2016; JIN et al., 2015; XIAO et al., 2015; NGUYEN et al., 2014; FUN et al., 2014; KORHONEN et al., 2011; CERVIN et al., 2012).

Mi et al. (2018) produziram aerogéis de celulose-grafeno como materiais absorventes de óleos. Os autores utilizaram uma concentração de 0,5% (m/m) de nanofibras de celulose extraída de polpa Kraft de *Eucalyptus* e variações de 5-40% (m/m de celulose) de óxido de grafeno (OG). A suspensão foi sonificada (por 30 min) e então congelada em uma configuração bi direcionada com nitrogênio líquido e água quente, para então ser liofilizada. Os aerogéis foram modificados com deposição a vapor de n-dodeciltrietoxissilano para torná-los hidrofóbicos. O aerogel de celulose-grafeno apresentou-se muito leve, sendo possível equilibrá-lo sob um dente-de-leão sem que a planta sofresse alteração como mostra a Figura 3.2. Nos ensaios de compressão os mesmos recuperaram-se totalmente após serem comprimidos, com carga de 54g, a 20% da sua altura original. Quando comprimidos a 10% da altura original, a recuperação foi de cerca de 96%. A influência da concentração do óxido de grafeno foi avaliada comprimindo os aerogéis a 60% de tensão, e os resultados sugerem que o módulo de compressão e a resistência foram maiores para os aerogéis com maior teor de OG, o que foi atribuído à rigidez das folhas de grafeno. Os aerogéis também mostraram uma notável capacidade de absorção de 80 ~ 197 vezes seu peso em relação a vários óleos e solventes químicos, o que segundo os autores supera os aerogéis hidrofóbicos de celulose e a maioria dos baseados em carbono.

Figura 3. 2 - Aerogel de celulose-grafeno sobre um dente-de-leão.
Fonte: (MI et al., 2018).

3.2 CELULOSE

A madeira é considerada um compósito natural, poroso, hidratado e tridimensional. Sua composição química elementar apresenta como principais elementos: carbono (49 – 50%), hidrogênio (6%), oxigênio (44 – 45%) e nitrogênio (0,1 – 1,0%). Presentes em todas as espécies, os principais componentes macromoleculares são a celulose (42 – 45%), hemicelulose (27 – 30%) e lignina (20 – 28%). A madeira ainda apresenta componentes minoritários como extrativos e substâncias minerais de baixa massa molar (KLOCK et al., 2005).

Sendo um polímero natural e orgânico, a celulose, está presente na parede celular das plantas, particularmente nos caules, talos e troncos e em todas as porções lenhosas dos tecidos vegetais. Também, está presente em bactérias, fungos, algas e mesmo em animais. Oriunda de um ciclo natural a celulose é considerada um recurso natural renovável e fonte quase inesgotável de matéria-prima para a crescente demanda por produtos ambientalmente corretos e biodegradáveis (KLEMM et al., 2005; O'SULLIVAN, 1997).

Em 2018, o Brasil produziu aproximadamente 19 mil toneladas de celulose, 98% do volume de celulose produzido é originário das florestas plantadas de *Pinus* sp. (conífera) e *Eucaliptus* sp.(folhosa) (IBÁ, 2019[3]). As fibras de celulose originárias da espécie *Pinus* sp. são nomeadas fibras longas pois possuem um comprimento de 3 a 6 mm, são utilizadas na fabricação de embalagens e papel cartão devido a sua maior resistência mecânica. As fibras obtidas a partir do *Eucaliptus* sp. chamadas fibras curtas possuem comprimento de 0,5 a 1,5 mm, têm resistência mecânica inferior à fibra longa e são utilizadas para fabricação de papéis para imprimir e escrever e com fins sanitários (BASSA et al., 2007).

A celulose é um polissacarídeo linear constituído da repetição de moléculas de β-D-glucopiranose (Figura 3.3), é uma cadeia polimérica extensa com um grau de polimerizaçao entre 1000 e 30.000 e com um grande número de hidroxilas (KLEMM et al., 2005).

[3] Disponível em: https://www.iba.org/. Acesso em: jan.2019.

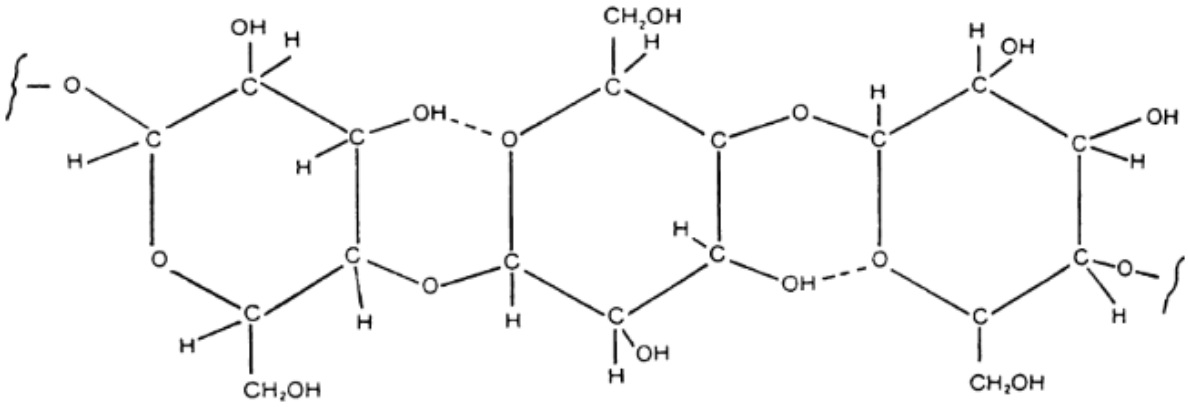

Figura 3. 3 – Estrutura molecular da celulose.
Fonte: BASU (2010).

Essa estrutura confere a celulose características como hidrofilicidade, quiralidade, degradabilidade e ampla variedade química devido reatividade dos grupos hidroxila. A cadeia de celulose tem três grupos hidroxila livres por unidade de glucose, possibilitando a formação das ligações de hidrogênio intra e intermoleculares, particularmente com as moléculas de água, que pode ser completamente ligadas à celulose. No entanto, a celulose não pode ser fundida ou dissolvida em solventes comuns, devido às suas fortes ligações de hidrogênio (GAVILLON, 2007; KLEMM et al., 2005).

Domínios cristalinos coexistem com regiões amorfas desordenadas (Figura 3.4). Por isso, as regiões amorfas são mais sucetíveis ao ataque de reagentes, enzimas ou até mesmo a absorção da água. A relação entre as regiões cristalina e amorfa determina o índice de cristalinidade (CrI) da celulose. As regiões cristalinas tem um papel estrutural, enquanto as regiões amorfas têm propriedades viscoelásticas (LENGOWSKI, 2012; GAVILLON, 2007).

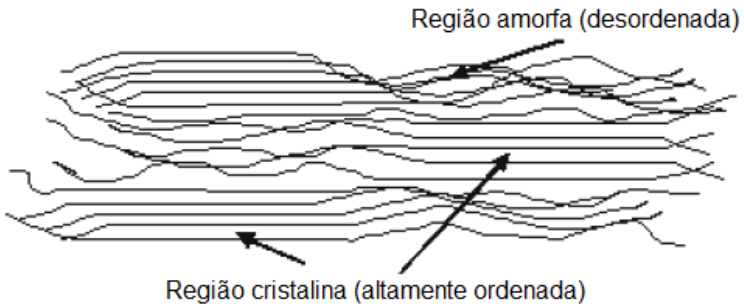

Figura 3. 4 - Microfibras de celulose.
Fonte: Adaptado de Gavillon, 2007.

O grau de cristalinidade depende da origem e o tratamento aplicado à celulose. Pode ser estimado por difração de raios-X de acordo com a intensidade relativa de certos picos. Os

vários estados cristalinos de celulose ocorrem de acordo com o arranjo das ligações de hidrogênio, a posição paralela ou antiparalela das cadeias de celulose e os parâmetros de unidade cristalina (GAVILLON, 2007; KLEMM et al., 2005; O'SULLIVAN, 1997).

Estes grupos hidroxila, concedem à fibra elevada polaridade o que acarreta em alta sorção de água. Uma abordagem fácil e eficaz para resolver este problema é encontrar meios de reduzir a energia superficial das fibras ou torná-las hidrofóbicas. Um método de simples operação e custo considerável é a modificação da superfície das fibras por silanos. No processo de silanização, há a formação de silanol pela hidrólise do silano, que em seguida, reage com o grupo hidroxila da fibra formando ligações covalentes quimicamente estáveis na superfície da fibra, enquanto que os grupos vinil, presentes no silano, ficam livres para interagirem com óleos e polímeros. Após o tratamento, as ligações (silano-fibra) formadas na interface agem como um sistema de separação, impedindo que a fibra interaja com a água presente no meio (HOKKANEN; BHATNAGAR; SILLANPÄÄ, 2016; ABDELMOULEH et al., 2004).

3.2.1 Pirólise da celulose

A pirólise envolve o aquecimento da biomassa na ausência de ar ou oxigênio a uma taxa de aquecimento específica até a temperatura máxima, mantendo-a nesta isoterma por um determinado período de tempo. O produto inicial da pirólise é composto de gases condensáveis e sólido (char). O gás condensável pode se decompor em gases não condensáveis (CO, CO_2, H_2 e CH_4), líquido e carvão. Essa decomposição ocorre parcialmente por meio de reações homogêneas em fase gasosa e em parte por reações térmicas heterogêneas da fase gás-sólido. Nas reações em fase gasosa, as ligações químicas das moléculas dos gases condensáveis são rompidas gerando moléculas menores de gases não condensáveis. A fração sólida (char), composta de aproximadamente 85% de carbono, pode ser coletada como produto final ou pode ser utilizada para produzir a energia necessária ao próprio processo (BASU, 2010). A pirólise pode ser representada pela reação geral abaixo:

$$C_nH_mO_p\ (biomassa) \rightarrow \Sigma_{líquido} C_xH_yO_z + \Sigma_{gás} C_aH_bO_c + H_2O + C(char)$$

O char, além de conter carbono, pode conter hidrogênio e oxigênio, e diferentemente dos combustíveis fósseis, as biomassas apresentam baixas frações de compostos inorgânicos. A uma temperatura moderadamente alta em uma atmosfera inerte, a pirólise decompõe

termicamente a estrutura de carboidratos da biomassa em resíduos sólidos carbonáceos (biochar) e vapores condensáveis e não condensáveis. É composto majoritariamente por carbono, possui um elevado valor energético, sendo um produto de valor agregado, que pode ser usado para muitos propósitos. A principal aplicação, atualmente, para o char/biochar é na produção de carvão ativado, muito utilizado como adsorvente devido a sua área superficial e estrutura de poros definidas, assim como a resistência química e capacidade de adsorção de compostos orgânicos (SKOUTERIS et al., 2015; LEE et al., 2013; BASU, 2010).

A fração líquida, também conhecida como alcatrão ou bio-óleo, é uma mistura de hidrocarbonetos complexos com grandes quantidades de oxigênio e água. É produzido pela rápida e simultânea despolimerização e fragmentação das moléculas de celulose, hemicelulose e lignina da biomassa. O bio-óleo é uma microemulsão, na qual a fase contínua é uma solução aquosa dos produtos da decomposição da celulose e da hemicelulose, e pequenas moléculas da decomposição da lignina. A fase descontínua é composta em grande parte por macromoléculas de lignina (BASU, 2010).

A primeira decomposição da biomassa que ocorre no processo de pirólise produz os gases condensáveis (vapor) e gases não-condensáveis. Os vapores, que são feitos de moléculas maiores, condensam no resfriamento, aumentando o rendimento líquido da pirólise. A mistura de gás não condensável contém gases de baixa massa molecular, como dióxido de carbono, monóxido de carbono, metano, etano e etileno. Estes não se condensam no resfriamento (BASU, 2010).

3.2.1.1 Mecanismos e reações envolvidos no processo de pirólise da celulose

Diversos modelos foram desenvolvidos para explicar os passos fundamentais da pirólise de biomassa, segundo Bridgwater; Czernik e Piskorz (2001) o modelo de Broido-Shafizadeh (apresentado na Figura 3.5) pode ser aplicado qualitativamente para as demais biomassas.

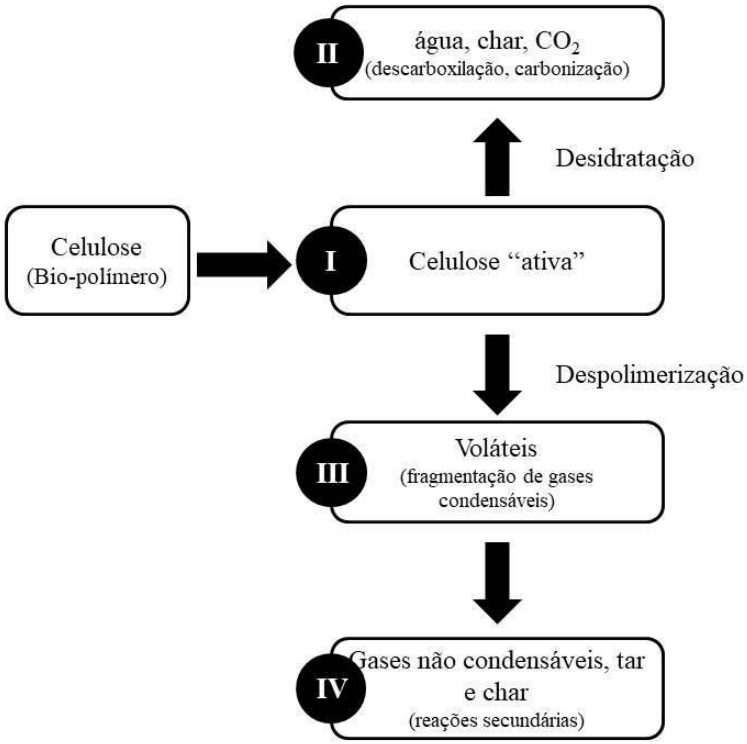

Figura 3. 5 – Modelo de decomposição típico da celulose.
Fonte: adaptado de BASU (2010) e (BRIDGWATER, 2011).

Durante a perda de massa inicial (T< 300°C), há a formação de um produto intermediário chamado celulose ativa (reação I), resultante da despolimerização parcial da celulose. As reações de desidratação (reação II) são responsáveis pela maior perda de massa antes dos 300°C, nessa fase, as moléculas de água já foram liberadas, porém o CO, CO_2 e compostos orgânicos raramente são detectados na fase volátil antes de 280ºC. As reações de desidratação são associadas com o rendimento de char e podem ocorrer intra e intermoleculares, e resultam em maior grau de reticulação e em maior estabilidade térmica do resíduo.

A despolimerização (reação III) da celulose é rápida e converte mais do que 80% dos compostos voláteis, que em sua maioria sçao compostos orgânicos condensáveis. Os gases condensáveis, se permitido escapar rapidamente do reator, pode condensar-se como bio-óleo ou alcatrão. Por outro lado, se for mantido em contato com a biomassa dentro do reator, pode sofrer reações secundárias (reação IV), quebrando o vapor em carvão, alcatrão e gases secundários.

A despolimerização (reação III) apresenta energias de ativação superiores às da desidratação (reação II). Assim, uma temperatura mais baixa e um tempo de residência mais longo favorecem essa reação, produzindo principalmente carvão, água e dióxido de carbono. Por outro lado, devido à sua maior energia de ativação, a reação III é favorecida em altas

temperaturas, rápida taxa de aquecimento e maior tempo de residência, produzindo principalmente gás. A temperatura moderada e o tempo de residência curto do vapor evitam o craqueamento secundário, produzindo principalmente vapor condensável - o precursor do bio-óleo, que é de grande importância comercial (COLLARD; BLIN, 2014; BRIDGWATER, 2011; BASU, 2010).

O calor da reação é inadequado para atender a todas as demandas de energia, que incluem calor necessário para elevar a alimentação e qualquer meio de transferência de calor inerte para a temperatura de reação, calor consumido por reações endotérmicas e perdas de calor do reator. Na maioria dos casos, é necessário queimar os gases não condensáveis e o carvão produzido para fornecer o calor necessário. Se isso não for adequado, outras fontes de calor são necessárias para fornecer a energia necessária para a pirólise.

O processo de desidratação (reação II) é exotérmico, enquanto a despolimerização (reação III) e o craqueamento secundário (reação IV) são endotérmicos. Entre as reações entre produtos intermediários da pirólise, algumas são exotérmicas e outras são endotérmicas. Em geral, a pirólise de hemicelulose e lignina é exotérmica. A pirólise da celulose é endotérmica em temperaturas mais baixas (<400–450°C) e se torna exotérmica em temperaturas mais altas devido às seguintes reações exotérmicas.

$CO + 3H_2 \rightarrow CH_4 + H_2O \ \Delta H = -226$ kJ gmol (1)

$CO + 2H_2 \rightarrow CH_3OH \ \Delta H = -105$ kJ gmol (2)

$0{,}17\ C_6H_{10}O_5 \rightarrow C + 0{,}85\ H_2O \ \Delta H = -80$ kJ gmol (3)

$CO + H_2O \rightarrow CO_2 + H_2 \ \Delta H = -42$ kJ gmol (4)

Por esta razão, um sistema adequadamente projetado inicialmente requer calor externo somente até que a temperatura necessária seja atingida. A produção de carvão a partir da celulose (Eq. 3) é levemente exotérmica. Entretanto, a uma temperatura mais alta, quando hidrogênio suficiente é produzido pela reação (Eq. 4), outras reações exotérmicas (Eqs. 1 e 2) podem prosseguir. Em baixas temperaturas (<400-450ºC) e tempos de residência curtos de voláteis, somente reações primárias endotérmicas são ativas (calor de reação -225 kJ kg^{-1}), enquanto que em altas temperaturas (>450ºC) reações secundárias exotérmicas (calor de reação 20 kJ kg^{-1}) são ativas.

Em conclusão, para fins de projeto pode-se negligenciar o calor de reação para o processo de pirólise, mas é necessário calcular a energia necessária para a vaporização de produtos e para aquecer os gases de alimentação até a temperatura de pirólise (BASU, 2010).

3.2.1.2 Fatores que influenciam no rendimento dos produtos

A fração dos produtos ao final da pirólise depende dos parâmetros de processo adotados, tais como, temperatura, taxa de aquecimento, pressão, meio reacional, tempo de residência e também das características da matéria-prima (PERONDI et al., 2017; DEMIRBAS, 2009).

Os constituintes individuais da biomassa, onde os três principais são a celulose, hemicelulose e lignina, fazem contribuições diferentes para os rendimentos da pirólise. Como por exemplo, a celulose e hemicelulose são as principais fontes de voláteis na biomassa, sendo que a celulose é uma fonte primária de gases condensáveis e a hemicelulose produz mais gases não condensáveis e menos alcatrão do que a celulose. Devido ao seu conteúdo aromático, a lignina se degrada lentamente, contribuindo significativamente para o rendimento do carvão (BASU, 2010).

O tamanho, a forma e a estrutura física da biomassa exercem influência nos produtos da pirólise. Partículas mais finas oferecem menos resistência ao escape de gases condensáveis ao ambiente, o que resulta em um maior rendimento de líquido. As partículas maiores, por outro lado, facilitam o craqueamento secundário devido à maior resistência que oferecem ao escape do produto primário de pirólise. Por essa razão, métodos mais antigos de produção de carvão usavam peças de madeira de grande porte em uma câmara selada (BASU, 2010).

Os parâmetros de temperatura e taxa de aquecimento apresentam a mesma influência sobre os rendimentos da pirólise, porém, a taxa de aquecimento sozinha não define os produtos. Ou seja, o aumento desses parâmetros favorece a formação de compostos voláteis (gases e líquidos). Enquanto que a diminuição favorece a produção de carvão (COLLARD; BLIN, 2014; DINIZ, 2005).

O tempo de residência também é um fator importante, pois em baixas taxas de aquecimento, a remoção lenta ou gradual de voláteis permite que uma reação secundária ocorra entre as partículas de char e de voláteis, levando a formação de char secundário (BASU, 2010).

Guerrero et al. (2005) avaliaram o rendimento de char obtido a partir de *Eucalyptus*

Globulus Labill em função da temperatura de pirólise (600-900°C), utilizando a taxa de aquecimento de 10°C.min^{-1}, tempo de residência de 1 hora e fluxo de N_2 de 1000 mL. min^{-1}. O maior rendimento obtido pelos autores foi na temperatura de 600°C (24%) cerca de 3% maior que o rendimento obtido a 900°C (21,4%). Os teores de C, N e H presentes no char foram calculados em relação aos teores desses componentes presentes na amostra de eucalipto. Os autores observaram um aumento no percentual de C e N e uma diminuição de H e O com o aumento da temperatura. A partícula carbonizada formada pela desvolatilização do eucalipto contém estruturas de poros complexos e é essencialmente uma estrutura micro-macroporosa. As áreas superficiais, medidas por adsorção de CO_2, aumentaram ligeiramente enquanto a temperatura de desvolatilização aumentava até 800ºC, e diminuía depois disso. O ordenamento estrutural e a coalescência de microporos são responsáveis pela diminuição do valor da área superficial observada a 900ºC (de 589 para 362 m².g^{-1}), o que resulta em uma desativação térmica do carvão.

3.2.1.3 Biochar

O elemento carbono (C) possui hibridizaçao sp^2, e por isso pode formar uma variedade de estruturas tais como grafite, grafeno, nanotubos de parede simples e múltipla, diamante e fulereno (ZARBIN; OLIVEIRA, 2013). Além das estruturas citadas, existem as formas de carbono amorfo, tais como, o negro de fumo, o carvão ativado, o carbono vítreo, o biochar, entre outros. O biochar é um material rico em carbono produzido a partir da pirólise da matéria orgânica na ausência total ou parcial de oxigênio. A conversão termoquímica de biomassas para a produção de biochar é um método comum e apresenta elevada eficiência em termos de qualidade e rendimento do produto, além disso, torna-se mais atrativa devido ao seu baixo custo, viabilidade, abundância e não toxicidade (BAKIERSKA et al., 2014; CHANG; CHEN; JIAO, 2010) (ZHANG et al., 2019) (YU et al., 2019). Sua estrutura morfológica carbônica inclui a estrutura de carbono amorfo e a estrutura condensada grafítica, que são a fração não carbonizada e a fração completamente carbonizada dos biochars, respectivamente (CHEN et al., 2018).

A adsorção é o principal mecanismo do biochar para remover metais e poluentes orgânicos. A capacidade de adsorção do biochar tem ligação direta com suas propriedades físico-químicas, como área superficial, distribuição do tamanho dos poros, grupos funcionais e capacidade de troca catiônica (WANG; WANG, 2019).

4 ARTIGO I

Lazzari, Lídia K.; Perondi, Daniele ; Zattera, Ademir J. ; Santana, Ruth M. C. . Influence of the addition of carbon structures in cellulose cryogels. Journal of Porous Materials, v. 28, p. 279-288, 2021.

Journal of Porous Materials
https://doi.org/10.1007/s10934-020-00972-3

Influence of the addition of carbon structures in cellulose cryogels

Lídia K. Lazzari[1] · Daniele Perondi[2] · Ademir J. Zattera[2] · Ruth M. C. Santana[1]

Abstract
The substitution of carbon structures, such as graphene and carbon nanotubes by biochar, is interesting, since the latter has considerably lower costs and similar properties to other structures. Therefore, the objective of the present paper was to evaluate the influence of the addition of biochar (BC), produced from the pyrolysis of cellulose residues, in order to substitute graphene nanoplatelets (GNP), regarding the thermal, mechanical and adsorption aspects. The cryogels were produced from the cellulose suspension with the addition of 50 and 100 (% w/w in relation to cellulose) of BC or GNP. Extremely light cryogels (with apparent density less than 0.033 g cm^{-3} and porosity greater than 90%) were produced. The addition of BC and GNP showed similar values in terms of compressive strength, temperature of degradation and thermal conductivity. In the heterogeneous adsorption capacity, however, a significant difference was observed between the two carbon structures studied, and for this property, the GNPs showed a slight increase in the adsorption capacity in relation to BC. In the general context of the properties studied, the biochar has the potential to be used to replace commercially used carbon structures, such as graphene nanoplatelets.

Keywords Cellulose cryogel · Biochar · Graphene nanoplatelets · Compressive strength · Thermal conductivity and adsorption

1 Introduction

The use of carbon structures (graphene and carbon nanotubes) as precursors in cryogels has become attractive due to its excellent thermal, mechanical and electrical properties. The addition of these materials in cryogels adds properties such as hydrophobicity and compressibility to the remarkable properties of aerogels, such as low density and high porosity [1, 2].

Several authors report research on the development of cellulose aerogels and allotropic forms of carbon, such as: graphene oxide [1, 3, 4] and carbon nanotubes [5, 6] (as a carbon source) for different applications. However, the large amount of chemical products and the generation of acidic residues during the synthesis of these precursors, associated with difficult and expensive technologies, in addition to the equipment involved in the preparation, restrict their production on a large-scale [3, 6, 7].

Due to its low cost, non-toxicity to humans and abundance in nature, the use of organic precursors as a source of carbonaceous raw material has received increasing attention in the last decade. Organic raw materials, when subjected to the pyrolysis process, produce a solid carbonaceous fraction (biochar) which has an elevated energy value, in addition to being an added value product. The combination of properties such as relatively high specific surface area, high pore volume, long-term stability and enriched surface functional groups, allows this material to be used for different purposes, such as wastewater treatment, precursor to catalysts, additives for digestion and anaerobic composting, energy storage, as well as reinforcement in aerogels. In addition, the inclusion of this biochar has some advantages such as high electrical conductivity, flame resistance and impermeability to water [4, 8–10].

Electronic supplementary material The online version of this article (https://doi.org/10.1007/s10934-020-00972-3) contains supplementary material, which is available to authorized users.

✉ Lídia K. Lazzari
lidia_lazzari@yahoo.com.br

[1] Post Graduation Program in Mining, Metallurgy and Materials Engineering, Federal University of Rio Grande Do Sul, Porto Alegre, RS, Brazil

[2] Post-Graduation Program in Process and Technology Engineering, University of Caxias Do Sul, Caxias Do Sul, RS, Brazil

Published online: 26 September 2020

Cryogels are derived from aerogel (microporous solid gel in which the dispersed phase is a gas), in which case the liquid present in the gel is removed from the pores by freeze-drying [11]. Currently, cryogels have been extensively studied for application purposes as adsorbents and thermal insulators. In the first case, due to their high specific surface area, carbon based aerogels have significant efficiency, high capacity and fast oil adsorption rate, associated with the combination of raw materials and simple and cheap synthesis methods, thus surpassing several other aerogels and commercial adsorbents [1, 3, 12]. For thermal insulation purposes, carbon structures have been used to increase the mechanical properties of aerogels (between 40 and 60% increase in compressive strength compared to aerogel without the addition of loads), since these particles do not affect their thermal conductivity [13, 14].

Considering the inferior mechanical properties of cellulose aerogels and the expensive precursors and technologies involved in the production process of graphene aerogels, studies are needed to replace more efficient precursors to improve them. Therefore, the objective of the present work was to evaluate the replacement of graphene nanopleletes by biochar and to determine its influence on the properties (thermal and mechanical) of cellulose cryogels, as well as on the application in adsorbents and thermal insulators. In this context, several authors research the addition of graphene oxide or carbon nanotubes to aerogel. However, no studies were found in the literature that present the addition of biochar in aerogels, except one carried out by our research group [13], that we have shown the influence of the concentration of biochar in cellulose aerogels under mechanical and thermal properties was evaluated.

2 Materials and methods

2.1 Materials

The materials used for the production of cryogels were: *Pinus elliotti* cellulose (provided by the company Trombini—RS/Brazil), waste from the pulp and paper industry (IPUSA—Uruguay), commercial graphene nanoplatelets—GNP (Strem Chemicals, INC.—USA)—6–8 nm thick with a bulk density of 0.03 to 0.1 g/cc, an oxygen content of < 1% and a carbon content of > 99.5 wt%. The petroleum was supplied by the Alberto Pasqualini Refinery, Canoas RS ($\rho = 891$ kg m^{-3} and $\mu = 62$ cP).

2.2 Production of cellulose suspension

Figure 1 (step 1) shows the flow chart of the cryogels production. Initially, *Pinus elliotti* cellulose was ground in a stone mill for 5 h at 4500 rpm with water, to obtain the

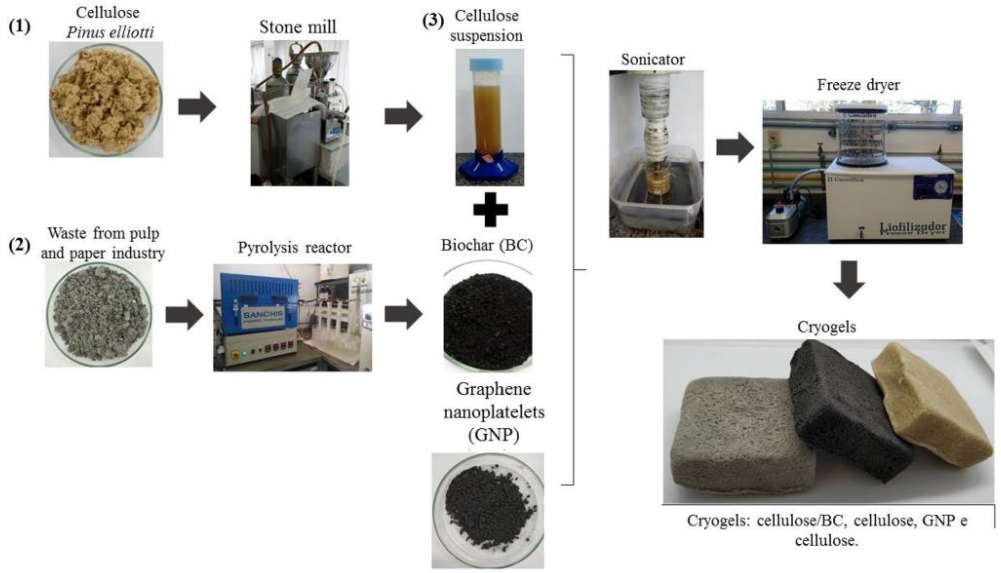

Fig. 1 Flowchart of production of cryogels

cellulose suspension with 1.43% (w/w) cellulose fiber concentration [15].

2.3 Production of biochar from cellulose residue

The biochar (BC) was produced from the pyrolysis of waste pulp and paper industry with a heating rate of 5 °C min^{-1}, isotherm time of 60 min, final operating temperature of 800 °C and N_2 flow of 150 mL min^{-1}. Figure 1 (step 2) shows the flowchart of the biochar production.

2.4 Production of cellulose/BC and cellulose/GNP cryogels

Figure 1 (step 3) shows the flowchart for the production of cryogels. Cryogels were produced by using the methodology presented by [13]. Initially, the cellulose suspension was centrifuged, and either BC or GNP was added to the supernatant in concentrations of 50 and 100% (w/w in relation to cellulose mass). The supernatant was drained over the precipitate and mechanically stirred for 5 min to completely homogenize the suspension. The final suspension was sonified for 30 min and with a 50% amplitude (maximum equipment capacity—500 W). Finally, the suspension was frozen in an ultrafreezer in square molds and then lyophilized for 72 h under vacuum at – 45 °C. After drying, silanization by vapor deposition was carried out in order to make the cryogel hydrophobic. The cryogel was then suspended by a screen in a beaker containing 2 ml of methyltrimethoxysilane (MTMS) and isolated inside another beaker for 48 h in an oven at 70 °C [16]. The nomenclature of cryogels was defined as: CC (cellulose cryogel); CC50BC (cellulose cryogel with addition of 50% w/w BC); CC100BC (cellulose cryogel with addition of 100% w/w BC); CC50GNP (cellulose cryogel with addition of 50% w/w GNP) and CC100GNP (cellulose cryogel with addition of 100% w/w GNP).

2.5 Characterization of cellulose/BC and cellulose/GNP cryogels

The density (ρ) of the cryogels was calculated by the ratio of mass (g) and volume (cm^3) [17].

The porosity (P) of cryogels was determined with Eq. 1 based on the methodology used by Wang et al. [18].

$$P = \left(1 - \frac{\rho}{\rho_{ts}}\right) * 100 \quad (1)$$

where ρ_{ts} is the theoretic density of cryogels calculated by Eq. 2.

$$\rho_{ts} = \frac{1}{\frac{\omega_{cel}}{\rho_{cel}} + \frac{\omega_{BC\ or\ GNP}}{\rho_{BC\ or\ GNP}}} \quad (2)$$

where ω_{cel}, $\omega_{BC\ and}$ ω_{GNP} are the mass fractions of cellulose, BC and GNP in the dry cryogels, respectively; ρ_{cel}, ρ_{BC} and ρ_{GNP} are the densities of cellulose, BC and GNP, respectively. These densities were determined using pycnometer in which dried cellulose (2.05 g cm^{-3}), BC (2.44 g cm^{-3}) and GNP (2.16 g cm^{-3}) powder was tested.

The surface area was measured by the method of Brunauer, Emmet and Teller (BET) using the Quantachrome Instruments equipment (model 1200e), managing the nitrogen adsorption/desorption process at − 196 °C. The samples went through a degassing process conducted under N2 flow without vacuum and temperature of 105 °C, for a period of 20 h.

The morphology of cryogels was assessed from optical microscopy analysis, using a Meterk opticaicroscope (China).

Fourier transform infrared spectroscopy (FTIR) performed on the Nicolet IS10 Thermo Scientific (USA) equipment, each spectrum was obtained by 32 scans, with wave number between 4000 and 400 cm^{-1} by ATR.

The compressive strength test was carried out on a universal test equipment EMIC—model DL 2000 (Brazil), with a compression speed of 1.3 mm min^{-1}, to measure the tension necessary to reduce the thickness of the specimen in 20, 50 and 70% of its initial thickness, according to adaptation of the ASTM D695-15 standard.

Thermogravimetry was performed using about 10 mg of sample at a heating rate of 10 °C min^{-1} over a temperature range of 23–600 °C in a nitrogen atmosphere with a flow of 50 mL min^{-1}. The equipment used was a thermobalance brand Shimadzu®—model TGA-50 (Japan).

The thermal conductivity of the cryogel was measured on the equipment TCi Thermal Conductivity Analyzer from C-Therm Technologies.

In order to evaluate the adsorption capacity of cryogels, adsorption tests were carried out in homogeneous medium (water and oil) and heterogeneous medium (water and oil), according to adaptation of the F726-12 standard of the American Society of Testing and Materials (ASTM, 2012). The cryogels were previously weighed and placed in a container with enough fluid (water and/or oil) so that they could float freely. The adsorption capacity test was performed by measuring the mass of fluid adsorbed by the cryogel for a time of 0.25; 0.5; 1; 3; 5; 10 and 15 min. The adsorption capacity was calculated according to Eq. 3. The tests were carried out in triplicate and the environment was controlled at 23 ± 2 °C.

$$C_{ads} = \frac{m_f - m_i}{m_i} \quad (3)$$

In which, C_{ads} is the adsorption capacity (g g^{-1}) and m_i and m_f the initial and final masses of cryogels (g).

3 Results and discussion

3.1 Characterization of BC and GNP

Cellulose has a specific surface area of 2.562 m^2 g^{-1}, after the pyrolysis of this raw material, the biochar produced presented a surface area of 153.948 m^2 g^{-1}, showing that the pyrolysis process considerably increases this property, which becomes very important when the purpose of using biochar for the application of adsorption. The GNP had a specific surface area of 127.621 m^2 g^{-1}, lower than that found for the biochar. this small difference found in the specific surface area of BC and GNP did not influence the porosity of the cryogels produced, as shown in Table 1.

3.2 Characterization of cryogels

Table 1 describes the cryogels produced and presents the results of apparent density and porosity of the samples produced.

The results presented in Table 1, show that with the addition of GNP and BC, the calculated value of the density of cryogels shows an increase in relation to cryogel CC. This increase is due to the increase of solid particles (BC and GNP) in the cellulose suspension. Yang et al. [19] also observed this behavior in their microcrystalline cellulose aerogels and graphene nanoplatelets, with a two-fold increase in density for the aerogel with a 1:1 cellulose/graphene nanoplatelets concentration, compared to microcrystalline cellulose aerogel.

The porosity of cryogels is inversely proportional to density, that is, the lower the density, the greater the porosity. This is because in the denser cryogel there is a greater amount of solid particles and cellulose fibers which reduces the free spaces (pores) between them, thus decreasing the porosity of cryogels. This behavior was observed for the studied cryogels, as seen in Table 1. Cryogels showed high porosity, above 98%, due to their low densities. Based on the data present in Table 1, it seems that the lower the apparent density is, the greater the porosity of the cryogel. With the addition of biochar and GNP causes an increase in the density of cryogels, consequently, there is a decrease in the porosity of the cryogel. Although CC100BC and CC100GNP cryogels have the same amount of solid particles, the CC100GNP showed higher porosity than the CC100BC, showing that GNPs have higher porosity than biochar.

Table 1 Apparent density and porosity of cryogels

Nomenclature	m (g)	Apparent density (g cm^{-3})	Porosity (%)
CC	0.79 ± 0.02	0.017 ± 0.0009	99.2 ± 0.04
CC50GNP	1.54 ± 0.02	0.029 ± 0.0002	98.6 ± 0.01
CC100GNP	1.19 ± 0.04	0.036 ± 0.0007	98.3 ± 0.03
CC50BC	1.47 ± 0.04	0.030 ± 0.001	98.6 ± 0.04
CC100BC	1.25 ± 0.05	0.043 ± 0.0008	98.1 ± 0.04

Figure 2 shows the photograph of the cryogels CC, CC100BC and CC100NPG and an increase in the surface made under an optical microscope to assess the porous surface of cryogels. In Fig. 2a and c, it is possible to observe that the cryogels CC100BC and CC100GNP, respectively, have a uniform color, showing that the mixture of BC and GNP in the cellulose suspension was homogeneous. Still, in the optical micrographs (Fig. 2b, d, f) it is possible to observe that the three-dimensional structure of the aerogel is heterogeneous and composed of voids of different sizes. In addition, at the edges of the cryogel, the pore sizes are smaller than in the center. This pore heterogeneity occurs during the gel freezing process, due to the freezing speed, according to which the faster the more homogeneous is the formation of the ice crystals, and the direction of the ice crystals formation happens, from the outside to the inside. The CC100BC cryogel has a greater amount of pores than the CC100GNP cryogel, in which a more compact pore structure is seen. In addition, the cryogel CC100BC, the presence of long fibers is observed, which can favor the mechanical performance of this reinforcement.

In the cryogel CC, although the cellulose suspension has undergone the mechanical grinding process, it is possible to see long and agglomerated fibers, in addition to a structure with visibly larger voids than the others. This behavior is also observed by [20], who justifies that the individual cellulose nanofibers are forced be joined into sheets due to the growth of ice crystals during freezing. Also, according to the authors, this agglomeration of nanofibers provides aerogel with greater mechanical stability.

Figure 3 and Table 2 shows the FTIR spectra and assignment bands obtained from the cryogels. As can be seen, most of the characteristic bands of cellulose remain in the other cryogels. Cryogels CC50GNP and CC100GNP present band in 1646 cm^{-1} assigning to C=C skeletal vibration from graphitic domains, in addition to presenting a more pronounced band in 1104 cm^{-1} indicate that many oxygen-containing functional groups existed on the surface of GNP. According to Ren et al. [16] the band's permanency at 3330 cm^{-1} in cryogels indicates the existence of the Strong hydrogen

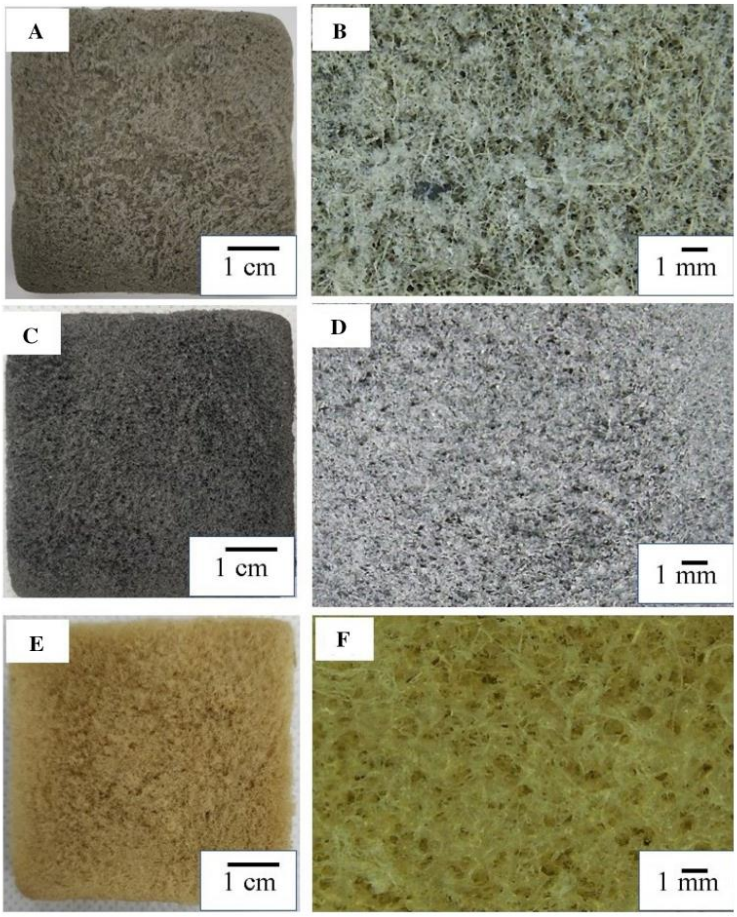

Fig. 2 Cryogels photography: **a** CC100BC, **c** CC100GNP and **e** CC; micrographs: **b** CC100BC, **d** CC100GNP and **f** CC

bonding interaction between cellulose and carbonaceous structures.

3.3 Compression strength

Figure 4 shows the stress–strain curves for the compressive strength test (for a deformation of 20, 50 and 70% of cryogels). The curves exhibit deformation behavior similar to that of foams. In Fig. 4, it is possible to verify two regions of deformation. The first, with deformation from 0 to 60% shows a gradual increase in tension, damaging the void walls irreversibly. And the second, with a densification region with greater stresses due to the densely compressed structure and, therefore, presenting a fast increase in the tension [3, 25]. The stress–strain curves presented for cryogels in the present study did not show the region of elastic deformation mentioned by other authors [2, 3, 26], which shows that these cryogels do not show elasticity, that is, after being subjected to tension, the cryogel structure does not have the capacity to return to its initial state [27].

In all deformations evaluated the behavior is the same. Compressive strength increases with the addition of 50 and 100% of the carbon structures, regardless of the type of structure added. For 70% deformation of the specimen, this increase was 50 and 160% in cryogels with the addition of 50 and 100% w/w of the carbon structures, respectively, either for GNP or for BC.

By comparing cryogels with the addition of carbon structures, for 50% deformation of the specimen, no significant difference between cryogels CC50BC and CC50GNP (item

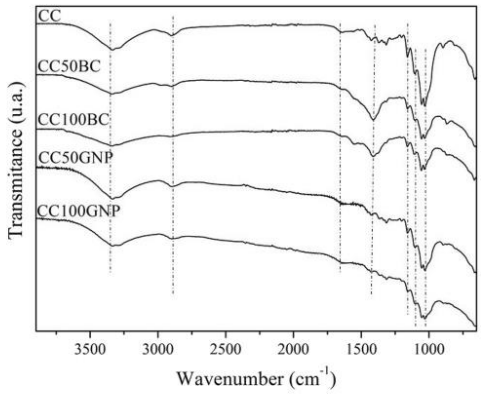

Fig. 3 FTIR spectra of cryogels

Table 2 FTIR assignment bands

Wavenumber (cm^{-1})	Assignment[a]
3330	Stretching vibration of O–H
2900	Symmetric ad asymmetric C–H vibration
1646	C=C skeletal vibration from graphitic domains
1415	Bending of $–CH_2$ and O–C–H
1159	$Si–CH_3$
1104	C–O stretching vibration
1054	Glycosidic bond vibration C–O–C overlpped with stretching vibration of C–OH
1031	Stretching of C–O and O–H groups bonds of cellulose polysaccharides

[a][16, 21–24]

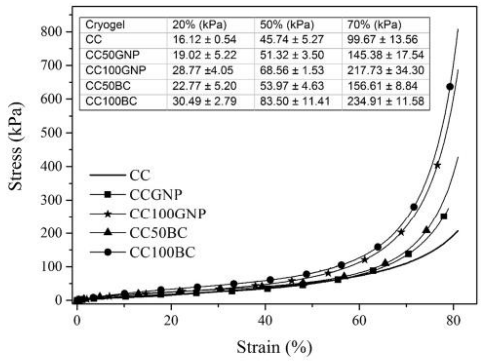

Fig. 4 Stress x strain curve with deformation of 20, 50 and 70% of the specimen

S.1.1 Statistical Analysis) was noted. However, between cryogels CC100BC and CC100GNP a significant difference is present, with the CC100BC cryogel presenting a higher compressive strength than CC100GNP. Regarding the 70% deformation of the specimen, the cryogels with the addition of carbon structures showed similar values of compressive strength, with no significant differences in compressive strength (item S.1.2 Statistical Analysis). Thus, it is possible to infer that the type of particle added (GNP or biochar) does not influence the compressive strength since the amount of solid particles (by mass) added in each cryogel is the same. It is important to highlight that due to the heterogeneity of the three-dimensional structure of the aerogels formed during their freezing, the standard deviation obtained in the test was high, mainly in the 70% deformation of the specimen.

Figure 5 shows the cryogenic resistance test at a standard weight of 1 kg. The figures shows that all cryogels supported the mass of the standard weight without undergoing visible changes in their structures. Therefore, the cryogels produced support approximately 1000 times their own mass.

Mi et al. [3] studied the behavior of adding graphene oxide to cellulose/graphene oxide aerogels and found that with the increase in the amount of graphene oxide, there is an increase in the compression and resistance modulus due to the rigidity of the graphene sheets, a behavior also observed per Ge et al. [14].

3.4 Thermal properties

3.4.1 Thermogravimetry

The thermogravimetric curves for cryogels are shown in Fig. 6a. For all cryogels produced, there is a mass loss event at approximately 100 °C, due to the loss of moisture present in the samples. For the cryogenic AC, there is a mass loss event between 200 and 400 °C, in which the highest percentage of mass loss occurs, due to the depolymerization of cellulose and after 400 °C, cellulose fiber degradation occurs with increasing temperature. For the other cryogels, because the carbon structures have been added to the cellulose suspension, the thermogravimetric curves also show a mass loss event between 200 and 400 °C due to cellulose degradation and the decomposition of oxygen present in the functional groups CO_2 and CO. The cryogels with the addition of GNP showed an initial temperature of degradation higher than the others, due to the greater thermal stability of these structures (see item S.4 of supplementary material).

The cellulose/biochar cryogels had a T_{max} lower than the CC, probably this was due to the biochar being produced from the waste pulp and paper industry, which may contain contaminants from the processing of cellulose for the production of paper.

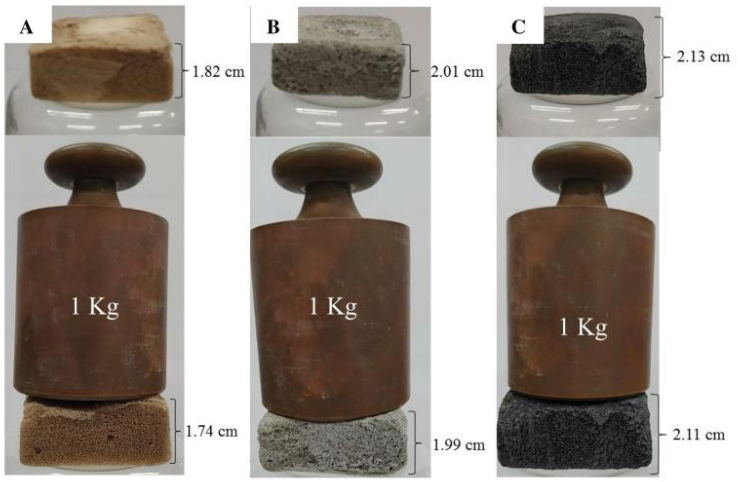

Fig. 5 Photograph of cryogels with standard weight of 1 kg: **a** CC, **b** CC100BC E **c** CC100GNP

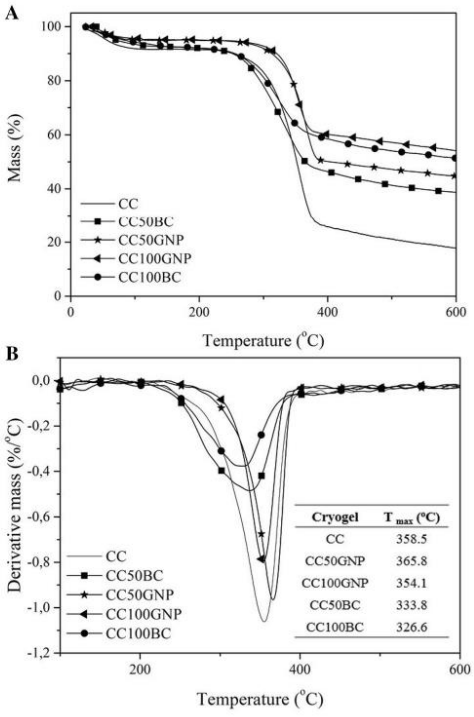

Fig. 6 **a** TGA curve and its **b** derivative (DTG) for cryogels

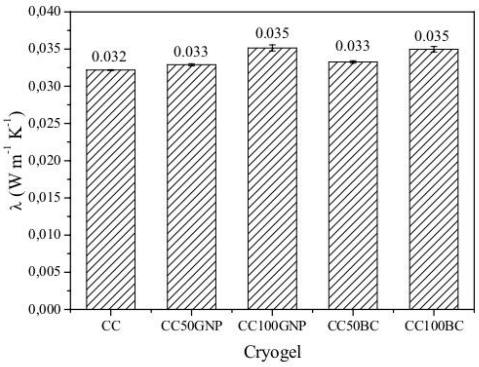

Fig. 7 Thermal conductivity of cryogels

Figure 6b shows that the addition of the carbon structures results in different outcomes. While the GNPs increase the T_{max}, the biochar decreases this temperature in relation to the raw material (see item S.4 of supplementary material). By doubling the carbon content in the foam, there is a shift towards lower peak temperatures. Furthermore, the decomposition kinetics of BC foams is slower (wide peaks) than samples with GNP.

3.4.2 Thermal conductivity

Figure 7 shows the thermal conductivity of cryogels. The thermal conductivity value found for cryogels, approximately 0.033 W m^{-1} K^{-1}, is comparable to polystyrene

foams (0.03–0.04 W m^{-1} K^{-1}), thus having the potential to replace commercial insulating materials [14]. The results obtained can also be compared to other materials studied by several researchers, such as: cellulose aerogel (0.029–0.032 W m^{-1} K^{-1}) [28]; aerogel/expanded perlite composite (0.030–0.038 W m^{-1} K^{-1}) [29]; carbon aerogels (0.054 W m^{-1} K^{-1}) [30] and cellulose/graphene aerogel supported phase change composites (1.35 W m^{-1} K^{-1}, 1:1 cellulose/graphene) [19].

According to Ge et al. [14] the thermal conductivity of an aerogel is determined from three factors: solid-state thermal conductivity, which depends on the conductivity of the solid material and the density of the aerogel; gaseous thermal conductivity, determined primarily by the pore size, in which the smaller the pore size is, the lower the thermal conductivity gets; and, thermal conductivity of radiation, which in the case of carbonaceous materials, as they present strong absorption in the infrared and insignificant radiation thermal conductivity. From these factors, the authors show that the thermal conductivity is influenced mainly by the type of solid material, density and pore size of the aerogel. In the present work, the proximity of the thermal conductivity found for all cryogels is explained due to the thermal conductivity factor and density increased after the addition of the carbon structures, although not significantly as seen in S.2—Statistical Analysis. In addition, as the porosity of cryogels is similar, so this factor did not influence thermal conductivity.

3.5 Sorption capacity

Figure 8 shows the results found in the adsorption capacity tests of the studied cryogels. As it is possible to observe, the cryogel CC presented the highest capacity of oil adsorption in homogeneous and heterogeneous medium in relation to the other cryogels, 33.5 and 34.2 g g^{-1} respectively. The adsorption occurs in the pores of the cryogels structure. Since the porosity of the cryogels was relatively close to each other (Table 1), it is clear that this factor was not decisive in the adsorption capacity of the cryogels. Therefore, the adsorption was higher in the cryogel CC due to its lower content of solids.

In an heterogeneous environment, considering the cryogels with particle addition (biochar or GNP), the ones with the greatest adsorption capacities were the cryogels CC50GNP and CC50BC, 23.3 and 22.3 g g^{-1} respectively. As seen in item S.3 (Statistical Analysis), between these cryogels there is no significant difference in the oil adsorption capacity. Hence, both have the same capacity and, therefore, biochar can be a good alternative as reinforcement for cellulose cryogels due to the lower cost raw material than GNP.

For cryogels with the addition of BC, it is possible to note that the adsorption capacity in heterogeneous medium is greater than the oil adsorption capacity, which shows that these cryogels may be adsorbing water together with oil. For cryogels with the addition of GNP, this behavior does not happen, showing that the GNP particles have a hydrophobic character [13, 31].

Other researchers have reported the adsorption capacity of aerogels and cryogels produced from different materials, such as: cellulose cryogels (25.9 g g^{-1}) [32]; hydrophobic silica aerogels (15.1 g g^{-1}) [33]; graphene/carbon nanotube aerogels (21–35 times their own weight—30 g g^{-1}) [34]. As seen in Fig. 8, cellulose/BC cryogels produced in this work have the capacity to adsorb above 23 times their own mass, compared to graphene/carbon nanotube aerogels. However, it is important to highlight that the cryogels produced in this work were obtained from a low-cost raw material.

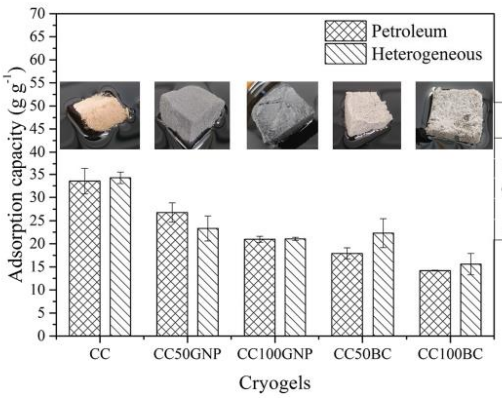

Cryogel	Petroleum (g g^{-1})	Heterogeneous (g g^{-1})
CC	33.5±2.2	34.2±1.0
CC50GNP	26.8±1.7	23.3±2.2
CC100GNP	21.0±0.5	21.1±0.3
CC50BC	17.9±1.0	22.3±3.1
CC100BC	14.2±0.1	15.6±1.9

Fig. 8 Adsorption capacity of cryogels. *Note* Water adsorption, in all cryogels it was less than 0.6 g g^{-1}, for this reason it was not shown in the graph

4 Conclusions

With the addition of carbon structures, an increase of 50 and 160% (with the addition of 50 and 100% w/w of the carbon structures) in the compressive strength of cellulose cryogels was obtained, which can be justified by the increase in the fraction of solids present in the cellulose suspension. In addition, the replacement of graphene nanoplatelets by biochar proved to be effective, since with the different carbon structures added, cryogels showed similar porosity, compressive strength, thermal conductivity and oil adsorption capacity. Therefore, it is possible to use a raw material from agricultural waste and of low cost, such as biochar, in the replacement of commercially used carbon structures.

Acknowledgements The authors are grateful for the National Council for Scientific and Technological Development (CNPq) and the Foundation for Research Support of the State of Rio Grande do Sul (FAPERGS).

References

1. C. Xiang, C. Wang, R. Guo, J. Lan, S. Lin, S. Jiang, X. Lai, Y. Zhang, H. Xiao, Synthesis of carboxymethyl cellulose-reduced graphene oxide aerogel for efficient removal of organic liquids and dyes. J. Mater. Sci. **54**, 1872–1883 (2019). https://doi.org/10.1007/s10853-018-2900-5
2. J. Li, H. Meng, S. Xie, B. Zhang, J. Li, L. Li, H. Ma, J. Zhang, M. Yu, Ultra-light, compressible and fire-resistant graphene aerogel as a highly efficient and recyclable absorbent for organic liquids. J. Mater. Chem. A. **2**, 2934–2941 (2014). https://doi.org/10.1039/c3ta14725h
3. H. Mi, X. Jing, A.L. Politowicz, E. Chen, H. Huang, L. Turng, Highly compressible ultra-light anisotropic cellulose/graphene aerogel fabricated by bidirectional freeze drying for selective oil absorption. Carbon N. Y. **132**, 199–209 (2018). https://doi.org/10.1016/j.carbon.2018.02.033
4. C. Wan, J. Li, Graphene oxide/cellulose aerogels nanocomposite: preparation, pyrolysis, and application for electromagnetic interference shielding. Carbohydr. Polym. **150**, 172–179 (2016). https://doi.org/10.1016/j.carbpol.2016.05.051
5. H.C. Hwang, J.S. Woo, S.Y. Park, Flexible carbonized cellulose/single-walled carbon nanotube films with high conductivity. Carbohydr. Polym. **196**, 168–175 (2018). https://doi.org/10.1016/j.carbpol.2018.05.013
6. L. Cong, X. Li, L. Ma, Z. Peng, C. Yang, P. Han, G. Wang, H. Li, W. Song, G. Song, High-performance graphene oxide/carbon nanotubes aerogel-polystyrene composites: preparation and mechanical properties. Mater. Lett. **214**, 190–193 (2018). https://doi.org/10.1016/j.matlet.2017.12.015
7. H. Bi, Z. Yin, X. Cao, X. Xie, C. Tan, X. Huang, B. Chen, F. Chen, Q. Yang, X. Bu, X. Lu, L. Sun, Carbon fiber aerogel made from raw cotton: a novel, efficient and recyclable sorbent for oils and organic solvents. Adv. Mater. (2013). https://doi.org/10.1002/adma.201302435
8. Z. Zhang, Z. Zhu, B. Shen, L. Liu, Insights into biochar and hydrochar production and applications: a review. Energy. **171**, 581–598 (2019). https://doi.org/10.1016/j.energy.2019.01.035
9. G. Skouteris, D. Saroj, P. Melidis, F.I. Hai, S. Ouki, The effect of activated carbon addition on membrane bioreactor processes for wastewater treatment and reclamation—a critical review. Bioresour. Technol. **185**, 399–410 (2015). https://doi.org/10.1016/j.biortech.2015.03.010
10. P. Basu, *Biomass Gasification and Pyrolysis: Pratical Design and Theory* (Eselvier, New York, 2010)
11. N. Hüsing, U. Schubert, Aerogels—airy materials: chemistry, structure, and properties. Angew. Chemie Int. Ed. **37**, 22–45 (2002). https://doi.org/10.1002/1521-3773(19980202)37:1/2<22:aid-anie22>3.3.co;2-9
12. S. Han, Q. Sun, H. Zheng, J. Li, C. Jin, Green and facile fabrication of carbon aerogels from cellulose-based waste newspaper for solving organic pollution. Carbohydr. Polym. **136**, 95–100 (2016). https://doi.org/10.1016/j.carbpol.2015.09.024
13. L.K. Lazzari, D. Perondi, V.B. Zampieri, A.J. Zattera, R.M.C. Santana, Cellulose/biochar aerogels with excellent mechanical and thermal insulation properties. Cellulose **26**, 9071–9083 (2019). https://doi.org/10.1007/s10570-019-02696-3
14. X. Ge, Y. Shan, L. Wu, X. Mu, H. Peng, Y. Jiang, High-strength and morphology-controlled aerogel based on carboxymethyl cellulose and graphene oxide. Carbohydr. Polym. **197**, 277–283 (2018). https://doi.org/10.1016/j.carbpol.2018.06.014
15. R.M. Neves, K.S. Lopes, M.V.G. Zimmermann, M. Poletto, A.J. Zattera, Characterization of polystyrene nanocomposites and expanded nanocomposites reinforced with cellulose nanofibers and nanocrystals. Cellulose **26**, 4417–4429 (2019). https://doi.org/10.1007/s10570-019-02392-2
16. L.K. Lazzari, V.B. Zampieri, M. Zanini, A.J. Zattera, C. Baldasso, Sorption capacity of hydrophobic cellulose cryogels silanized by two different methods. Cellulose **24**, 3421–3431 (2017). https://doi.org/10.1007/s10570-017-1349-z
17. P. Gupta, B. Singh, A.K. Agrawal, P.K. Maji, Low density and high strength nanofibrillated cellulose aerogel for thermal insulation application. Mater. Des. **158**, 224–236 (2018). https://doi.org/10.1016/j.matdes.2018.08.031
18. L. Wang, M. Sánchez-Soto, T. Abt, Properties of bio-based gum Arabic/clay aerogels. Ind. Crops Prod. **91**, 15–21 (2016). https://doi.org/10.1016/j.indcrop.2016.05.001
19. J. Yang, E. Zhang, X. Li, Y. Zhang, J. Qu, Z. Yu, Cellulose/graphene aerogel supported phase change composites with high thermal conductivity and good shape stability for thermal energy storage. Carbon N. Y. **98**, 50–57 (2016). https://doi.org/10.1016/j.carbon.2015.10.082
20. J.T. Korhonen, M. Kettunen, R.H.A. Ras, O. Ikkala, Hydrophobic nanocellulose aerogels as floating, sustainable, reusable, and recyclable oil absorbents. ACS Appl. Mater. Interfaces. **3**, 1813–1816 (2011)
21. R.M. Neves, H.L. Ornaghi, A.J. Zattera, S.C. Amico, The influence of silane surface modification on microcrystalline cellulose characteristics. Carbohydr. Polym. (2020). https://doi.org/10.1016/j.carbpol.2019.115595
22. R.J. Mo, Y. Zhao, M.M. Zhao, M. Wu, C. Wang, J.P. Li, S. Kuga, Y. Huang, Graphene-like porous carbon from sheet cellulose as electrodes for supercapacitors. Chem. Eng. J. **346**, 104–112 (2018). https://doi.org/10.1016/j.cej.2018.04.010
23. F. Ren, Z. Li, W.Z. Tan, X.H. Liu, Z.F. Sun, P.G. Ren, D.X. Yan, Facile preparation of 3D regenerated cellulose/graphene oxide composite aerogel with high-efficiency adsorption towards methylene blue. J. Colloid Interface Sci. **532**, 58–67 (2018). https://doi.org/10.1016/j.jcis.2018.07.101
24. N. Lobos, J. Manuel, V. Comignani, E. Laura, M. Duarte, Biochar from pyrolysis of cellulose: an alternative catalyst support for the electro-oxidation of methanol. Int. J. Hydrogen Energy. **41**, 10695–10706 (2016). https://doi.org/10.1016/j.ijhydene.2016.04.041

25. Q. Zheng, A. Javadi, R. Sabo, Z. Cai, S. Gong, Polyvinyl alcohol (PVA)-cellulose nanofibril (CNF)-multiwalled carbon nanotube (MWCNT) hybrid organic aerogels with superior mechanical properties. RSC Adv. **3**, 20816–20823 (2013). https://doi.org/10.1039/c3ra42321b
26. H. Hu, Z. Zhao, W. Wan, Y. Gogotsi, J. Qiu, Polymer/graphene hybrid aerogel with high compressibility, conductivity, and "sticky" superhydrophobicity. ACS Appl. Mater. Interfaces. **6**, 3242–3249 (2014). https://doi.org/10.1021/am4050647%7C
27. C. Chen, F. Li, Y. Zhang, B. Wang, Y. Fan, X. Wang, R. Sun, Compressive, ultralight and fire-resistant lignin-modified graphene aerogels as recyclable absorbents for oil and organic solvents. Chem. Eng. J. **350**, 173–180 (2018). https://doi.org/10.1016/j.cej.2018.05.189
28. S.T. Nguyen, J. Feng, S.K. Ng, J.P.W. Wong, V.B.C. Tan, H.M. Duong, Advanced thermal insulation and absorption properties of recycled cellulose aerogels. Colloids Surfaces A Physicochem. Eng. Asp. **445**, 128–134 (2014). https://doi.org/10.1016/j.colsurfa.2014.01.015
29. G. Jia, Z. Li, P. Liu, Q. Jing, Preparation and characterization of aerogel/expanded perlite composite as building thermal insulation material. J. Non. Cryst. Solids. **482**, 192–202 (2018). https://doi.org/10.1016/j.jnoncrysol.2017.12.047
30. M. Wiener, G. Reichenauer, F. Hemberger, H. Ebert, Thermal conductivity of carbon aerogels as a function of pyrolysis temperature. Int. J. Thermophys. **27**, 1826–1843 (2006). https://doi.org/10.1007/s10765-006-0086-6
31. C. Jin, S. Han, J. Li, Q. Sun, Fabrication of cellulose-based aerogels from waste newspaper without any pretreatment and their use for absorbents. Carbohydr. Polym. **123**, 150–156 (2015). https://doi.org/10.1016/j.carbpol.2015.01.056
32. L.K. Lazzari, V.B. Zampieri, R.M. Neves, M. Zanini, A.J. Zattera, C. Baldasso, A study on adsorption isotherm and kinetics of petroleum by cellulose cryogels. Cellulose **26**, 1231–1246 (2018). https://doi.org/10.1007/s10570-018-2111-x
33. D. Wang, E. McLaughlin, R. Pfeffer, Y.S. Lin, Adsorption of oils from pure liquid and oil-water emulsion on hydrophobic silica aerogels. Sep. Purif. Technol. **99**, 28–35 (2012). https://doi.org/10.1016/j.seppur.2012.08.001
34. S. Kabiri, D.N.H. Tran, T. Altalhi, D. Losic, Outstanding adsorption performance of graphene-carbon nanotube aerogels for continuous oil removal. Carbon N. Y. **80**, 523–533 (2014). https://doi.org/10.1016/j.carbon.2014.08.092

SUPPLEMENTARY MATERIAL

STATISTICAL ANALYSIS

Statistical analyses of the results were performed by using the one-way analysis of variance function in Excel software. Based on the ANOVA data generated, the interaction between the groups was evaluated in order to verify the presence of significant differences between the groups. The data presented in the ANOVA table, shows that when "p" is lower than 0.05 (degree of reliability), there is a significant difference between the groups; when "*p*" is greater than 0.05 (degree of reliability), there is no significant difference between the groups.

In cases in which there was a significant difference between the groups, a multiple comparison of averages was performed to verify among which groups there is a significant difference. Hence, the decision limit (Dl) was calculated and compared to the value of the means difference (Δm) of 2 groups: when Dl> Δm, there is a significant difference between the groups and when Dl <Δm, there is no difference between the groups. Based on the result, letters were associated to each group to identify the significant differences between groups.

S.1 COMPRESSION STRENGTH

S.1.1 DEFORMATION OF 50% OF PROOF BODY

The values for 50% deformation of the cryogels proof body are presented in Table S.1.

Table S.1 – Compression strength for 50% deformation of cellulose cyogels.

	AC	AC50NPG	AC100NPG	AC50BC	AC100BC
Compression strength (kPa)	41.87	49.49	69.25	48.87	95.69
	43.61	49.12	66.77	57.89	81.72
	34.22	55.35	69.55	55.16	73.09
Average	39.90	51.32	68.53	53.97	83.50
Standard deviation	4.08	2.85	1.25	3.78	9.31

The data collected during the test and presented in Table S.1 was used to produce the ANOVA table in the Excel software, presented in Table S.2.

Table S.2 – ANOVA table.

Effect	*SQ*	*gl*	*MQ*	*F*	*P value*	*F critical*
Var 1	3416.95	4	854.24	22.36	5.66E-05	3.48
Error	382.07	10	38.21			
Total	3799.02	14				

Given that the "P value" is lower than 0.05 and "F" is higher than "Fcritical", there is a significant difference between the groups. Therefore the decision limit (Dl) of 10.71 was found and the multiple comparisons of averages were done as shown in Table S.3.

Table S.3 Multiple comparison of averages.

	Δm	Result	
AC/AC50NPG	11.42	Δm > Dl	significant
AC/AC100NPG	28.62	Δm > Dl	significant
AC/AC50BC	14.07	Δm > Dl	significant
AC/AC100BC	43.60	Δm > Dl	significant
AC50NPG/AC100NPG	17.21	Δm > Dl	significant
AC50NPG/AC50BC	2.65	Δm < Dl	not significant
AC50NPG/AC100BC	32.18	Δm > Dl	significant
AC100NPG/AC50BC	14.55	Δm > Dl	significant
AC100NPG/AC100BC	14.97	Δm > Dl	significant
AC50BC/AC100BC	29.53	Δm > Dl	significant

Considering that the difference between AC50NPG and AC50BC was not significant for compression strength, the cryogel AC50BC is a better option than NPG, due to added biochar, which is a cost-free raw material.

S.1.2 50% DEFORMATION OF THE PROOF BODY

The calculated values of the compression strength for 50% deformation of the proof body of the cryogels are presented in Table S.1.

Table S.1 – Compression strength for 50% deformation of cellulose aerogels.

	AC	AC50NPG	AC100NPG	AC50BC	AC100BC
Compression strength (kPa)	104.82	134.17	250.19	162.93	238.29
	84.29	165.59	181.84	160.40	244.43
	109.91	136.37	221.16	146.51	222.02
Average	99.67	145.38	217.73	156.61	234.91
Standard deviation	11.07	14.32	28.01	7.22	9.46

The ANOVA table was generated based on the data collected during the test, as per Table S.1. Results are presented in Table S.2.

Table S.2 – ANOVA table.

Effect	*SQ*	*gl*	*MQ*	*F*	*P value*	*F critical*
Var 1	36658.06	4	9164.51	24.37	3.86E-05	3.48
Error	3760.94	10	376.09			
Total	40419.00	14				

Since the "P-value" is lower than 0.05 and "F" is higher than "Fcritical", a significant difference between the groups is present. Therefore, the decision limit (Dl) of 33.59 was found and the multiple comparisons of averages were done as shown in Table S.3.

Table S.3 Multiple comparison of averages.

	Δm	Result	
AC/AC50NPG	45.70	Δm > Dl	significant
AC/AC100NPG	118.06	Δm > Dl	significant
AC/AC50BC	56.94	Δm > Dl	significant
AC/AC100BC	135.28	Δm > Dl	significant
AC50NPG/AC100NPG	72.3	Δm > Dl	significant
AC50NPG/AC50BC	11.23	Δm < Dl	not significant
AC50NPG/AC100BC	89.53	Δm > Dl	significant
AC100NPG/AC50BC	61.12	Δm > Dl	significant
AC100NPG/AC100BC	17.19	Δm < Dl	not significant
AC50BC/AC100BC	78.30	Δm > Dl	significant

Considering that the difference between AC50NPG-AC50BC and AC100NPG-AC100BC for compression strength was not significant, the cryogel with biochar is a better option than NPG, as it is cost-free raw material.

S.2 THERMAL CONDUCTIVITY

The calculated values of the thermal conductivity (k) of the cellulose aerogels are presented in Table S.1.

Table S.1 – Thermal conductivity of cellulose aerogels.

	AC	AC50NPG	AC100NPG	AC50BC	AC100BC

Thermal conductivity ($W\ m^{-1}\ K^{-1}$)	0.0263	0.0257	0.0246	0.0280	0.0255
	0.0220	0.0245	0.0229	0.0207	0.0231
	0.0256	0.0245	0.0250	0.0256	0.0291
Average	0.0246	0.0249	0.0242	0.0248	0.0259
Standard deviation	0.0019	0.0005	0.0009	0.0030	0.0025

The ANOVA table was generated based on the data collected during the test, as per Table S.1. Results are presented in Table S.2.

Table S.2 – ANOVA table.

Effect	*SQ*	*gl*	*MQ*	*F*	*P value*	*F critical*
Var 1	1.0483E-05	4	2.6208E-06	0.6460	0.6422	3.4780
Error	4.0569E-05	10	4.0569E-06			
Total	5.1052E-05	14				

Since the "P-value" is higher than 0.05 and "F" is lowest than "Fcritical", there is no significant difference between the groups. The lack of significant differences between the groups for thermal conductivity makes AC the best cryogel because there is no cargo added in it.

S.3 ADSORPTION CAPACITY

S.3.1 PETROLEUM (HOMOGENEOUS)

The calculated values of the petroleum adsorption capacity for the cryogels are presented in Table S.1.

Table S.1 – Petroleum adsorption capacity of cryogels.

	AC	AC50NPG	AC100NPG	AC50BC	AC100BC
Adsorption capacity ($g\ g^{-1}$)	30.54	27.33	21.64	16.77	14.30
	34.02	28.50	20.36	17.82	14.15
	35.97	24.50	20.95	19.16	14.13
Average	33.51	26.77	20.98	17.92	14.20
Standard deviation	2.25	1.68	0.52	0.98	0.07

The ANOVA table was generated based on the data collected during the test, as per Table S.1. Results are presented in Table S.2.

Table S.2 – ANOVA table.

Effect	*SQ*	*gl*	*MQ*	*F*	*P value*	*F critical*
Var 1	694.71	4	173.68	63.56	4.51E-07	3.48
Error	27.32	10	2.73			
Total	722.03	14				

Since the "P-value" is lower than 0.05 and "F" is higher than "Fcritical", a significant difference between the groups is present. Therefore, the decision limit (Dl) of 2.86 was found and the multiple comparisons of averages were done as shown in Table S.3.

Table S.3 Multiple comparison of averages.

	Δm	Result	
AC/AC50NPG	6.73	Δm > Dl	significant
AC/AC100NPG	12.52	Δm > Dl	significant
AC/AC50BC	15.59	Δm > Dl	significant
AC/AC100BC	19.31	Δm > Dl	significant
AC50NPG/AC100NPG	5.79	Δm > Dl	significant
AC50NPG/AC50BC	8.86	Δm > Dl	significant
AC50NPG/AC100BC	12.58	Δm > Dl	significant
AC100NPG/AC50BC	3.07	Δm > Dl	significant
AC100NPG/AC100BC	6.79	Δm > Dl	significant
AC50BC/AC100BC	3.72	Δm > Dl	significant

Given that, all groups present a significance different for petroleum adsorption capacity, the cryogel with the highest adsorption capacity is AC.

S.3.2 HETEROGENEOUS

The calculated values of the petroleum adsorption capacity for the cryogels are presented in Table S.1.

Table S.1 – Heterogeneous adsorption capacity of cryogels.

	AC	AC50NPG	AC100NPG	AC50BC	AC100BC
Soption capacity ($g\ g^{-1}$)	32.98	25.69	21.24	23.53	17.07
	35.45	20.35	20.70	18.73	12.92
	34.27	23.92	21.25	24.64	16.73
Average	34.23	23.32	21.06	22.30	15.58
Standard deviation	1.01	2.22	0.26	3.14	1.88

The ANOVA table was generated based on the data collected during the test, as per Table S.1. Results are presented in Table S.2.

Table S.2 – ANOVA table.

Effect	*SQ*	*gl*	*MQ*	*F*	*P value*	*F critical*
Var 1	555.55	4	138.89	28.67	1.858E-05	3.48
Error	48.44	10	4.84			
Total	603.99	14				

Since the "Pvalue" is lower than 0.05 and "F" is higher than "Fcritical", there is a significant difference between the groups. Therefore, the decision limit (Dl) of 3.81 was found and the multiple comparisons of averages was performed as shown in Table S.3.

Table S.3 Multiple comparison of averages.

	Δm	Result
AC/AC50NPG	10.91	Δm > Dl
AC/AC100NPG	13.17	Δm > Dl
AC/AC50BC	11.93	Δm > Dl
AC/AC100BC	18.66	Δm > Dl
AC50NPG/AC100NPG	2.26	Δm < Dl
AC50NPG/AC50BC	1.02	Δm < Dl
AC50NPG/AC100BC	7.75	Δm > Dl
AC100NPG/AC50BC	1.24	Δm < Dl
AC100NPG/AC100BC	5.48	Δm > Dl
AC50BC/AC100BC	6.72	Δm > Dl

Considering that the difference between AC50NPG and AC50BC for heterogeneous adsorption capacity was not significant, the cryogel AC50BC is a better option than NPG due the to added biochar, which is a cost-free raw material.

CHARACTERIZATION OF RAW MATERIALS

S.4 THERMOGRAVIMETRY

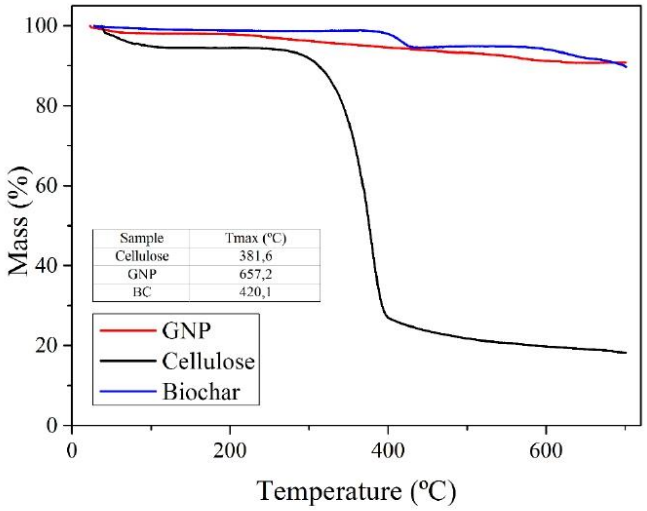

Fig. 1 – TGA curve for Cellulose, GNP and BC.

5 ARTIGO II

Lazzari, Lídia K.; Perondi, Daniele; Zampieri, Vitória B.; Zattera, Ademir J. ; Santana, Ruth M. C. . Cellulose/biochar aerogels with excellent mechanical and thermal insulation properties. Cellulose, v. 26, p. 9071-9083, 2019.

Cellulose
https://doi.org/10.1007/s10570-019-02696-3

ORIGINAL RESEARCH

Cellulose/biochar aerogels with excellent mechanical and thermal insulation properties

Lídia K. Lazzari · Daniele Perondi · Vitória B. Zampieri · Ademir J. Zattera · Ruth M. C. Santana

Received: 22 July 2019 / Accepted: 19 August 2019

Abstract Aiming at investigating the use of alternative materials for the production of thermal insulation and, mainly, to replace the carbon structures (graphene and nanotubes), extensively used in the development of aerogels, the present study had the objective to produce cellulose/biochar aerogels and to evaluate their properties. The aerogels were produced from *Pinus elliottii* cellulose fibers and biochar produced from these fibers. The materials were characterized in their physical, thermal and mechanical properties. They were extremely light and porous, with a density between 0.01 and 0.027 g cm^{-3} and porosity between 93 and 97%. Several percentages of biochars were added to the cellulose suspension (0–100% w/w). The use of 40 wt% biochar provided a 60% increase in the compressive strength of the aerogel in relation to the cellulose aerogel. Besides that, the addition of this carbonaceous structure did not influence significantly the thermal conductivity of the aerogels, which presented a thermal conductivity of 0.021–0.026 W m^{-1} K^{-1}. The materials produced in the present research present a great potential to be used as insulators due to the low thermal conductivity found, which was very similar to the thermal conductivity of the air and also of commercial materials such as polyurethane foam and expanded polystyrene.

Keywords *Pinus elliottii* cellulose · Biochar · Carbon structure · Aerogel · Thermal insulation

Introduction

According to data from the International Energy Agency (IEA 2019), in the member countries in 2016, the residential sector accounted for 20% of energy consumption. In Brazil, in 2017 alone, the sector accounted for 28.8% of energy consumption (EPE 2018). Given that this percentage is a considerable part of the total energy consumption in the sector, there is a need to improve the energy performance of buildings by reducing the energy consumed. Considering that the orientation of a building and its architectural features are subject to constraints imposed by the densely built urban environment and also by architectural desires and restrictions, thermal

Electronic supplementary material The online version of this article (https://doi.org/10.1007/s10570-019-02696-3) contains supplementary material, which is available to authorized users.

L. K. Lazzari (✉) · R. M. C. Santana
Post Graduation Program in Mining, Metallurgy and Materials Engineering, Universidade Federal do Rio Grande do Sul, Porto Alegre, RS, Brazil
e-mail: lidia_lazzari@yahoo.com.br

D. Perondi · V. B. Zampieri · A. J. Zattera
Post-Graduation Program in Process and Technology Engineering, Universidade de Caxias do Sul, Francisco Getúlio Vargas Street, 1130, Bloco V - Room 408B, Bairro Petrópolis, Caxias do Sul, RS, Brazil

Published online: 28 August 2019

insulation remains a vital tool for optimizing the energy behavior of buildings (Papadopoulos and Giama 2007).

Materials, or fluids, of low thermal conductivity are considered thermally insulating, that is, they offer resistance to heat transfer between the system and the medium. In civil construction, they are used to prevent internal heat from spreading to the external environment. In this way, synthetic materials such as polyurethane (PU) and expanded polystyrene (EPS) are used on a large scale. The insulation capacity of a material is measured according to the thermal conductivity, that is, the lower the thermal conductivity, the greater the insulation capacity (Silva 2013).

In order to minimize the energy consumption of a building, by means of thermal protection, conductivity values of insulation materials (values less than 0.04 W m^{-1} K^{-1}) are in constant development. Among the most used categories of insulation materials are inorganic fibers (glass wool and rock wool) and organic foams (expanded polystyrene and polyurethane foams). These materials have a high performance in heat transfer resistance. However, their use causes some adversities such as: emission of greenhouse gases during their production, release of toxic gases when vaporized and high flammability (Cetiner and Shea 2018; Papadopoulos and Giama 2007; Silva 2013). Thus, the research and development of more sustainable and minimally processed insulators, such as aerogels, become fundamental.

Aerogels (porous solids) are considered very interesting materials for thermal insulation purposes because they present a high performance as a result of their extremely low thermal conductivity. In addition, they are characterized by their highly porous structure, reduced solids content and highly specific surface area. These properties make aerogels suitable for thermal insulation applications, electrodes in supercapacitors, advanced catalyst carriers and adsorbents (Du et al. 2013; Lei et al. 2018).

In recent years, the development of aerogels produced from different allotropic forms of carbon, such as graphene and nanotubes, attracted attention because of their superior properties, such as electrical and thermal conductivity, low density and mechanical strength. However, the high cost and toxicity of precursors added to the difficult and expensive technologies they require, as well as the equipment involved in the preparation, hinder their large-scale production (Hu et al. 2014; Lei et al. 2018).

Several authors present research on the development of cellulose aerogels and allotropic carbon forms, such as graphene oxide (Ge et al. 2018; Mi et al. 2018; Wan and Li 2016) and carbon nanotubes (Cong et al. 2018; Hwang et al. 2018) (as carbon source) for different applications, including thermal insulation. The results found in these studies show that the addition of these carbon structures to the cellulose aerogels does not present changes in the thermal conductivity of the same. The thermal conductivity of the cellulose aerogels (CMC)/graphene oxide (GO) remained around 0.04 W m^{-1} K^{-1} with the addition of 5% GO to the mass of CMC used (Ge et al. 2018). And for polyglycolic alcohol (PVA) aerogels, cellulose nanofibers (CNFs) and graphene oxide nanoparticles (GONSs) the thermal conductivity was 0.045 W m^{-1} K^{-1}.

Furthermore, according to the studies carried out by the aforementioned authors, the addition of carbon structures in cellulose aerogels improves the mechanical properties of the material, where the compression modulus and the resistance are larger proportionally with the increase of the carbonaceous particles content, which can be attributed to the well-defined crystalline structure of these materials (Ge et al. 2018; Zheng et al. 2013).

With an environment of harnessing industrial and agricultural waste for the production of new thermal insulators has also been much studied. The use of organic precursors subjected to the pyrolysis process, which thermally decomposes the biomass structure, produces carbonaceous solid waste (biochar) and condensable and non-condensable vapors. This biochar is highly carbonous and therefore has a high energy value. In addition, it is an added-value product that can be used for many purposes (Basu 2010; Lee et al. 2013; Skouteris et al. 2015). Cellulose is not only a qualified raw material for the preparation of carbon materials and is attractive due to its low cost, viability, abundance and non-toxicity, but also a renewable resource (Bakierska et al. 2014; Chang et al. 2010; Dunnigan et al. 2018; Han et al. 2016; Lazzari et al. 2018).

Cellulose aerogels, being produced from renewable sources (plants, wood, algae and animals), can be considered environmentally friendly and can reduce the manufacturing cost due to the low cost of the raw

material. The low density of cellulose fibers provides cellulose aerogels with high porosity and high surface area, as well as high mechanical strength due to the three-dimensional structure formed by cellulose fibers (Feng et al. 2015; Xiao et al. 2015; Innerlohinger et al. 2006).

Within this context, cellulose/biochar aerogels were produced aiming at their use thermal insulators. *Pinus elliottii* pulp was used as raw material for the production of aerogel and also for biochar, making it possible to add a high value to this biomass allied to a low processing cost. The thermal, chemical and morphological properties of the aerogels were studied in order to evaluate their use as thermal insulators.

Materials and methods

Materials

The cellulose used in the present work was supplied by the company Trombini (Brazil). The type of cellulose used was the unbleached long fiber of *Pinus elliottii*. Cellulose was further characterized as to its composition, chemical, physical, thermal and morphological properties.

Obtaining the *Pinus elliottii* cellulose biochar

Initially the cellulose was comminuted in a knife mill (10 mm size) and dried in an oven at 105 °C for 24 h, so that pyrolysis could be performed in a bench reactor, which operates in a batch system. A detailed description of this equipment was recently reported by Perondi et al. (2017). The parameters used in the pyrolysis were: heating rate of 5 °C min^{-1}, final operating temperature of 800 °C and N_2 flow of 150 mL min^{-1}. The cellulose mass used in the feed was approximately 35 g. The biochar was obtained after the cooling stage of the reactor. Due to differences in the size of the resulting particles, maceration was conducted, resulting in homogenous particles.

Obtaining the cellulose/biochar aerogels

The cellulose/biochar aerogels were produced according to the methodology presented by Lazzari et al. (2017). Initially, *Pinus elliottii* cellulose was milled in a knife mill. Thereafter, a suspension was produced with distilled water and cellulose in the concentration of 1.5% (w/w). This suspension was later placed in a Masuko Sangyo stone micronizer, model MKCA6-2J (Japan) for the fiber milling for 5 h (Neves et al. 2019). The aerogels were produced from the actual cellulose concentration (1.43 and 0.715% w/w) and biochar (0.5, 10, 20, 40, 80 and 100% w/w, relative to the cellulose mass). In the following step, the cellulose suspension was centrifuged for 5 min at 4500 rpm. To the supernatant, a certain concentration of biochar was added and maintained on mechanical agitation for 5 min for homogenization of the mixture. Thereafter, the supernatant was mixed to the pellet, also by mechanical agitation and for 5 min. The suspension obtained after the milling process was sonicated for 30 min in a Sonics Sonifier Model VC505 Sonifier, with an amplitude of 50% measured in relation to the maximum equipment capacity (500 W). Then, metal molds were used to condition the samples. These molds have the following dimensions: 5 cm (side) × 2.5 cm (thickness). The samples (packaged in the molds) were then frozen in a Panasonic MDF PRO Series freezer at a temperature of − 80 °C for 24 h. Freeze drying was carried out in a Lio Top lyophilizer, Model L101 (Brazil). The samples were placed in a chamber and subjected to vacuum at a temperature of − 40 °C for about 70 h for the sublimation of the ice and drying of the aerogel.

Characterization of the aerogels

The bulk density of the aerogels was measured according to ASTM D1622-08, and calculated according to Eq. 1.

$$\rho_{aerogel} = \frac{m}{v} \tag{1}$$

in which $\rho_{aerogel}$ is the apparent density of aerogel (g cm^{-3}); m is the mass of the aerogel (g) and v is the volume of the aerogel (cm^3).

The porosity of the aerogels was determined by a method presented by Sehaqui et al. (2011), by using Eq. 2.

$$\text{Porosity}\,(\%) = \left(1 - \frac{\rho_{aerogel}}{\rho_{cellulose}}\right) \times 100 \tag{2}$$

in which $\rho_{aerogel}$ is the apparent density of aerogel (g cm^{-3}) and $\rho_{cellulose}$ is the apparent density of cellulose (0.39 g cm^{-3}).

The thermal properties of the aerogels were evaluated by thermogravimetry (TG) using a Shimadzu model, TGA-50, with a heating rate of 10 °C min^{-1}, from 30 to 800 °C, under a nitrogen atmosphere (N_2) with a flux of 50 mL min^{-1}.

Thermal conductivity of aerogels

The thermal conductivity of the aerogels was determined according to the norm NBR 15220-5 (2003). Samples with the following dimensions were used: 50 × 50 × 20 mm width, length and thickness, respectively, in duplicate. The heat flux applied to the system was determined by measurements with PSI-20 glass wool (density 0.020 g cm^{-3}), which is known for its thermal conductivity (0.038 W m^{-1} K^{-1}). The glass wool was supplied by Tecnotermo Isolantes Térmicos (Brazil). The thermal conductivity of the samples was determined by Eq. 3.

$$\lambda = \frac{q \times e}{\Delta t} \tag{3}$$

in which λ is the thermal conductivity (W m^{-1} K^{-1}); q is the heat flux density (W m^{-2}); e is the thickness of the sample (m) and Δt is the temperature difference between the hot and the cold faces of the sample (K).

Compressive strength of aerogels

The compressive strength tests were performed in a universal testing machine (EMIC, model DL 2000, Brazil), with a compression speed of 1.3 mm min^{-1}. The assay was performed in duplicate, the samples were 5 cm (side) × 2.5 cm (thickness). They were used to measure the tension required to reduce the thickness of the specimen in 20, 50 and 70% of their initial thickness, and were adapted from ASTM D695-15.

Results and discussion

Cellulose aerogels

The cellulose suspension was produced from a mixture with 1.5% (w/w) cellulose. However, the actual concentration of cellulose after the milling process was 1.43 ± 0.02%. This decrease occurred due to the losses in the walls of the mill. Therefore, the cellulose concentration of the AC-1 and AC-2 aerogels was 1.43 ± 0.02% and 0.715 ± 0.02%, respectively (as reported in Table 1).

Table 1 presents the results of apparent density and calculated porosity of AC-1 and AC-2 aerogels. Density values between 0.010 and 0.019 g cm^{-3} and porosity between 97.3 and 95.1% were results found for samples AC-1 and AC-2, respectively. It is possible to verify that the apparent density is proportional to the cellulose concentration used, since the AC-1 aerogel had an apparent density about 50% higher than the aerogels AC-2.

The porosity is inversely proportional to the apparent density, that is, the greater the apparent density of the aerogel, the smaller its porosity. The aerogel that presented greater porosity was AC-2, at about 97%. This result, is due to the lower concentration of fibers present in it.

The process of mechanical grinding of cellulose promotes defibrillation and breaking of fibers from the micrometric scale to the nanometric. Besides, it more economical and beneficial to the environment as no chemical reagents are used. Figure 1 shows the micrographs of cellulose and cellulose/biochar aerogels.

In the observed structure of the cellulose aerogels in Fig. 1b, d, it is possible to notice that the fibers remain long, with length in the micrometric and agglomerated. On the other hand, the thickness of the fibers decreased, presenting several fibers with thickness in nanoscale. In addition, due to the hydrophilic nature of the cellulose, the fibers agglomerate when in suspension. Thus, even after drying the aerogels, there is the formation of extended "sheets" forming macroscopic open channels and large pores with several micrometers wide, which connect the different cells and thin sheets of aerogel (Aulin et al. 2010).

Rapid freezing is known to be accompanied by the formation of amorphous ice which, in turn, can lead to a more homogeneous fibrillar aerogel structure with smaller pores and less pronounced structure. In contrast, slow freezing increases the formation of non-amorphous ice (crystals) which contributes to the formation of "sheets". The structure of aerogel is therefore directly related to the size and distribution of ice crystals in the frozen system. In addition, the thickness of the aerogels plays an important role in the

Table 1 Nomenclature, composition, density and porosity of cellulose/biochar aerogels

Nomenclature	Cellulose concentration (% w/w)	Biochar concentration[a] (% w/w)	Apparent density (g cm^{-3})	Porosity (%)
AC-1	1.43 ± 0.02	0.0	0.019 ± 0.0005	95.15 ± 0.12
AC-1.B5	1.43 ± 0.02	5.0	0.021 ± 0.0005	94.55 ± 0.12
AC-1.B10	1.43 ± 0.02	10.0	0.025 ± 0.001	93.67 ± 0.21
AC-1.B20	1.43 ± 0.02	20.0	0.024 ± 0.001	93.93 ± 0.13
AC-1.B40	1.43 ± 0.02	40.0	0.022 ± 0.001	94.31 ± 0.15
AC-1.B80	1.43 ± 0.02	80.0	0.026 ± 0.001	93.31 ± 0.20
AC-1.B100	1.43 ± 0.02	100.0	0.027 ± 0.001	93.10 ± 0.17
AC-2	0.715 ± 0.02	0.0	0.010 ± 0.0002	97.35 ± 0.06

[a]The biochar concentration was a function of the cellulose concentration

freezing rate. Therefore, thicker samples freeze more slowly (Aulin et al. 2010).

Figure 2a shows the thermogravimetry of the *Pinus elliottii* cellulose sample and the AC-1 and AC-2 aerogels. The cellulose aerogels showed a mass loss below 100 °C, due to the presence of moisture in the samples. In addition, the highest percentage of mass loss was observed between 250 and 450 °C, due to the degradation of the hemicelluloses, cellulose and a lower degradation of part of the lignin.

A difference is noted in T_{onset} (temperature at which sample degradation starts) and T_{max} (temperature at which the rate of degradation is maximal), as shown in Table 2. These temperatures of the cellulose aerogels decreased in relation to the *Pinus elliottii* cellulose fiber, probably due to the increase of the specific surface area obtained after the mechanical process, which facilitates the degradation process when compared to the original material, and contributes to thermal stability decrease (Zanini et al. 2017). The residual mass of the aerogels had a slight decrease compared to the original cellulose.

Gupta et al. (2018) obtained an increase in the thermal stability of the aerogels due to the presence of fibers on the nanometer scale in their cellulose aerogels. However, they performed a chemical treatment before the mechanical milling on the fibers for the removal of lignin, hemicellulose and pectin. This treatment increased the initial degradation temperature to about 80 °C.

Figure 3a shows the stress × strain curves and the compressive strength of aerogels AC-1, AC-1.B40 and AC-2.

The stress × strain curves presented in Fig. 3a present different stages according to the slope of the curve: a linear stage with a fixed slope of the curve, a long regime of elastic–plastic deformation, and a stage in which the compression stress increases significantly due to the gradual densification of the porous structure. This behavior was also observed for silica aerogels reinforced with glass fibers (Li et al. 2017) and cellulose nanofibers aerogels (Jiménez-Saelices et al. 2017).

The AC-1 aerogel has a compressive strength about 35% higher than the AC-2 aerogel, for deformation of 70%. According to Jiménez-Saelices et al. (2017) the apparent density (from 0.010 to 0.019 g cm^{-3} of aerogels AC-2 and AC-1, respectively) causes an increase in pore wall thickness, causing a greater resistance of the structure to curvature and collapse of the wall cells.

The statistical analysis was performed for the deformation of 70% of the specimen, as shown in Table S.2 (complementary information). Between AC-1 and AC-2 (identified by 2 different letters in Fig. 3b) there is a significant difference in compressive strength. Therefore, the cellulose concentration impacts significantly, that is, the amount of cellulose used influences the compressive strength of the cellulose aerogels for a 70% deformation of the sample.

Figure 4 shows the thermal conductivity of the cellulose/biochar aerogels. The AC-1 and AC-2 cellulose aerogels presented thermal conductivity of 0.024 and 0.021 W m^{-1} K^{-1}, respectively.

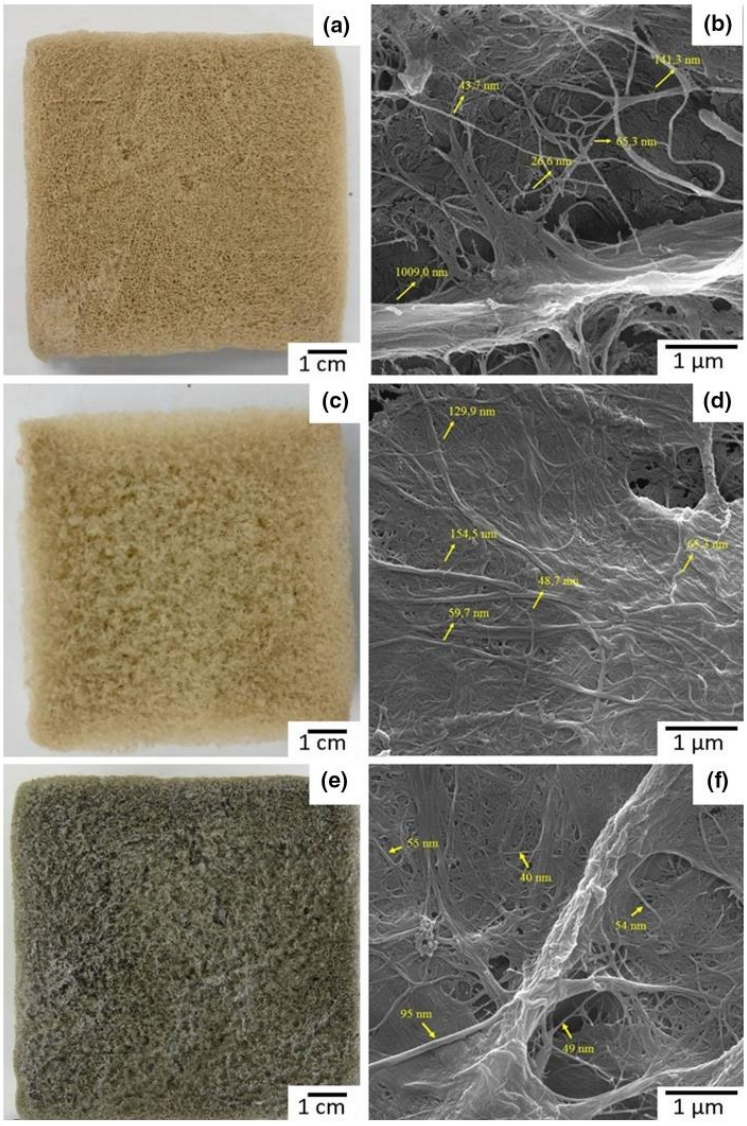

Fig. 1 Photos of aerogels: AC-1 (**a**); AC-2 (**c**) and AC-1.B40 (**e**). Micrographs of aerogels: AC-1 (**b**), AC-2 (**d**) and AC-1.B40 (**f**)

According to the statistical analysis presented in item S.5 (complementary information) and multiple comparison of means (Table S.3), we concluded that the concentration of cellulose does not cause significant difference, i.e. the amount of cellulose used does not influence the conductivity of the aerogels. This is because, as can be seen from Table 1, there is not a considerable difference in the porosity of aerogel, about 2% only.

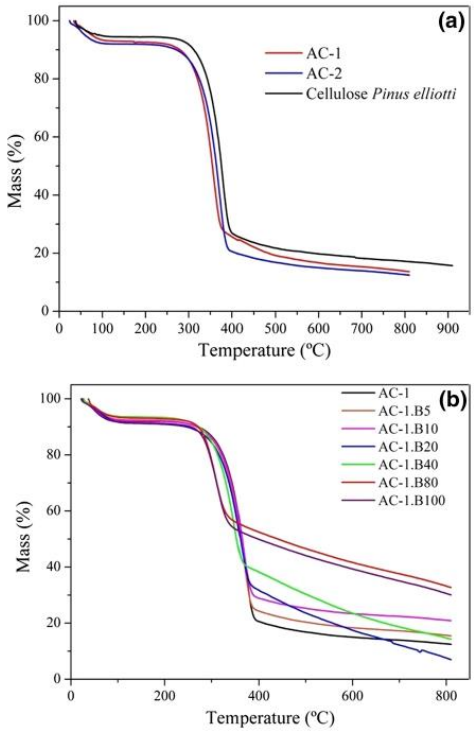

Fig. 2 Thermogravimetry of *Pinus elliottii* fiber and aerogels of **a** cellulose and **b** cellulose/biochar

The high porosity of the aerogels (more than 95% of the aerogel structure is composed by air) provides them with a thermal conductivity inferior to the thermal conductivity of the air (0.026 W m^{-1} K^{-1}) (Incropera et al. 2007).

Karadagli et al. (2015) used cellulose fibers to produce aerogels by extrusion. The authors evaluated the influence of fiber concentration (0.5–6 % w/w) on bulk density (0.009 and 0.137 g cm^{-3}), porosity (99 and 91%), compressive strength ($\sim$ 0.3 to 1.5 MPa, for deformation of 50% of the specimen) and thermal conductivity (0.04 and 0.075 W m^{-1} K^{-1}). The results found by the authors showed the same behavior found in the present study for density and porosity. However, for the thermal conductivity, the authors found values superior to those found in the present study, which shows that AC-1 and AC-2 present a better thermal insulation than others aerogels. Regarding the compressive strength, the authors found extremely high values when compared with the aerogels of the present study.

By means of statistical analysis, we found that the cellulose concentration significantly influenced the compressive strength of the aerogels, because there is an increase in the fraction of solids present in AC-1 aerogel compared to AC-2 aerogel. On the other hand, in the thermal conductivity test, the cellulose concentration did not present significant influence. Considering these tests as the main results for the determination of the cellulose concentration for the production of the aerogels, it was decided to choose sample AC-1, with cellulose concentration of 1.43% for the continuation of this research, mainly due to its compressive strength being superior to the sample AC-2, since the thermal conductivity is not influenced by cellulose concentration.

Cellulose/biochar aerogels

Figure 5 shows the cellulose/biochar aerogels produced with different concentrations of biochar,

Table 2 Results of the analysis of thermogravimetry of the *Pinus elliottii* cellulose fiber, cellulose aerogels and cellulose/biochar aerogels

Sample	T_{onset} (°C)	$T_{máx}$ (°C)	Residual mass (%)
Pinus elliottii cellulose	342	382	15.80
AC-1	333	372	12.50
AC-1.B5	316	370	15.80
AC-1.B10	323	368	20.98
AC-1.B20	315	360	5.14
AC-1.B40	297	349	14.38
AC-1.B80	276	313	32.83
AC-1.B100	272	315	30.08
AC-2	315	358	13.70

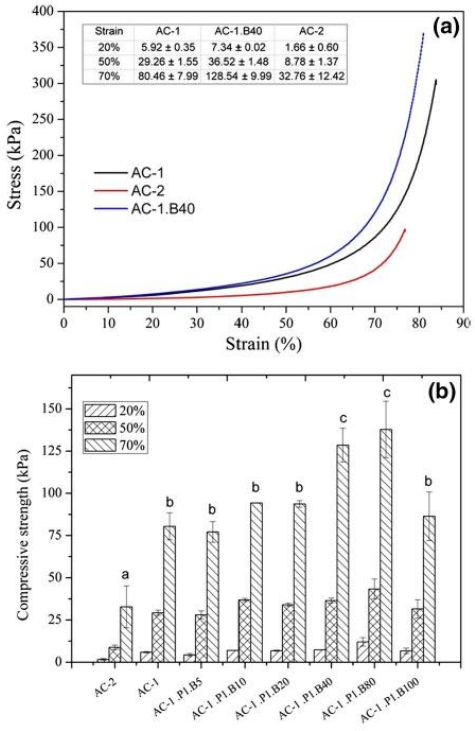

Fig. 3 **a** Stress × strain curves and **b** Compressive strength of *Pinus elliottii* AC-1 and AC-2 cellulose aerogels with deformation of 20, 50 and 70% of the specimen. *Note*: Different letters indicate the significant difference between groups

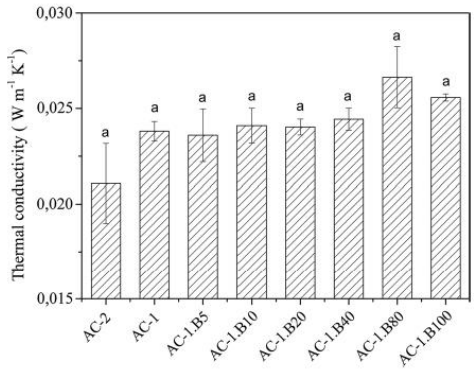

Fig. 4 Thermal conductivity of cellulose and cellulose/biochar aerogels

according to the nomenclature presented in Table 1. Due to the increase of the concentration of biochar in the cellulose aerogel, its coloration changes gradually into a dark gray tone. The aerogels have a uniform coloration, showing that the mixture of the biochar in the cellulose suspension was homogeneous. In addition, the three-dimensional structure of aerogels is composed of pores of different sizes. However, by adding the biochar, the pore size reduces, due to the higher amount of solids in the cellulose/biochar suspension.

Table 1 shows the bulk density and porosity of the cellulose/biochar aerogels. With the addition of the biochar to the cellulose suspension, the calculated value of the apparent density of the aerogels presents a slight increase, from 0.0189 to 0.0269 (higher value found for aerogel AC-1.B100). As the porosity is inversely proportional to the bulk density, the porosity decreased from 95.15 to 93.10% for aerogels AC-1 and AC-1.B100, respectively.

Yang et al. (2016) also observed this behavior in their aerogels of microcrystalline cellulose and graphene nanoplatelets, having a two fold increase in density for aerogel with cellulose/nanoplatelet concentration of 1:1 compared to microcrystalline cellulose aerogel. Consequently, there was a decrease in porosity of about 5% between these same aerogels.

Figure 1e, f present the image and micrograph, respectively, of aerogel AC-1.B40, in order to compare the micrographs of this aerogel with AC-1 and AC-2 aerogels. The structure of the aerogel was not altered with the addition of the biochar, remaining with long and very agglomerated fibers. The fact that biochar is produced from cellulose itself hinders its identification, and through them it can be noticed that there was homogenization of the biochar to the cellulose suspension.

Several authors report that the addition of graphene oxide (GO), a carbonaceous structure such as biochar, in cellulose aerogels provides changes in the structure of aerogels, for example, the porous structure becomes more heterogeneous, the interaction and entanglement of the GO and cellulose form denser networks, the porous structure of the wall is replaced by a lamellar structure, among others (Ren et al. 2018; Wan and Li 2016; Xiang et al. 2019).

Figure 2b shows the thermogravimetry of the cellulose/biochar aerogels, where it can be observed that the addition of the biochar, even in homogeneity

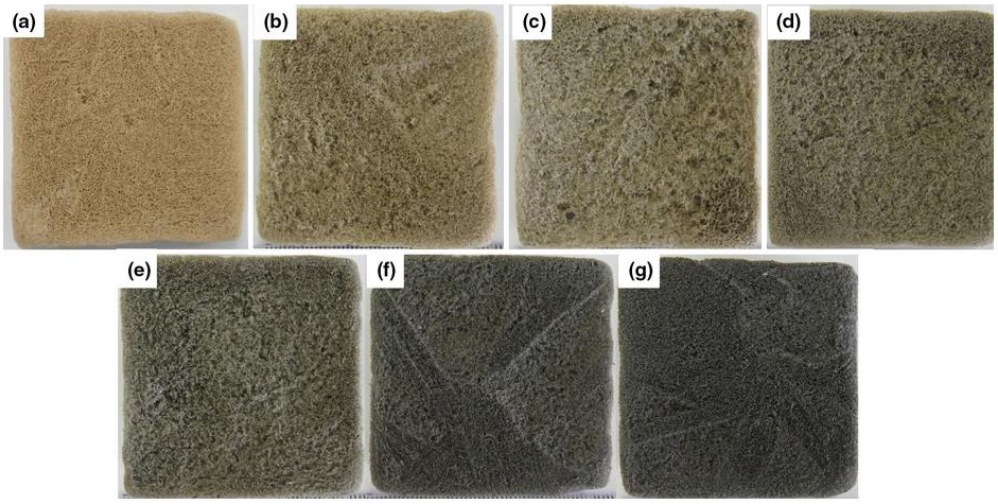

Fig. 5 Cellulose/biochar aerogels: **a** AC-1, **b** AC-1. B5, **c** AC-1.B10, **d** AC-1.B20, **e** AC-1.B40, **f** AC-1.B80 and **g** AC-1.B100

with the cellulose suspension and having already had its organic matter degraded, decreased the thermal stability of the aerogels.

The presence of the biochar in the aerogels causes the decrease of the T_{onset} and T_{max} temperatures (obtained by thermogravimetry derived from the curves), as can be seen in Table 2. However, its presence increases the residual mass, due to the submission of the raw material to the pyrolysis process, before the production of the aerogel, during which the organic matter was degraded.

In a study carried out by Wan and Li (2016) the authors also noted this behavior among their samples, where T_{onset} decreased from 363 to 353 °C in the aerogels of bamboo fiber cellulose and the aerogel with 5% of graphene oxide (GO), respectively. Furthermore, the authors reported that there is no mass loss related to the decomposition of the oxygen receptor groups on the surface of the GO due to deoxygenation and low proportion of the same in the aerogels.

Figure 3a shows the stress–strain curves of aerogels AC-1 and AC-1.B40. Curves exhibit foam-like deformation behavior. The aerogels suffered a plastic deformation, a deformation of 0–70%, irreversibly. After this region, due to the densely compressed structure, the aerogels become resistant, and therefore the tension increases rapidly. Ge et al. (2018) observed the same behavior for their GO/CMC aerogels, but in the deformation range of 0–7%, there was an elastic deformation. The authors obtained a 62% increase in compressive strength with the addition of 5% graphene oxide in CMC aerogels.

Figure 3b shows the compressive strength of the cellulose/biochar aerogels for deformations of 20, 50 and 70% of the sample. In all evaluated deformation, the behavior is the same, presenting a slight tendency to increase until the concentration of 80% of biochar in cellulose mass and, subsequently, a considerable decrease of resistance takes place, of about 60%. For deformation of 70% of the specimen, there was an increase from 80 to 128 kPa (aerogels AC-1 and AC-1.B40, respectively), about 60% greater.

Due to the high standard deviation associated with some aerogels, a statistical analysis was presented in Table S.2 (complementary information) and multiple comparison of means presented in Table S.3 (complementary information). From the results, we concluded that the compressive strength of the cellulose/biochar aerogels presents a significant difference, that is, the amount of biochar used influences the compressive strength between some cellulose1/biochar aerogels for deformation of 50% of the sample (see association of letters).

Considering that the aerogels AC-1.B40 and AC-1.B80 had the highest resistance values (128 and

137 kPa, respectively), and that between the two there is no significant difference (both are identified with the letter "*c*"), it can be considered that with the addition of 40% of biochar in relation to the mass of cellulose one obtains the greatest resistance to the compression of the aerogels.

Mi et al. (2018) obtained the greatest compressive strength in their study with the increase of graphene oxide in the aerogels of cellulose nanofibers, and attributed this improvement to the stiffness of the graphene sheets. Ge et al. (2018) compared the compressive strength of aerogels of carboxymethyl cellulose and cellulose/graphene oxide nanosheets (GOS), and with the addition of 5.0% of GOS, the compressive strength reached 349 kPa, which were 1.6 times that of CMC aerogels. This increase is attributed to the good dispersion of GOS in the cellulose suspension and the strong interfacial adhesion to the matrix.

Figure 6 shows the aerogels AC-1 and AC-1.B40 during the compression test. It is possible to verify that the aerogel has a rigid structure, because after the aerogel load is removed, it does not return to its original state, having a plastic deformation known as permanent deformation. At the end of the trial, the aerogels were reduced by about 80% of their original height.

Figure 4 shows the thermal conductivity of the cellulose/biochar aerogels. The values found ranged from 0.024 to 0.027 W m^{-1} K^{-1}, the first being found for AC-1 and the second for AC-1.B80. Due to the small difference found, a statistical analysis of the results was performed, as presented in Table S.5 (complementary information). The conductivity of the aerogels did not present significant difference, that is, the addition of the biochar did not influence in the thermal conductivity of the aerogels.

Considering that the thermal conductivity of aerogels is determined mainly by the thermal conductivity factor of the solid material, density and pore size, and since having a significant, yet very small, difference in density and porosity of the aerogels, the absence of significant differences in the thermal conductivity of non-aerogels is justified (Wiener et al. 2006).

According to Wiener et al. (2006), the transport of heat through a porous solid, consists of radioactive, gaseous and solid contributions. Therefore, the change in thermal conductivity is due to changes in the solid phase of the material. In the aerogels produced in the present study, there were no changes in structure due to the addition of the biochar, as shown in Fig. 1. The influence that the biochars caused in the aerogels was the increase of the apparent density and the decrease of the porosity, which resulted in an increase in

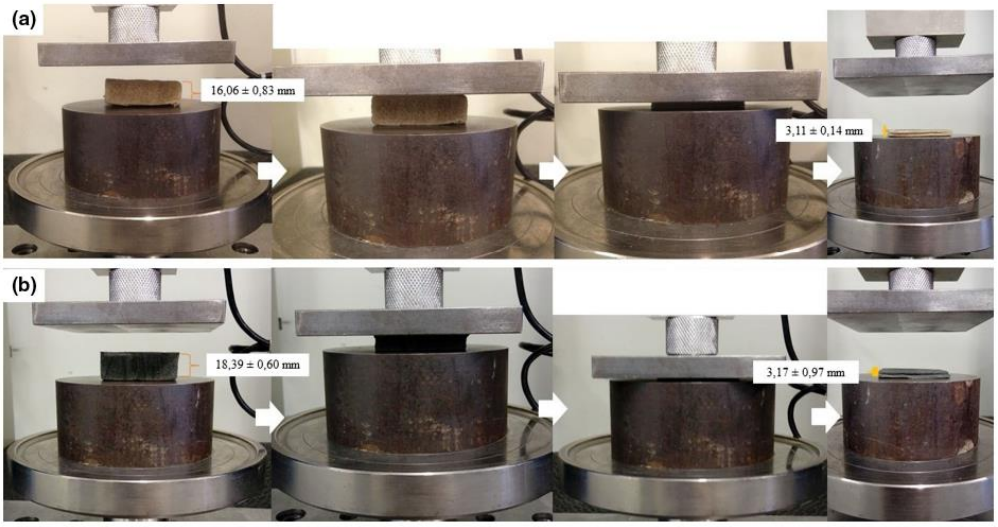

Fig. 6 Images of the compression test of cellulose/biochar aerogels. **a** AC-1 and **b** AC-1.P1.B40

Table 3 Thermal conductivity of thermal insulators materials

Sample	Thermal conductivity (W m^{-1} K^{-1})	Reference
AC-1.B40	0.024	–
Polyurethane foam	0.02–0.03	Zhang et al. (2017)
CMC/GO aerogels	0.04	Ge et al. (2018)
Silica aerogel	0.0338	Zhao et al. (2018)
Recycled cellulose aerogel	0.032	Nguyen et al. (2014)
Expanded polystyrene	0.04	Silva (2013)
Cellulose nanofiber aerogel	0.018–0.028	Jiménez-Saelices et al. (2017)
Silica cellulose aerogel	0.0236	Fu et al. (2016)
Wood waste	0.048–0.055	Cetiner and Shea (2018)

conductivity, but not enough to show significant differences between them.

Ge et al. (2018) developed aerogels of carboxymethylcellulose (CMC) and graphene oxide (GO) in a concentration of up to 5% mass of cellulose. When comparing cellulose aerogel with CMC/GO aerogels, both the thermal conductivity factor (between 0.038 and 0.042 W m^{-1} K^{-1}) and the density (between 24.3 and 25.5 kg m^{-3}) of the composite aerogel increased at a small rate after the addition of GO, so the solid-state thermal conductivity increased as well. Furthermore, in the absence of obvious changes in density and pore structure, the thermal conductivities of aerogels tended to increase slowly with increasing GO content. This is because the thermal conductivity factor of the aerogel increased with increasing GO content.

The thermal conductivity of the aerogels found in the present study, about 0.025 W m^{-1} K^{-1}, is comparable to the thermal conductivity of commercial materials such as polyurethane foams and expanded polystyrene and other thermal insulator aerogels, as noted in Table 3.

Conclusion

In relation to the cellulose concentration, the results obtained in the statistical analysis present in Supplementary Material were evaluated, and, the thermal conductivity and compressive strength tests were considered the main results for the determination of the cellulose concentration for the production two aerogels. These results were the basis for the choice of the aerogels AC-1, with a cellulose concentration of 1.43% for the continuation of the studies in the present study, mainly due to its compressive strength being superior to AC-2, given that the thermal conductivity is not influenced by the cellulose concentration.

The cellulose/biochar aerogels produced presented good characteristics to be used as thermal insulators. Although they had a heterogeneous structure, the porosity was high, higher than 95%, and the bulk density (about 0.025 g cm^{-3}) was close to that of materials such as glass wool, widely used in construction. The addition of biochar did not increase the thermal stability of aerogels as expected. On the contrary, the higher the concentration used the lower the maximum degradation temperature. On the other hand, the biochar had no influence on the thermal conductivity of the aerogels (about 0.025 W m^{-1} K^{-1}), which was close to that of the polyurethane foams (0.02–0.03 W m^{-1} K^{-1}). However, an increase in the compressive strength of the cellulose/biochar aerogels (AC-1.B40) of 60% in relation to the cellulose aerogel (AC-1) can be verified.

For these, they presented more thermal insulation than aerogels produced with carbon structures as precursors, in addition to having very close compressive strength to these aerogels. Finally, the cellulose/biochar aerogels are promising for the thermal insulation application proposed for the present work.

Acknowledgments The authors are grateful for the National Council for Scientific and Technological Development (CNPq)

and the Foundation for Research Support of the State of Rio Grande do Sul (FAPERGS).

References

Aulin C, Netrval J, Wagberg L, Lindstrom T (2010) Aerogels from nanofibrillated cellulose with tunable oleophobicity. Soft Matter 6(14):3298–3305

Bakierska M, Molenda M, Majda D, Dziembaj R (2014) Functional starch based carbon aerogels for energy applications. Procedia Eng 98:14–19

Basu P (2010) Biomass gasification and pyrolysis: practical design and theory. Academic Press, Burlington

Cetiner I, Shea AD (2018) Wood waste as an alternative thermal insulation for buildings. Energy Build 168:374–384

Chang X, Chen D, Jiao X (2010) Starch-derived carbon aerogels with high-performance for sorption of cationic dyes. Polymer 51(16):3801–3807

Cong L, Li X, Ma L, Peng Z, Yang C, Han P, Wang G, Li H, Song W, Song G (2018) High-performance graphene oxide/carbon nanotubes aerogel-polystyrene composites: preparation and mechanical properties. Mater Lett 214:190–193

Du A, Zhou B, Zhang Z, Shen J (2013) A special material or a new state of matter: a review and reconsideration of the aerogel. Materials 6(3):941–968

Dunnigan L, Ashman PJ, Zhang X, Kwong CW (2018) Production of biochar from rice husk: particulate emissions from the combustion of raw pyrolysis volatiles. J Clean Prod 172:1639–1645

EPE (2018) Anuário estatístico de energia elétrica 2018. Empresa de pesquisa energética. http://www.epe.gov.br/en/publicacoes-dados-abertos/publicacoes/anuario-estatistico-de-energia-electrica. Accessed 25 Apr 2019

Feng J, Nguyen ST, Fan Z, Duong HM (2015) Advanced fabrication and oil absorption properties of super-hydrophobic recycled cellulose aerogels. Chem Eng J 270:168–175

Fu J, Wang S, He C, Lu Z, Huang J, Chen Z (2016) Facilitated fabrication of high strength silica aerogels using cellulose nanofibrils as scaffold. Carbohydr Polym 147:89–96

Ge X, Shan Y, Wu L, Um X, Peng H, Jiang Y (2018) High-strength and morphology-controlled aerogel based on carboxymethyl cellulose and graphene oxide. Carbohydr Polym 197(June):277–283

Gupta P, Singh B, Agrawal AK, Maji PK (2018) Low density and high strength nanofibrillated cellulose aerogel for thermal insulation application. Mater Des 158:224–236

Han S, Sun Q, Zheng H, Li J, Jin C (2016) Green and facile fabrication of carbon aerogels from cellulose-based waste newspaper for solving organic pollution. Carbohydr Polym 136:95–100

Hu H, Zhao Z, Wan W, Gogotsi Y, Qiu J (2014) Polymer/graphene hybrid aerogel with high compressibility, conductivity, and "sticky" superhydrophobicity. ACS Appl Mater Interfaces 6:3242–3249

Hwang HC, Woo JS, Park SY (2018) Flexible carbonized cellulose/single-walled carbon nanotube films with high conductivity. Carbohydr Polym 196:168–175

IEA (2019) Energy Efficiency Indicators Database. International Energy Agency. https://www.iea.org/statistics/efficiency/. Accessed 25 Apr 2019

Incropera FP, Dewitt DP, Bergman TL, Lavine AS (2007) Fundamentos de transferência de calor e massa. Wiley, New York

Innerlohinger J, Weber HK, Kraft G (2006) Aerocellulose: aerogels and aerogel-like materials made from cellulose. Macromol Symp 244:126–135

Jiménez-Saelices C, Seantier B, Cathala B, Grohens Y (2017) Spray freeze-dried nanofibrillated cellulose aerogels with thermal superinsulating properties. Carbohydr Polym 157:105–113

Karadagli I, Schulz B, Schestakow M, Milow B, Gries T, Ratke L (2015) The Journal of Supercritical Fluids Production of porous cellulose aerogel fibers by an extrusion process. J Supercrit Fluids 106:105–114

Lazzari LK, Zampieri VB, Zanini M, Zattera AJ, Baldasso C (2017) Sorption capacity of hydrophobic cellulose cryogels silanized by two different methods. Cellulose 24(8):3421–3431

Lazzari E, Schena T, Marcelo MCA, Primaz CT, Silva AN, Ferrao MF, Bjerk T, Caramao EB (2018) Classification of biomass through their pyrolytic bio-oil composition using FTIR and PCA analysis. Ind Crops Prod 111(November 2017):856–864

Lee Y, Park J, Ryu C, Gang KS, Yang W, Park YK, Jung J, Hyun S (2013) Comparison of biochar properties from biomass residues produced by slow pyrolysis at 500°C. Bioresour Technol 148:196–201

Lei E, Li W, Ma C, Liu S (2018) An ultra-lightweight recyclable carbon aerogel from bleached softwood kraft pulp for efficient oil and organic absorption. Mater Chem Phys 214:291–296. https://doi.org/10.1016/j.matchemphys.2018.04.075

Li C, Cheng X, Li Z, Pan Y, Huang Y, Gong L (2017) Mechanical, thermal and flammability properties of glass fiber film/silica aerogel composites. J Non-Cryst Solids 457:52–59

Mi HY, Jing X, Politowicz AL, Chen E, Huang HX, Turng LS (2018) Highly compressible ultra-light anisotropic cellulose/graphene aerogel fabricated by bidirectional freeze drying for selective oil absorption. Carbon 132:199–209

Nguyen ST, Feng J, Ng SK, Wong JPW, Tan VBC, Duong HM (2014) Advanced thermal insulation and absorption properties of recycled cellulose aerogels. Colloids Surf A 445:128–134

Neves RM, Lopes KS, Zimmermann MGV, Polleto M, Zattera AJ (2019) Cellulose nanowhiskers extracted from Tempo-oxidized curaua fibers. J Nat Fibers. https://doi.org/10.1080/15440478.2019.1568346

Papadopoulos AM, Giama E (2007) Environmental performance evaluation of thermal insulation materials and its impact on the building. Build Environ 42(5):2178–2187

Perondi D, Poletto P, Restelatto D, Manera C, Silva JC, Junges J, Collazo GC, Dettmer A, Godinho M, Vilela ACF (2017) Steam gasification of poultry litter biochar for bio-syngas production. Process Saf Environ Prot 109:478–488

Ren F, Li Z, Tan WZ, Liu XH, Sun ZF, Ren PG, Yan DX (2018) Facile preparation of 3D regenerated cellulose/graphene

oxide composite aerogel with high-efficiency adsorption towards methylene blue. J Colloid Interface Sci 532:58–67

Sehaqui H, Zhou Q, Berglund LA (2011) High-porosity aerogels of high specific surface area prepared from nanofibrillated cellulose (NFC). Compos Sci Technol 71(13):1593–1599

Silva FMF (2013) Estudo de materiais de isolamento térmico inovadores. Universidade do Porto, Porto

Skouteris G, Saroj D, Melidis P, Hai FI, Ouki S (2015) The effect of activated carbon addition on membrane bioreactor processes for wastewater treatment and reclamation—a critical review. Bioresour Technol 185:399–410

Wan C, Li J (2016) Graphene oxide/cellulose aerogels nanocomposite: preparation, pyrolysis, and application for electromagnetic interference shielding. Carbohydr Polym 150:172–179

Wiener M, Reichenauer G, Hemberger F, Ebert HP (2006) Thermal conductivity of carbon aerogels as a function of pyrolysis temperature. Int J Thermophys 27(6):1826–1843

Xiang C, Wang C, Guo R, Lan J, Lin S, Jiang S, Lai X, Zhang Y, Xiao H (2019) Synthesis of carboxymethyl cellulose-reduced graphene oxide aerogel for efficient removal of organic liquids and dyes. J Mater Sci 54(2):1872–1883

Xiao S, Gao R, Lu Y, Li J, Sun Q (2015) Fabrication and characterization of nanofibrillated cellulose and its aerogels from natural pine needles. Carbohydr Polym 119:202–209

Yang J, Zhang E, Li X, Zhang Y, Qu J, Yu ZZ (2016) Cellulose/graphene aerogel supported phase change composites with high thermal conductivity and good shape stability for thermal energy storage. Carbon 98:50–57

Zanini M, Lavoratti A, Zimmermann MVG, Galiotto D, Matana F, Baldasso C, Zattera AJ (2017) Aerogel preparation from short cellulose nanofiber of the Eucalyptus species. J Cell Plast 53(5):503–512

Zhang H, Fang WH, Li YM, Tao WQ (2017) Experimental study of the thermal conductivity of polyurethane foams. Appl Therm Eng 115:528–538

Zhao Y, Li Y, Zhang R (2018) Silica aerogels having high flexibility and hydrophobicity prepared by sol–gel method. Ceram Int 44(17):21262–21268

Zheng Q, Javadi A, Sabo R, Cai Z, Gong S (2013) Polyvinyl alcohol (PVA)-cellulose nanofibril (CNF)-multiwalled carbon nanotube (MWCNT) hybrid organic aerogels with superior mechanical properties. RSC Adv 3(43):20816–20823

COMPLEMENTARY INFORMATION

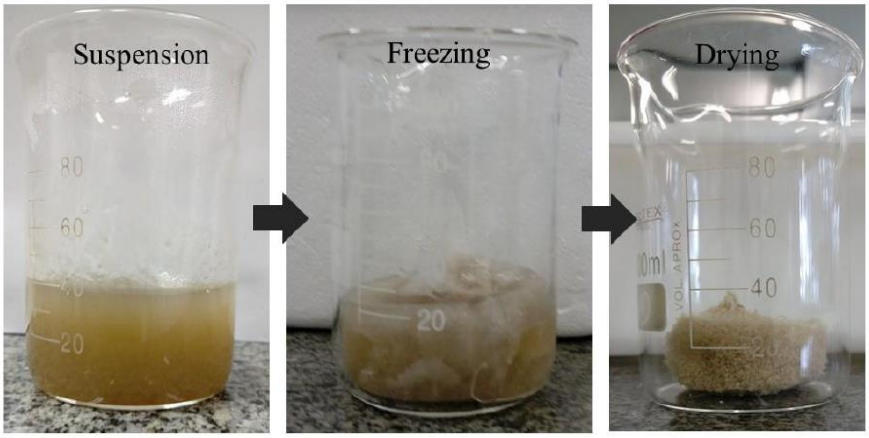

Figure S.1 - Stages of production of Pinus elliotti AC-2 cellulose aerogel.

STATISTICAL ANALYSIS

Statistical analyses of the results were performed using the one way analysis of variance function in Excel software. The concentration levels of cellulose and biochar were evaluated with n levels: two for the cellulose concentration (0.5 and 1.0 wt%) and seven for the biochar concentration (0.0, 5.0, 10.0; 20.0, 40.0, 80.0 and 100.0%). The ANOVA table was generated in the Excel software, based on it, the interaction between the groups was evaluated in order to verify if there were significant differences between the groups. From the data presented in the ANOVA table, it is possible to conclude the following: when "*p*" is lower than 0.05 (degree of reliability), there is a significant difference between the groups; when "*p*" is greater than 0.05 (degree of reliability), there is no significant difference between the groups.

In cases in which there was significant difference between the groups, a Multiple Comparison of Averages was performed to verify among which groups there is a significant difference. For this, the decision limit (Dl) was calculated and compared to the value of the means difference (Δm) of 2 groups: when Dl> Δm, there is a significant difference between the groups and when Dl <Δm, there is no difference between the groups. From the result,

letters were associated to each group to identify between which groups there was a significant difference.

Compressive strength

The values obtained in the compressive strength test of the cellulose aerogels for 70% deformation are presented in Table S.1.

Table S.1 - Compressive strength of the cellulose/biochar aerogels for 70% deformation.

	Aerogel							
	AC-2	**AC-1**	**AC-1.B5**	**AC-1.B10**	**AC-1.B20**	**AC-1.B40**	**AC-1.B80**	**AC-1.B100**
Strength compressive (kPa)	41.54	74.81	72.83	94.4	95.09	135.6	149.65	76.25
	23.98	86.11	81.44	94.3	92.34	121.5	125.99	96.56
Average	32.76	80.46	77.14	94.33	93.72	128.55	137.82	86.41
Standard deviation	8.78	5.65	4.305	0.065	1.375	7.05	11.83	10.155

With the data collected during the test and presented in Table S.1, the ANOVA table was generated in the Statistics software, presented in Table S.2.

Table S.2 – ANOVA table.

Effect	*SQ*	*gl*	*MQ*	*F*	*P value*	*F critical*
Var 1	14671	7	2096	19.85	0.000184	3.50
Error	844	8	106			
Total	15516	15				

Since the "P-value" is lower than 0.05 and "F" is higher than "Fcritical", there is a significant difference between the groups. Therefore the decision limit (Dl) of 21.79 was found and the multiple comparisons of means were done as shown in Table S.3.

Table S.3 Multiple comparison of averages.

Decision limit (Dl) = 21.79		
Aerogels	**Δm**	**Result**
AC-1/AC-2	47.70	Significant
AC-1/AC-1.B5	3.33	Not significant
AC-1/AC-1.B10	13.87	Not significant
AC-1/AC-1.B20	13.26	Not significant
AC-1/AC-1.B40	48.09	Significant
AC-1/AC-1.80	57.36	Significant
AC-1/AC-1.B100	5.94	Not significant
AC-1.B5/AC-1.B10	17.19	Not significant
AC-1.B5/AC-1.B20	16.58	Not significant
AC-1.B5/AC-1.B40	51.42	Significant
AC-1.B5/AC-1.B80	60.69	Significant
AC-1.B5/AC-1.B100	9.27	Not significant

AC-1.B10/AC-1.B20	0.61	Not significant
AC-1.B10/AC-1.B40	34.23	Significant
AC-1.B10/AC-1.B80	43.50	Significant
AC-1.B10/AC-1.B100	7.92	Not significant
AC-1.B20/AC-1.B40	34.84	Significant
AC-1.B20/AC-1.B80	44.11	Significant
AC-1.B20/AC-1.B100	7.31	Not significant
AC-1.B40/AC-1.B80	9.27	Not significant
AC-1.B40/AC-1.B100	42.15	Significant
AC-1.B80/AC-1.B100	51.42	Significant

Thermal Conductivity

The calculated values of the thermal conductivity (k) of the cellulose aerogels are presented in Table S.4.

Table S.4 – Thermal conductivity of cellulose aerogels.

	Aerogel							
	AC-2	**AC-1**	**AC-1.B5**	**AC-1.B10**	**AC-1.B20**	**AC-1.B40**	**AC-1.B80**	**AC-1.B100**
Thermal conductivity ($W\ m^{-1}\ K^{-1}$)	0.020	0.024	0.022	0.023	0.024	0.025	0.026	0.025
	0.023	0.023	0.025	0.025	0.024	0.024	0.028	0.026
Average	0.021	0.024	0.024	0.024	0.024	0.024	0.027	0.026
Standard deviation	0.001	0.001	0.001	0.001	0.000	0.000	0.001	0.000

With the data collected during the test and presented in Table S.4, the ANOVA table was generated in the Statistics software, presented in Table S.5.

Table S.5 – ANOVA table.

Effect	*SQ*	*gl*	*MQ*	*F*	*P-value*	*F critical*
Var 1	3.636E-05	7	5.19E-06	3.037	0.071	3.500
Error	1.368E-05	8	1.71E-06			
Total	5.004E-05	15				

Since the "P-value" is higher than 0.05 and "F" is lower than "Fcritical" there is no significant difference between the groups.

6 ARTIGO III

Lazzari, Lídia K.; Perondi, Daniele ; Zattera, Ademir J. ; Santana, Ruth M. C. . Cellulose/Biochar Cryogels: A Study of Adsorption Kinetics and Isotherms. Langmuir, v. 37, p. 3180-3188, 2021.

LANGMUIR

pubs.acs.org/Langmuir Article

Cellulose/Biochar Cryogels: A Study of Adsorption Kinetics and Isotherms

Lídia Kunz Lazzari,* Daniele Perondi, Ademir José Zattera, and Ruth Marlene Campomanes Santana

Cite This: *Langmuir* 2021, 37, 3180−3188 Read Online

ACCESS | Metrics & More | Article Recommendations | Supporting Information

ABSTRACT: The objective of this work was to characterize and study the behavior of the adsorption process of cellulose/biochar cryogels through isotherm models and adsorption kinetics. The cryogels were produced from a cellulose suspension obtained by mechanical fibrillation of 0.75 and 1.5% w/w unbleached long-fiber cellulose of the *Pinus elliotti* species. Into this suspension, 5, 10, and 20% w/w (relative to cellulose mass) biochar were added; then, the suspension was frozen and freeze-dried. After this, 2 mL of methyltrimethoxysilane (MTMS) was deposited on the cryogels. Characterization analyses were performed on the cryogels, including specific mass and porosity and sorption capacity, in addition to the study of adsorption kinetics and isotherms. The cryogels showed a porosity of above 90% and a specific gravity of less than 0.035 g cm^{-3}. The heterogeneous sorption capacity varied according to the concentration of cellulose used, and with the addition of 5% w/w biochar in the cellulose cryogel, the highest sorption capacity was obtained, 73 g g^{-1} of petroleum and 54 g g^{-1} of SAE20W50 oil. In the study of adsorption isotherms, the Freundlich model best fitted the process. Therefore, it was concluded that the process of petroleum adsorption by the cellulose cryogel occurs in multiple layers. In addition, the cellulose/biochar cryogel developed in the present work is suitable for use in the adsorption of organic liquids.

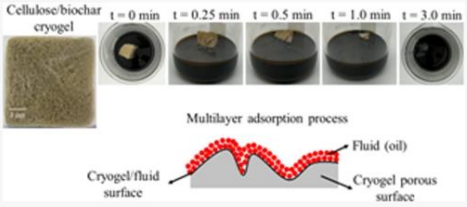

INTRODUCTION

Adsorption is a superficial phenomenon where a fluid of various components (gas or liquid) is attracted by an adsorbent surface of a solid forming physical or chemical bonds. It is recognized as an effective, promising, affordable, and widely used alternative for removing organic compounds in aqueous media.[1,2]

To obtain an ideal adsorption system, when exploring new adsorbent materials, it is essential to establish the most appropriate equilibrium ratio for the system. The way in which the pollutants interact with the adsorbent materials is described through the equilibrium relationships of the system (adsorption isotherms), being critical points for the optimization of the adsorption mechanism, expression of the properties, and surface capacities of the adsorbents, in addition to the effective planning of adsorption systems.[1]

In addition to the study of equilibrium, thermodynamic and kinetic aspects must be known to obtain more details of the mechanism and performance of the adsorption process. From the kinetic analysis, it is possible to determine the residence time necessary for the adsorbent to reach its maximum adsorption capacity and also to be able to scale the adsorption system.[2]

Thermodynamic parameters can indicate the spontaneity of the adsorption process, the affinity of the adsorbent for the adsorbate, the endothermic or exothermic nature, and whether physical or chemical adsorption and randomness in the solid/solution interface occur.[3]

Allotropic carbon structures such as graphene and carbon nanotubes have significant advantages over synthetic and natural adsorbent materials due to their high adsorption capacity and reusability. Nevertheless, the adsorbents used based on activated carbon and carbon nanotubes have high production costs and are difficult to recycle. In search of more accessible materials for such applications, biochar research has increased in recent years, due to the high cost of other adsorbents. According to Tan et al.,[4] the production of activated carbon needs higher temperatures and an additional activation process. Comparatively, the production of biochar is cheaper, with lower energy requirements.[5−9] Also, highly ordered structures of carbonaceous materials, providing high surface areas and malleable porosity, can be produced from different sources of biomass, including agricultural, forestry, and animal residues, among others.[10−12] In this way, the conversion of biomass into biochar as a sorbent is a "win−win"

Received: January 14, 2021
Revised: February 18, 2021
Published: March 5, 2021

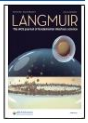

https://dx.doi.org/10.1021/acs.langmuir.1c00123
Langmuir 2021, 37, 3180−3188

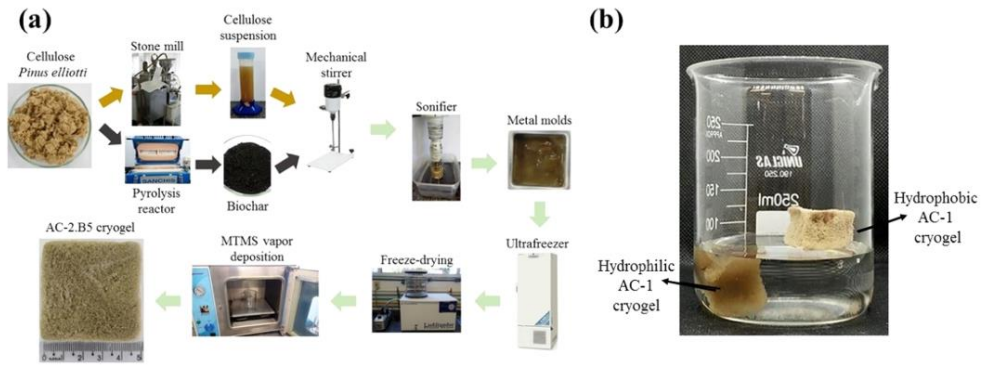

Figure 1. (a) Production flowchart for cryogels and (b) AC-1 cryogel before and after silanization.

solution both for improving waste management and protecting the environment.[5,6]

Biochar is a carbonaceous material, produced from the thermochemical conversion of biomass[13] in an inert environment of biomasses; it is commonly used and presents high efficiency in terms of product quality and yield.[14,15] Several studies report biochar as an excellent adsorbent for gases,[16] metal ions,[17] organic and inorganic liquids,[18,19] and dyes,[20] among others. In addition to being an interesting material for removing pollutants in water treatment,[17,21−23] this material is interesting for these applications due to its low cost, large surface area, microporosity, and adsorption capacity.[13] Because of its surface morphology, porous structure, specific surface area, and surface functionality, it can replace other carbon-based adsorbents such as graphene oxide and carbon nanotubes.[11]

Cryogels have three-dimensional network structures in which their micro/macropores are filled with air by freeze-drying. The production process of cryogels is similar to that of aerogels; the difference between them lies in the drying process. Initially, formation of a solution occurs in which particles are formed spontaneously or through catalysis yielding a colloidal suspension (sol) through the process of polycondensation/gelation forming a three-dimensional solid matrix. Finally, the liquid phase present in this gel is replaced by air without damaging the formed structure. In this last step, cryogels (freeze-drying) differ from aerogels (supercritical drying). Specifically, in freeze-drying, the gel is frozen and thus kept for a certain period so that ice crystals are formed. Then, the frozen suspension is freeze-dried so that sublimation of ice crystals occurs and pores are formed.[24,25] Several studies used the freeze-drying technique for the production of cryogels.[24,26−30] Their main applications are in the field of adsorption of dyes, petroleum, and solvents and also as thermal insulators due to their low thermal conductivity.[26]

In this context, cellulose/biochar cryogels were produced for the kinetic and isotherm study of the petroleum and motor petroleum sorption process. *Pinus elliotti* cellulose was used as a raw material for the production of cryogels and also biochar (a substitute for other carbon structures, such as graphene), thus making it possible to add a high value to the aforementioned biomass, an organic and abundant raw material in nature, combined with a low processing cost.

MATERIALS AND METHODS

Materials. Cellulose fibers from *P. elliotti* species were used and were supplied by the company Trombini (Fraiburgo—SC, Brazil). Petroleum (ρ = 0.891 g cm^{-3}) was supplied by Refinaria Alberto Pasqualini (Canoas—RS, Brazil), and SAE20W50 oil (ρ = 0.864 g cm^{-3}) was obtained from Ipiranga Petroquímica.

Biochar Production. Initially, the *P. elliotti* cellulose fibers were comminuted in a knife mill and dried in an oven at 105 °C for 24 h. Afterward, pyrolysis was performed in a bench reactor, which operates on a batch system. A detailed description of this reactor has been reported by Perondi et al.[31] It is a Sanchis brand furnace, which has an internally coupled reactor. Inert gas flow (N_2) is controlled by a flow meter (from 0 to 1 L min^{-1}). The reactor is electrically heated by two resistors, each with a power of 1900 W, with a maximum oven operating temperature of 1200 °C. Condensation of pyrolysis vapors was conducted according to CEN BT/TF 143 (adapted). The parameters used in the pyrolysis process were a heating rate of 5 °C min^{-1}, a holding time of 60 min, and a final operating temperature of 800 °C. The experiment was conducted in an inert environment with a N_2 flow of 150 mL min^{-1}.

Obtaining of Cellulose/Biochar Cryogels. Cellulose/biochar cryogels were produced according to the methodology presented in Lazzari et al.[27] Initially, the cellulose suspension was obtained by grinding the fibers in a stone mill (Masuko Sangyo, model MKCA6-2J) for 5 h at 2500 rpm in two different concentrations of fibers (1.5 and 0.75 wt %). This suspension was centrifuged for 5 min at 4500 rpm, and the biochar (in different concentrations of 5, 10, and 20% by weight of cellulose fibers) was added to the supernatant under mechanical agitation. Finally, the supernatant was mixed again with the precipitate and thus the cellulose/biochar suspension was obtained. The cellulose/biochar suspension was sonicated for 30 min, in a Sonics Model VC505 sonicator, with an amplitude of 50% measured in relation to the maximum equipment capacity (500 W). The suspension was then placed in metal molds, frozen at −80 °C, and lyophilized for approximately 72 h. After drying, silanization was carried out to make the cryogel hydrophobic (as shown in Figure 1). The cryogel was then suspended by a screen in a beaker containing 2 mL of methyltrimethoxysilane (MTMS) and isolated inside another beaker for 48 h in an oven at 70 °C.

Cryogel Characterization. The specific mass and porosity were determined from eqs 1[32] and 2,[33] respectively.

$$\rho_c = \frac{m_c}{v_c} \tag{1}$$

where ρ_c is the cryogel-specific mass (g cm^{-3}), m_c is the cryogel mass (g), and v_c is the cryogel volume (cm^3).

https://dx.doi.org/10.1021/acs.langmuir.1c00123
Langmuir 2021, 37, 3180−3188

$$P = \frac{\rho_c}{\rho_{cel}} \times 100 \quad (2)$$

where P is the porosity (%) and ρ_{cel} is the cellulose-specific mass (0.39 g cm^{-3}).

The pore size distribution was measured by the method of Barrett, Joyner, and Halenda (BJH) using the Quantachrome Instruments equipment (model 1200e), managing the nitrogen adsorption/desorption process at −196 °C. The samples were subjected to a degassing process conducted under a N_2 flow without vacuum and at a temperature of 105 °C for a period of 20 h.

The morphology of the cryogels was assessed by optical microscopy analysis using a Meterk optical microscope (China).

Sorption in a Homogeneous Medium of Short Duration. To assess the sorption capacity of cryogels, sorption tests were carried out in a homogeneous medium (petroleum), according to the adaptation of the F726-12 standard of the American Society of Testing and Materials (ASTM, 2012). The cryogels were previously weighed and placed in a container containing enough petroleum so that they could float freely. The petroleum sorption capacity experiments were performed, in triplicate, in a homogeneous medium (petroleum); the sorbed petroleum mass by the cryogel was determined for the time points of 0.25, 0.5, 1, 3, 5, 10, 15, and 20 min. The sorption capacity was calculated using eq 3.[34] The tests were carried out in a controlled environment at 23 ± 2 °C.

$$C_E = \frac{m_f - m_i}{m_i} \quad (3)$$

where C_E is the experimental sorption capacity (g g^{-1}), m_i is the initial mass of the cryogel (g), and m_f is the final mass of the cryogel (g).

A two-way-type statistical analysis was performed to define the cryogels that had the highest petroleum sorption capacity and, thus, the study of the adsorption kinetics and isotherms for petroleum and motor oil was carried out.

Adsorption Kinetics in a Heterogeneous Medium. The petroleum adsorption kinetics study was carried out in a heterogeneous medium, in triplicate, where the cryogels' adsorption capacity was evaluated as a function of the contact time. The contact time was determined from the result obtained in the test of adsorption in a homogeneous medium of short duration. To perform the adsorption test, a certain mass (g) of petroleum/SAE20W50 oil was used in 100 mL of distilled water in a controlled environment at 23 ± 2 °C. These concentrations were chosen to represent a capacity for removing petroleum from the medium between 10 and 100% of the adsorption capacity.

To determine the constants of the adsorption rate and adsorption capacity at equilibrium, the nonlinear kinetic equations of the reaction models were used: pseudo-first-order and pseudo-second-order models according to eqs 4[35] and 5,[36] respectively.

$$q_t = q_e(1 - e^{k_1 t}) \quad (4)$$

$$q_t = \frac{k_2 q_e^2 t}{1 + k_2 q_e t} \quad (5)$$

where q_t is the quantity of solute adsorbed (g g^{-1}) at time t, q_e is the quantity of solute adsorbed (g g^{-1}) at equilibrium, k_1 is the constant of the pseudo-first-order equation (min^{-1}), k_2 is the constant of the pseudo-second-order equation (g g^{-1} min^{-1}), and t is the time (min).

Adsorption Isotherm. The study of petroleum adsorption isotherms was carried out in a heterogeneous medium with a mass of 8.75, 17.5, 35.0, and 70.0 g of petroleum in 100 mL of water and 5.7, 11.4, 28.5, and 57.0 g of SAE20W50 oil petroleum in 100 mL of water. Isotherms were constructed from the analysis of the relationship between the amount of petroleum adsorbed in equilibrium and the final concentration of petroleum, also in equilibrium, using the Langmuir (eqs 6 and 7), Freundlich (eq 8), Redlich–Peterson (eq 9), Temkin (eq 10), and Sips (eq 11) isotherms.[1] The tests were carried out in a controlled environment at 23 ± 2 °C.

$$q_e = \frac{q_m K_L C_e}{1 + K_L C_e} \quad (6)$$

$$R_L = \frac{1}{1 + K_L C_o} \quad (7)$$

where q_m is the theoretical maximum adsorption maximum monolayer coverage capacity (mg g^{-1}), C_e is the concentration at equilibrium (mg L^{-1}), K_L is the constant of the Langmuir isotherm (L mg^{-1}), R_L is the separation factor, and C_o is the initial adsorbate concentration (mg L^{-1}).

$$q_e = K_F C_e^{1/n} \quad (8)$$

where K_F is the constant of the Freundlich isotherm (mg g^{-1}) (dm^3 g^{-1})^n and $1/n$ is the empirical parameter of the adsorption intensity, which varies according to the heterogeneity of the material.

$$q_e = \frac{K_R C_e}{1 + a_R C_e^g} \quad (9)$$

where K_R is the Redlich–Peterson isotherm constant (L g^{-1}), a_R is the Redlich–Peterson linear constant (1 mg^{-1}), R is the universal gas constant (8.314 J mol^{-1} K^{-1}), and g is the Redlich–Peterson isotherm exponent.

$$q_e = \frac{RT}{b_T} \ln A_T C_e \quad (10)$$

where b_T is the Tempkin isotherm constant and A_T is the Tempkin isotherm equilibrium binding constant (L g^{-1}).

$$q_e = \frac{K_S C_e^{\beta_S}}{1 + a_S C_e^{\beta_S}} \quad (11)$$

where K_S is the Sips isotherm model constant (L g^{-1}), β_S is the Sips isotherm model exponent, and a_S is the Sips isotherm model constant (L mg^{-1}).

RESULTS AND DISCUSSION

Porosity and Specific Mass of Cellulose/Biochar Cryogels. The specific mass and porosity of cellulose/biochar cryogels are shown in Table 1. It is noteworthy that the apparent density of cryogels is inversely proportional to porosity, that is, the higher the density, the lower the porosity. The specific mass of AC-1 cryogels was twice as high as that of AC-2 cryogels, due to their higher fiber concentration. Consequently, the porosity was about 4% lower for these cryogels. Due to the small concentrations of biochar (5, 10, and 20% w/w) used, there was no influence of its addition on the density and porosity of the studied cryogels.

Table 1. Nomenclature, Specific Mass, and Porosity of Cellulose/Biochar Cryogels

cryogel	cellulose fibers (% w/w)	biochar (% w/w)[a]	specific mass (g cm^{-3})	porosity (%)
AC-1	1.43	0.0	0.032 ± 0.004	91.9 ± 1.1
AC-2	0.715	0.0	0.015 ± 0.001	96.3 ± 0.4
AC-2.B5	0.715	5.0	0.019 ± 0.001	95.2 ± 0.4
AC-2.B10	0.715	10.0	0.017 ± 0.001	95.8 ± 0.3
AC-2.B20	0.715	20.0	0.017 ± 0.001	95.5 ± 0.4

[a]Biochar concentration was a function of cellulose concentration.

During the pyrolysis process, a thermal breakdown of the organic components present in the biomass is seen, which

https://dx.doi.org/10.1021/acs.langmuir.1c00123
Langmuir 2021, 37, 3180−3188

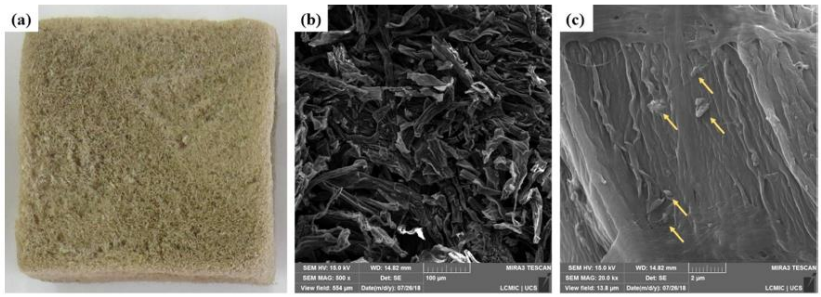

Figure 2. AC-2.B5: (a) photograph, (b) SEM image (500× magnification), and (c) SEM image (20k× magnification).

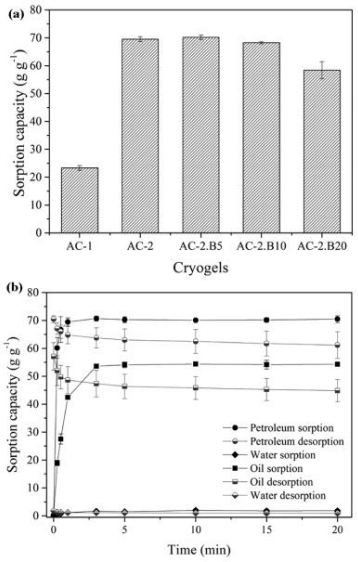

Figure 3. (a) Petroleum sorption capacity of cellulose/biochar cryogels. (b) Sorption and sorption capacity of the AC-2.B5 cryogel as a function of time.

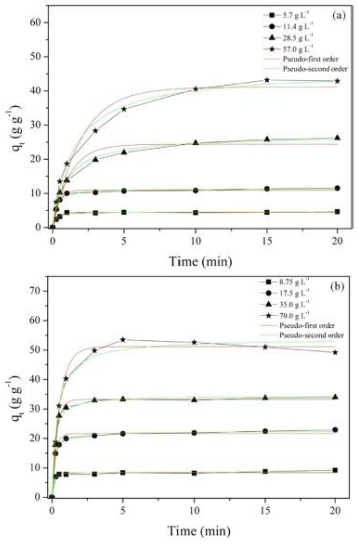

Figure 4. Nonlinear regression for the pseudo-first-order and pseudo-second-order reaction kinetic models for the AC-2.B5 cryogel: (a) SAE20W50 oil and (b) petroleum.

generates the formation of micropores in the biochar, due to water loss during the dehydration process. The pore size varies from nanopores to micropores, and for application as an adsorbent of organic liquids, such as oil, the larger the pore size the better, due to the large molecules of oil.[13]

In Figure 2a,b, the three-dimensional and porous structure of the AC-2.B5 cryogel can be seen from the micrographs. The porous structure is composed of mesopores (±36 Å), determined by the BJH method. It is also noteworthy that the color of the cryogel is homogeneous (Figure 2a), revealing that the biochar was effectively mixed with the cellulose suspension. Figure 2b shows the cellulose fibers used as raw materials with an average thickness of 50 μm. Because the concentration of biochar is only 5% w/w (relative to the concentration of cellulose) and also since it is composed mainly of carbon (80% w/w), there is a certain difficulty in identifying the biochar particles adhered to the cellulose fibers; however, in Figure 2c, it is possible to identify some.

Sorption Capacity of Cellulose/Biochar Cryogels in a Homogeneous Medium. Figure 3a shows the petroleum sorption capacity of cellulose/biochar cryogels after 15 min of testing, according to ASTM 726-12. It is possible to compare the sorption capacity between cryogels, where it is noted that the concentration of cellulose fibers influences the sorption capacity, that is, the AC-1 cryogels showed a lower capacity than the AC-2 cryogels, which is why they contain twice the fiber concentration, greater apparent density, and, as previously discussed, lower porosity. The petroleum sorption capacity of the AC-1 cryogel was about 50% (22.3 g g^{-1}) less than that of the AC-2 cryogel (41.3 g g^{-1}). The pores of cryogels are formed during the freezing of the gel, which, in this case, was carried out in an ultrafreezer at a T of −80°C. During this freezing step, ice crystals are formed in different sizes, and after

https://dx.doi.org/10.1021/acs.langmuir.1c00123
Langmuir 2021, 37, 3180−3188

Table 2. Kinetic Parameters of the Pseudo-First-Order and Pseudo-Second-Order Reaction Models of the AC-2.B5 Cryogel

	initial petroleum concentration (g L^{-1})			
	8.75	17.5	35.0	70.0
	Pseudo-First-Order			
q_e	8.33 ± 0.19	21.63 ± 0.41	33.24 ± 0.35	51.13 ± 0.73
k_1	7.00 ± 1.37	4.14 ± 0.46	3.20 ± 0.18	1.75 ± 0.11
R^2	0.9740	0.9839	0.9955	0.9932
R_{adj}^2	0.9704	0.9816	0.9948	0.9922
χ^2	0.23	0.96	0.67	2.66
	Pseudo-Second-Order			
q_e	8.54 ± 0.18	22.40 ± 0.18	34.52 ± 0.68	53.97 ± 1.30
k_2	2.02 ± 0.63	0.35 ± 0.03	0.16 ± 0.03	0.05 ± 0.007
R^2	0.9832	0.9977	0.9871	0.9853
R_{adj}^2	0.9808	0.9974	0.9852	0.9833
χ^2	0.15	0.13	1.91	5.75
	initial SAE20W50 oil concentration (g L^{-1})			
	5.7	11.4	28.5	57.0
	Pseudo-First-Order			
q_e	4.46 ± 0.07	10.93 ± 0.16	30.66 ± 2.54	40.78 ± 1.76
k_1	2.89 ± 0.22	2.67 ± 0.19	0.39 ± 0.12	0.49 ± 0.08
R^2	0.9912	0.9914	0.8891	0.9667
R_{adj}^2	0.9899	0.9902	0.8733	0.9620
χ^2	0.02	0.14	17.94	9.80
	Pseudo-Second-Order			
q_e	4.63 ± 0.12	11.43 ± 0.21	34.38 ± 2.62	45.73 ± 1.23
k_2	1.10 ± 0.22	0.36 ± 0.05	0.02 ± 0.01	0.02 ± 0.002
R^2	0.9786	0.9890	0.9434	0.9920
R_{adj}^2	0.9756	0.9874	0.9353	0.9909
χ^2	0.06	0.18	9.16	2.34

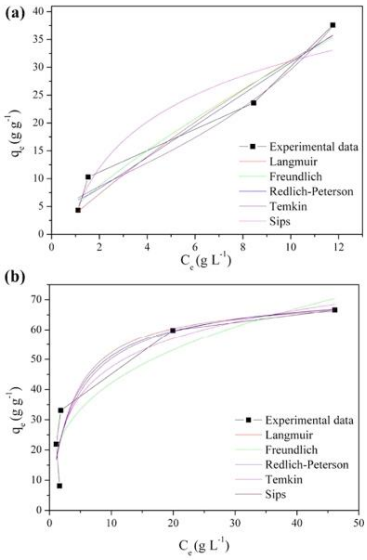

Figure 5. Nonlinear regression for the Langmuir, Freundlich, Redlich−Peterson, Temkin, and Sips isotherms models for the AC-2.B5 cryogels: (a) SAE20W50 oil and (b) petroleum, T = 23 °C.

lyophilization, these crystals formed the pores in the material's structure. As it is not a controllable process in terms of freezing speed and thus does not guarantee a homogeneous formation of pore sizes, the three-dimensional structures of cryogels are heterogeneous,[24,26] which might consequently affect the cryogel's adsorption capacity. In addition, cellulose fibers tend to agglomerate during freezing, yielding filmlike masses (Figure 2c), thus decreasing the number of pores in the structure, being a plausible explanation for the differences in behavior between cryogels. In AC-1 cryogels, there is a higher concentration of fibers, which results in greater agglomeration of fibers, compared to AC-2 cryogels.

The cryogel that showed the highest petroleum sorption capacity was AC-2.B5 (approximately 73 g g^{-1}), 76% higher than the AC-2 cryogel. The presence of functional groups such as carboxyl, hydroxyl, and phenolic on the biochar surface allows this material to adsorb organic and inorganic contaminants from water and petroleum.[37]

Due to the small difference found between the sorption capacity of cryogels AC-2.B5 and AC-2.B10, a statistical analysis was performed to verify if there is a difference between the sorption capacity of cryogels. The results presented in item Table S.1 of the Supporting Information show that between cryogels AC-2.B5 and AC-2.B10, there is no significant difference in the sorption capacity. This result shows that the concentration of biochar used has no influence on the sorption capacity of the cryogel, so the lowest concentration (5% w/w of biochar) was chosen as a result of the lower amount of biochar to be used in the production of the same for the adsorption kinetics and isotherm studies. The decrease in the sorption capacity of the AC-2.B5 cryogel might be attributed to a large amount of biochar added, which considerably increases the content of solids present in the cryogel, thus leading to an increase in the number of cellulose fibers and biochar agglomeration and then decreasing the active sites for oil sorption. The sorption capacity is dependent on the pores of cryogels, where the sorption sites are located.

In a study performed by Niu et al.,[38] in which they obtained reduced graphene oxide foams, the sorption capacity of motor oil for this material was about 37 times its mass. Xiang et al.[39] obtained a sorption capacity of different organic liquids in the range of 10−21 times the mass of the carboxymethyl cellulose−graphene oxide aerogel. These values were lower than those of the AC-2.B5 cryogel (73 times its own mass) produced with cellulose and biochar, which allows us to consider that biochar is more effective than graphene oxide for adsorbent application.

The sorption capacity test as a function of time was performed to determine the maximum sorption capacity of the AC-2.B5 cryogel in a homogeneous medium (water, SAE20W50 oil, and petroleum). As seen in Figure 3b, the AC-2.B5 cryogel reached equilibrium within 3 min of testing in a homogeneous medium. After reaching equilibrium, the cryogel does not sorb a significant amount of sorbate and there is no need to keep it in contact with the medium. As the test was carried out in a homogeneous environment, it is possible to conclude that at 3 min, the cryogel has reached its maximum sorption capacity, being approximately 1.5, 54, and 73 g g^{-1} of water, SAE20W50 oil, and petroleum, respectively (for the AC-2.B5 cryogel).

https://dx.doi.org/10.1021/acs.langmuir.1c00123
Langmuir 2021, 37, 3180−3188

Table 3. Values of the Parameters of the Petroleum and SAE20W50 Oil Adsorption Isotherm Models

	AC-2.B5	
	petroleum	SAE20W50 oil
	Langmuir	
R^2	0.874	0.942
R_{adj}^2	0.833	0.913
χ^2	103.06	19.11
Q_m	71.37 ± 10.21	179.16 ± 436.28
K_L	0.274 ± 0.138	0.021 ± 0.062
R_L	0.286−0.037	0.889−0.469
	Freundlich	
R^2	0.922	0.954
R_{adj}^2	0.801	0.932
χ^2	122.57	14.96
K_F	19.48 ± 6.06	5.02 ± 2.33
n	2.98 ± 0.86	1.26 ± 0.32
	Redlich−Peterson	
R^2	0.875	0.961
R_{adj}^2	0.750	0.885
χ^2	154.14	24.25
K_R	20.82 ± 21.07	2.76 ± 3.76
A_R	0.33 ± 0.89	−0.54 ± 0.48
g	0.96 ± 0.46	−0.72 ± 4.94
	Temkin	
R^2	0.869	0.918
R_{adj}^2	0.826	0.877
χ^2	107.62	26.86
b_T	167.47 ± 37.91	198.87 ± 41.08
A_T	3.18 ± 2.25	1.36 ± 0.54
	Sips	
R^2	0.876	0.981
R_{adj}^2	0.751	0.942
χ^2	153.46	12.76
α_S	0.268 ± 0.197	−0.57 ± 4.70
K_S	20.46 ± 12.07	2.67 ± 27.88
β_S	0.86 ± 1.10	0.18 ± 2.33

The time taken for the system to reach equilibrium and the sorption capacity of the aerogel/cryogel vary with the type of raw material used and the process of surface modification. In comparison to studies in the literature, the cryogels produced in the present study show superior results. For recycled cellulose aerogel (2% w/w), the equilibrium of the sorption system for crude petroleum was reached after 20 min of testing, and the maximum sorption capacity was approximately 20 g g^{-1}.[40] In studies conducted by Karatum et al.,[41] with commercial silica aerogels, the equilibrium of the petroleum sorption system was also achieved in short times (<6 min), but this type of aerogel has a lower sorption capacity (10 g g^{-1}) than those of the cryogels of cellulose/biochar of the present study.

Besides, in Figure 3b, it is noted that the desorption capacity of the AC-2.B5 cryogel also achieves equilibrium after 3 min of testing, with the petroleum loss being about 3 g g^{-1}, showing the petroleum-holding capacity of the AC-2.B5 cryogel. This is an important feature when used in petroleum spills (for example) so that there are no losses during the maintenance and transport of the previously used cryogel.

In the case of petroleum/oil motor sorption by cryogels, the petroleum/oil motor molecules are adhered to the surface of cryogels and also to the active sites present in them, causing the two sorption phenomena (adsorption and absorption). The study of the adsorption kinetics and isotherms carried out in the present work was based on the studies carried out in refs 28, 42, where the researchers report and study only the adsorption kinetics and isotherms.

Adsorption Kinetics in a Heterogeneous Medium. The results for the adsorption kinetics dependent on the initial concentrations of petroleum and SAE20W50 oil for the AC-2.B5 cryogel are shown in Figure 4.

The results revealed that the adsorption occurs by intraparticle diffusion, presenting two stages in the adsorption process. In the initial stages of the contact period, adsorption occurs on the adsorbate's external surface and at a rapid adsorption rate (greater slope of the curve); thus, the rate of petroleum/SAE20W50 oil removal is higher. Subsequently, close to equilibrium, the adsorption rate becomes slower, decreasing the petroleum removal rate. This phenomenon might be due to the presence of a large number of sites on the cryogel's surface available for adsorption during the initial stage and, after a certain time, the remaining sites become difficult to be occupied due to the repulsive forces between the molecules of petroleum.[28,42] It appears that the adsorption capacity of the cryogel is influenced by the initial concentration of the solute, where the higher the initial concentration, the greater the adsorption capacity of the cryogel.

To determine the time in which the system reaches equilibrium in heterogeneous adsorption tests, the two-way analysis of variance was performed and also the multiple comparisons of means as shown in the Supporting Information (Table S.2). Whenever the value of the multiple comparisons of means is lower than the value of DL, there is no significant difference between the results. Therefore, the equilibrium of the system, in each heterogeneous adsorption test, was obtained at different times as follows:

- AC-2.B5 (SAE20W50 oil adsorption capacity—Figure 4a): as seen in Table S.3 of the Supporting Information; at lower concentrations (5.7 and 11.4 g L^{-1}), the system equilibrium was reached at 3 min of the assay because the difference between the means was less than DL. At higher concentrations (28.5 and 57 g L^{-1}), equilibrium was reached at 10 min of the assay because the difference between the means was less than DL.
- AC-2.B5 (petroleum adsorption capacity—Figure 4b): as seen in Table S.4 of the Supporting Information, the system equilibrium was reached at 3 min of the assay. Since the difference between the means is smaller than DL, there is no significant difference. That is, from the 3 min test, there is no significant amount of adsorbed fluid to keep the cryogel in contact with the medium.

Once the system is in equilibrium, there is no longer an adsorbed amount of SAE20W50 oil or significant petroleum, so there is no longer a need to keep the cryogel in contact with the fluid.

Differently, Figure 4 shows the adjustments to the reactive pseudo-first-order and pseudo-second-order kinetic models from the analysis of nonlinear regression. The values of the parameters related to these models are shown in Table 2.

The values of R^2 and R_{adj}^2 were calculated to determine the best regression fit and to obtain a better prediction of the kinetic behavior of the adsorption of petroleum by the cryogel. For the AC-2.B5 cryogel, at low initial petroleum concentrations (<25% w/w), the pseudo-second-order model showed

https://dx.doi.org/10.1021/acs.langmuir.1c00123
Langmuir 2021, 37, 3180−3188

higher R^2 and R_{adj}^2 values; this means that the adsorption process includes external liquid film diffusion, particle internal diffusion, and surface adsorption.[43] As for initial concentrations of adsorbate above 25% w/w, the pseudo-first-order kinetic model showed higher R^2 and R_{adj}^2 values, showing that the adsorption process is controlled by intraparticle and extraparticle diffusion.[44,45] For SAE20W50 oil, the behavior was contrary to that of petroleum, which can be attributed to the smaller size of the molecules of SAE20W50 oil compared to petroleum and its lower density.

In our previous study,[28] with cellulose cryogels, the pseudo-second-order kinetic model presented the best linear regression adjustment for all initial concentrations. The comparison between the two studies showed that at low initial concentrations of the adsorbate, there may be differences in the results. However, for initial concentrations of the adsorbate close to the adsorption capacity of the adsorbent at equilibrium, the results found were the same, where the pseudo-second-order kinetic model governs the adsorption process of cellulose/biochar cryogels.

According to Plazinski et al.,[46] the constants k_1 and k_2 are dependent on the initial concentration of the adsorbate; the higher the initial concentration, the lower the constant and the longer the time required for the system to reach equilibrium. This phenomenon might be attributed to the presence of a greater number of active molecules for adsorption at high initial concentrations of the adsorbate.[47]

Finally, evaluating the results of Table 2, it is noted that the values of the quantity (qe) of petroleum/SAE20W50 oil adsorbed by the AC-2.B5 cryogel are in agreement with the experimental data.

Equilibrium of the Adsorption Process (Adsorption Isotherms). Based on cryogenic adsorption kinetics studies, presented above, and, which show that the systems reached equilibrium at different test times, and to standardize the results, it was determined that for all studied systems the equilibrium of the same was reached at 10 min of the test, to standardize the results in the study of adsorption isotherms. Figure 5 shows the nonlinear regression for the Langmuir, Freundlich, Redlich−Peterson, Temkin, and Sips isotherms for the AC-2.B5 cryogel. According to Weber and Chakravorti, the AC-2.B5 cryogel shows an "extremely favorable" behavior,[48] due to the behavior of the isotherms presented in Figure 5.

The values of the parameters studied for the different models of isotherms are presented in Table 3. As noted, the values of R^2 and R_{adj}^2 that are closest to the unit are Freundlich for petroleum and Sips for SAE20W50 oil, showing that these are the models that present the best regression fit.

The Freundlich model assumes that the surface of the adsorbent is heterogeneous in terms of shape and energy, which indicates that the interaction between adsorbed molecules is not limited to the formation of just a single layer. Also, this model assumes that the process is unlimited; in other words, it does not provide for adsorbent saturation.[1]

The Sips model is related to the Langmuir and Freundlich models, but this model presents a third parameter (β_S—Sips exponential constant). According to Foo and Hamed,[1] when a small amount of adsorbate is retained in the solid, the model behaves like the Freundlich model ($\beta_S \rightarrow 0$) and when the quantity is high, the model behaves like the Langmuir model ($\beta_S \rightarrow 1$). In the case of the AC-2.B5 cryogel, for the SAE20W50 oil, the parameter β_S approaches 0 (0.18), showing that this model is reduced to the Freundlich equation. Hence, it is possible to state that for both studied fluids (petroleum and SAE20W50 oil), the Freundlich model best fits the experimental data, indicating that the process occurs through the formation of multiple layers and the cryogel adsorption sites are energetically heterogeneous.

CONCLUSIONS

The use of biochar as a substitute for carbon structures, such as graphene and nanotubes, proved to be efficient in the adsorption of organic liquids, which shows its potential to be applied in adsorbents. The petroleum adsorption capacity was influenced by the concentration of cellulose, and the addition of biochar to the cellulose cryogel caused a 70% increase in adsorption capacity. In the study of adsorption kinetics, the equilibrium of the system was reached at 3 min of testing. For petroleum, the kinetic model that best fitted the system was the pseudo-first-order model (R^2 0.9932), while for SAE20W50 oil, it was the pseudo-second-order model (R^2 0.9920). Concerning the process equilibrium, the Freundlich model best fit the petroleum system. As for the SAE20W50 oil system, the best-fit model was Sips, with exponential constant $\beta_S \rightarrow 0$, thus reducing the equation to the Freundlich model. Herewith, it might be concluded that the petroleum/SAE20W50 oil adsorption process occurs in multiple layers and the adsorption sites are energetically heterogeneous. Finally, the addition of biochar to the cellulose cryogel confers benefits to the final products as it increases the adsorption capacity of the studied fluids and also increases the adsorption speed of the solute, petroleum, and possibly of its derivatives.

ASSOCIATED CONTENT

Supporting Information

The Supporting Information is available free of charge at https://pubs.acs.org/doi/10.1021/acs.langmuir.1c00123.

Statistical analyses performed in the adsorption capacity tests; adsorption capacity of the cellulose/biochar aerogels (Table S.1); ANOVA table (Tables S.2 and S.5); Tukey HSD test (Tables S.3 and S.6); and petroleum adsorption capacity of the cellulose/biochar aerogels (Table S.4) (PDF)

AUTHOR INFORMATION

Corresponding Author

Lídia Kunz Lazzari − *Postgraduate Program in Mining, Metallurgical and Materials Engineering, Federal University of Rio Grande do Sul, Porto Alegre 91501-970, Brazil*; Email: lidia_lazzari@yahoo.com.br

Authors

Daniele Perondi − *Postgraduate Program in Engineering of Processes and Technologies, University of Caxias do Sul., Caxias do Sul 95070-560, Brazil*

Ademir José Zattera − *Postgraduate Program in Engineering of Processes and Technologies, University of Caxias do Sul., Caxias do Sul 95070-560, Brazil*

Ruth Marlene Campomanes Santana − *Postgraduate Program in Mining, Metallurgical and Materials Engineering, Federal University of Rio Grande do Sul., Porto Alegre 91501-970, Brazil*

Complete contact information is available at: https://pubs.acs.org/10.1021/acs.langmuir.1c00123

https://dx.doi.org/10.1021/acs.langmuir.1c00123
Langmuir 2021, 37, 3180−3188

Notes

The authors declare no competing financial interest.

■ ACKNOWLEDGMENTS

The authors would like to thank the Federal University of Rio Grande do Sul (UFRGS), the University of Caxias do Sul (UCS), and the National Council for Scientific and Technological Development (CNPq).

■ REFERENCES

(1) Foo, K. Y.; Hameed, B. H. Insights into the modeling of adsorption isotherm systems. *Chem. Eng. J.* **2010**, *156*, 2−10.
(2) Qiu, H.; Lv, L.; Pan, B.; Zhang, Q.; Zhang, W.; Zhang, Q. Critical review in adsorption kinetic models*. *J. Zhejiang Univ., Sci., A* **2009**, *10*, 716−724.
(3) Ramesh, A.; Lee, D. J.; Wong, J. W. C. Thermodynamic parameters for adsorption equilibrium of heavy metals and dyes from waste water with low-cost adsorbents. *J. Colloid Interface Sci.* **2005**, *291*, 588−592.
(4) Tan, X.; Liu, Y.; Zeng, G.; Wang, X.; Hu, X.; Gu, Y.; Yang, Z. Application of biochar for the 461 removal of pollutants from aqueous solutions. *Chemosphere* **2015**, *125*, 70−85.
(5) Cao, X.; Ma, L.; Gao, B.; Harris, W. Dairy-manure derived biochar effectively sorbs lead and atrazine. *Environ. Sci. Technol.* **2009**, *43*, 3285−3291.
(6) Zheng, W.; Guo, M.; Chow, T.; Bennett, D. N.; Rajagopalan, N. Sorption properties of greenwaste biochar for two triazine pesticides. *J. Hazard. Mater.* **2010**, *181*, 121−126.
(7) Karakoyun, N.; Kubilay, S.; Aktas, N.; Turhan, O.; Kasimoglu, M.; Yilmaz, S.; Sahiner, N. Hydrogel-Biochar composites for effective organic contaminant removal from aqueous media. *Desalination* **2011**, *280*, 319−325.
(8) Ahmad, M.; Lee, S. S.; Dou, X.; Mohan, D.; Sung, J. K.; Yang, J. E.; Ok, Y. S. Effects of pyrolysis temperature on soybean stover- and peanut shell-derived biochar properties and TCE adsorption in water. *Bioresour. Technol.* **2012**, *118*, 536−544.
(9) Lu, H.; Zhang, W.; Yang, Y.; Huang, X.; Wang, S.; Qiu, R. Relative distribution of Pb2+ sorption mechanisms by sludge-derived biochar. *Water Res.* **2012**, *46*, 854−862.
(10) Tang, L.; Yu, J.; Pang, Y.; Zeng, G.; Deng, Y.; Wang, J.; Ren, X.; Ye, S.; Peng, B.; Feng, H. Sustainable efficient adsorbent: Alkali-acid modified magnetic biochar derived from sewage sludge for aqueous organic contaminant removal. *Chem. Eng. J.* **2018**, *336*, 160−169.
(11) Lobos, M. L. N.; Sieben, J. M.; Comignani, V.; Duarte, M.; Volpe, M. A.; Moyano, E. L. Biochar from pyrolysis of cellulose: An alternative catalyst support for the electro-oxidation of methanol. *Int. J. Hydrogen Energy* **2016**, *41*, 10695−10706.
(12) Kabiri, S.; Tran, D. N. H.; Altalhi, T.; Losic, D. Outstanding adsorption performance of graphene-carbon nanotube aerogels for continuous oil removal. *Carbon* **2014**, *80*, 523−533.
(13) Tareq, R.; Akter, N.; Azam, S. M. Chapter 10 - Biochars and Biochar Composites: Low-Cost Adsorbents for Environmental Remediation. In *Biochar from Biomass and Waste*; Elsevier, 2019; Vol. 25, pp 169−209.
(14) Zhang, Z.; Zhu, Z.; Shen, B.; Liu, L. Insights into biochar and hydrochar production and 493 applications: A review. *Energy* **2019**, *171*, 581−598.
(15) Yu, S.; Park, J.; Kim, M.; Ryu, C.; Park, J. Characterization of biochar and byproducts 496 from slow pyrolysis of hinoki cypress. *Bioresour. Technol. Rep.* **2019**, *6*, 217−222.
(16) Jung, S.; Park, Y. K.; Kwon, E. E. Strategic use of biochar for CO2 capture and 499 sequestration. *J. CO2 Util.* **2019**, 32, 128−139.
(17) Godwin, P. M.; Pan, Y.; Xiao, H.; Afzal, M. T. Progress in preparation and application of modified biochar for improving heavy metal ion removal from wastewater. *J. Bioresour. Bioprod.* **2019**, *4*, 31−42.
(18) Yu, J.; Feng, H.; Tang, L.; Pang, Y.; Wang, J.; Zou, J.; Xie, Q.; Liu, Y.; Feng, C.; Wang, J. Insight into the key factors in fast adsorption of organic pollutants by hierarchical porous biochar. *J. Hazard. Mater.* **2021**, *403*, No. 123610.
(19) Yang, J.; Ji, G.; Gao, Y.; Fu, W.; Irfan, M.; Mu, L.; Zhang, Y.; Li, A. High-yield and high-performance porous biochar produced from pyrolysis of peanut shell with low-dose ammonium polyphosphate for chloramphenicol adsorption. *J. Cleaner Prod.* **2020**, *264*, No. 121516.
(20) Zazycki, M. A.; Godinho, M.; Perondi, P.; Foletto, E. L.; Collazzo, G. C.; Dotto, G. L. New biochar from pecan nutshells as an alternative adsorbent for removing reactive red 141 from aqueous solutions. *J. Cleaner Prod.* **2018**, *171*, 57−65.
(21) Zhang, L.; Tang, S.; He, F.; Liu, Y.; Mao, W.; Guan, Y. Highly efficient and selective capture of heavy metals by poly(acrylic acid) grafted chitosan and biochar composite for wastewater treatment. *Chem. Eng. J.* **2019**, *378*, No. 122215.
(22) Chen, W.; Wei, R.; Ni, J.; Yang, L.; Qian, W.; Yang, Y. Sorption of chlorinated 521 hydrocarbons to biochars in aqueous environment: Effects of the amorphous carbon 522 structure of biochars and the molecular properties of adsorbates. *Chemosphere* **2018**, *210*, 753−761.
(23) Li, X.; Zhao, C.; Zhang, M. Chapter 8 - Biochar for anionic contaminants removal from water. In *Biochar from Biomass and Waste*; Elsevier, 2019; pp 143−160.
(24) Gun'ko, V. M.; Savina, I. N.; Mikhalovsky, S. V. Cryogels: morphological, structural and adsorption characterization. *Adv. Colloid Interface Sci.* **2013**, *187*−*188*, 1−46.
(25) Husing, N.; Schubert, U. Aerogels—airy materials: chemistry, structure, and properties. *Angew. Chem., Int. Ed.* **2002**, *37*, 22−45.
(26) Darpentigny, C.; Nonglaton, G.; Bras, J.; Jean, B. Highly absorbent cellulose nanofibrils aerogels prepared by supercritical drying. *Carbohydr. Polym.* **2020**, *229*, No. 115560.
(27) Lazzari, L. K.; Perondi, D.; Zampieri, V. B.; Zattera, A. J.; Santana, R. M. C. Cellulose/biochar aerogels with excellent mechanical and thermal insulation properties. *Cellulose* **2019**, *26*, 9071−9083.
(28) Lazzari, L. K.; Zampieri, V. B.; Neves, R. M.; Zanini, M.; Zattera, A. J.; Baldasso, C. A study on adsorption isotherm and kinetics of petroleum by cellulose cryogels. *Cellulose* **2019**, *26*, 1231−1246.
(29) Zanini, M.; Lavoratti, A.; Lazzari, L. K.; Galiotto, D.; Pagnocelli, M.; Baldasso, C.; Zattera, A. J. Producing aerogels from silanized cellulose nanofiber suspension. *Cellulose* **2017**, *24*, 769−779.
(30) Ganesan, K.; Dennstedt, A.; Barowski, A.; Ratke, L. Design of aerogels, cryogels and xerogels of cellulose with hierarchical porous structures. *Mater. Des.* **2016**, *92*, 345−355.
(31) Perondi, D.; Polleto, P.; Restelatto, D.; Manera, C.; Silva, J. P.; Junges, J.; Collazzo, G. C.; Dettmer, A.; Godinho, M.; Vilela, A. C. F. Steam gasification of poultry litter biochar for 550 bio-syngas production. *Process Saf. Environ. Prot.* **2017**, *109*, 478−488.
(32) Sescousse, R.; Gavillon, R.; Budtova, T. erocellulose from cellulose-ionic liquid solutions: Preparation, properties and comparison with cellulose-NaOH and cellulose- NMMO routes. *Carbohydr. Polym.* **2011**, *83*, 1766−1774.
(33) Fu, J.; Wang, S.; He, C.; Lu, Z.; Huang, J.; Chen, Z. Facilitated fabrication of high strength silica aerogels using cellulose nanofibrils as scaffold. *Carbohydr. Polym.* **2016**, *147*, 89−96.
(34) Lazzari, L. K.; Zampieri, V. B.; Zanini, M.; Zattera, A. J.; Baldasso, C. Sorption capacity of hydrophobic cellulose cryogels silanized by two different methods. *Cellulose* **2017**, *24*, 3421−3431.
(35) Lei, E.; Li, W.; Ma, C.; Liu, S. An ultra-lightweight recyclable carbon aerogel from bleached softwood kraft pulp for efficient oil and organic absorption. *Mater. Chem. Phys.* **2018**, *214*, 291−296.
(36) Lazzari, E.; Schena, T.; Marcelo, M. C. A.; Primaz, T. C.; Silva, A. N.; Ferrao, M. F.; Bjerk, T.; Caramao, E. B. Classification of biomass through their pyrolytic bio-oil composition using FTIR and PCA analysis. *Ind. Crops Prod.* **2018**, *111*, 856−864.
(37) Godlewska, P.; Bogusz, A.; Dobrzynska, J.; Dobrowolski, R.; Oleszczuk, P. Engineered biochar modified with iron as a new adsorbent for treatment of water contaminated by selenium. *J. Saudi Chem. Soc.* **2020**, *24*, 824−834.

https://dx.doi.org/10.1021/acs.langmuir.1c00123
Langmuir 2021, 37, 3180−3188

(38) Niu, Z.; Chen, J.; Hng, H. H.; Ma, J.; Chen, X. A leavening strategy to prepare reduced graphene oxide foams. *Adv. Mater.* **2012**, *24*, 4144−4150.
(39) Xiang, C.; Wang, C.; Guo, R.; Lan, J.; Lin, S.; Jiang, S.; Lai, X.; Zhang, Y.; Xiao, H. ynthesis of carboxymethyl cellulose-reduced graphene oxide aerogel for efficient removal of organic liquids and dyes. *J. Mater. Sci.* **2019**, *54*, 1872−1883.
(40) Nguyen, S. T.; Feng, J.; Le, N. T.; Le, A. T. T.; Hoang, N.; Tan, V. B. C.; Duong, H. M. *Ind. Eng. Chem. Res.* **2013**, *52*, 18386−18391.
(41) Karatum, O.; Shi, W.; Plata, D. L.; Steiner, S. A.; Griffin, J. S. Flexible, mechanically durable aerogel composites for oil capture and recovery. *ACS Appl. Mater. Interfaces* **2016**, *8*, 215−224.
(42) Rahmani, Z.; Rashidi, A. M.; Kazemi, A.; Samadi, M. T.; Rahmani, A. R. N-doped reduced graphene oxide aerogel for the selective adsorption of oil pollutants from water: Isotherm and kinetic study. *J. Ind. Eng. Chem.* **2018**, *61*, 416−426.
(43) Tang, M.; Jia, R.; Kan, H.; Liu, Z.; Yang, S.; Sun, L.; Yang, Y. Kinetic, isotherm, and thermodynamic studies of the adsorption of dye from aqueous solution by propylene glycol adipate-modified cellulose aerogel. *Colloids Surf., A* **2020**, *602*, No. 125009.
(44) Wang, J.; Guo, X. Adsorption kinetic models: Physical meanings, applications, and solving methods. *J. Hazard. Mater.* **2020**, *390*, No. 122156.
(45) Simonin, J. On the comparison of pseudo-first order and pseudo-second order rate laws in the modeling of adsorption kinetics. *Chem. Eng. J.* **2016**, *300*, 254−263.
(46) Plazinski, W.; Rudzinski, W.; Plazinska, A. Theoretical models of sorption kinetics including a surface reaction mechanism: A review. *Adv. Colloid Interface Sci.* **2009**, *152*, 2−13.
(47) Pan, Y.; Wang, F.; Wei, T.; Zhang, C.; Xiao, H. Hydrophobic modification of bagasse cellulose fibers with cationic latex: Adsorption kinetics and mechanism. *Chem. Eng. J.* **2016**, *302*, 33−43.
(48) Weber, T. W.; Chakravorti, R. K. Pore and Solid Diffusion Models for fixed-bed adsorbers. *AIChE J.* **1974**, *20*, 228−238.

https://dx.doi.org/10.1021/acs.langmuir.1c00123
Langmuir 2021, 37, 3180−3188

CELLULOSE/BIOCHAR CRYOGELS: STUDY OF ADSORPTION KINETICS AND ISOTHERMS

Lídia Kunz Lazzari[1], Daniele Perondi[2], Ademir José Zattera[2] and Ruth Marlene Campomanes Santana[1]

SUPPLEMENTARY INFORMATION

STATISTICAL ANALYSIS

S.1 Cellulose/biochar cryogels adsorption capacity

The values obtained in the petroleum adsorption capacity test of the cellulose/biochar aerogels for are presented in Table S.1.

Table S.1 – Adsorption capacity of the cellulose/biochar aerogels.

		Concentração de biochar (%)			
		0	**5**	**10**	**20**
Concentração de celulose (%)	**1.43**	24.16	22.71	20.89	26.07
		22.43	22.81	25.71	23.22
		20.36	28.34	24.46	23.99
	0.715	40.83	70.97	70.32	55.34
		39.77	72.55	67.86	50.90
		43.31	75.47	68.63	61.46

With the data collected during the test and presented in Table S.1, the ANOVA table was generated in the Statistics software, presented in Table S.2.

Table S.2 - Table ANOVA.

Effect	*SQ*	*gl*	*MQ*	*F*	*P value*
% cellulose	7785.25	1	7785.25	5525.40	0.0000
%biochar	1031.86	3	343.95	1027.031	0.0000
interaction	823.02	3	274.34	45.375	0.0000
Error	121.29	16	7.58	36.191	0.0000

Since the "P-value" is less than 0.05, there is a significant difference between the groups. For this, the Tukey HSD test was performed for determined between the groups there is a significant difference. The result found is shown in the Table S.3.

Table S.3 Tukey HSD test.

Cryogel	AC-.2	AC-2.B5	AC-2.B10	AC-2.B20	AC-1	AC-1.B5	AC-1.B10	AC-1.B20
AC-2		0.000175	0.000175	0.000311	0.000177	0.000193	0.000182	0.000190
AC-2.B5	0.000175		0.624930	0.000187	0.000175	0.000175	0.000175	0.000175
AC-2.B10	0.000175	0.624930		0.000689	0.000175	0.000175	0.000175	0.000175
AC-2.B20	0.000311	0.000187	0.000689		0.000175	0.000175	0.000175	0.000175
AC-1	0.000177	0.000175	0.000175	0.000175		0.963344	0.998225	0.977092
AC-1.B5	0.000193	0.000175	0.000175	0.000175	0.963344		0.999853	1.000000
AC-1.B10	0.000182	0.000175	0.000175	0.000175	0.998225	0.999853		0.999970
AC-1.B20	0.000190	0.000175	0.000175	0.000175	0.977092	1.000000	0.999970	

The results presented in Table S.3, show significant difference between the groups that presents values < 0.05. Thereby, there is a significant difference between the concentrations of cellulose, therefore, in their choice, the 0.715% of cellulose presents the greatest capacity. Analyzing the results the biochar concentration with the highest capacity is 5%, due to the non-significant difference between 5 and 10%, preferred to 5%.

S.2 Petroleum adsorption capacity AC-2.B5 cryogel

The values obtained in the adsorption capacity test of the cellulose/biochar aerogels for are presented in Table S.4.

Table S.4 – Petroleum adsorption capacity of the cellulose/biochar aerogels.

		Petroleum concentration (g L^{-1})			
		8.75	**17.5**	**35.0**	**70.0**
Tempo (min)	**0**	0.085	0.000	0.000	0.000
		0.130	0.000	0.000	0.000
	0.25	7.022	10.161	17.594	12.622
		6.504	19.154	17.536	24.582
	0.5	8.067	14.343	30.185	22.100
		7.177	20.861	24.867	39.625
	1	8.494	17.228	33.332	29.469
		6.826	22.408	27.399	50.840
	3	8.327	18.461	34.517	43.589
		6.073	21.841	30.129	54.802
	5	8.156	18.444	33.664	48.569
		6.248	22.039	30.862	56.281
	10	8.624	19.104	33.454	46.415
		6.577	23.230	31.523	57.670
	15	9.566	20.242	34.539	45.930
		8.328	25.081	33.194	56.406

20	8.895	19.225	33.443	42.735
	8.042	24.865	33.211	54.251

With the data collected during the test and presented in Table S.4, the ANOVA table was generated in the Statistics software, presented in Table S.5.

Table S.5 - Table ANOVA.

Effect	*SQ*	*gl*	*MQ*	*F*	*P value*
Time (min)	5913.60	8	739.20	29.193	0.00000
Petroleum concentration (g L^{-1})	9534.90	3	3178.30	125.520	0.00000
Interaction	2368.63	24	98.69	3.898	0.00012
Error	911.56	36	25.32		

Since the "P-value" is less than 0.05, there is a significant difference between the groups. For this, the Tukey HSD test was performed for determined between the groups there is a significant difference. The result found is shown in the Table S.6.

Table S.6 Tukey HSD test.

		t = 3 min			
Petroleum conc (g L^{-1})		8.75	17.5	35.0	70.0
Time (min)	5	1,000	1,000	1,000	1,000
	10	1,000	1,000	1,000	1,000
	15	1,000	1,000	1,000	1,000
	20	1,000	1,000	1,000	1,000

The results presented in Table S.3, show not significant difference between the groups that presents values in black writing.

7 INTEGRAÇÃO DOS ARTIGOS

Os materiais alotrópicos de carbono, principalmente o grafeno e os nanotubos de carbono, são amplamente utilizados nos aerogéis/criogéis encontrados na literatura. Porém por apresentarem elevados custos e alta tecnologia para serem produzidos, estudou-se a possibilidade de substituição desses materiais pelo biochar (**Artigo I**), produto este derivado de fontes vegetais e renováveis, com baixo custo associado à sua obtenção. A base dos criogéis produzidos no presente trabalho foi a celulose *Pinus elliotti* e para a comparação com o biochar, foram utilizadas nanoplaquetas de grafeno. Os criogéis de celulose foram produzidos com concentrações de biochar e NPG muito superiores (>50% m/m) as utilizadas na literatura (<20% m/m) para que assim pudesse verificar se essas partículas realmente apresentam influência nas propriedades físicas, químicas e mecânicas dos criogéis de celulose.

Os criogéis de celulose/NPG e criogéis de celulose/biochar apresentam elevada porosidade (>90%) devido suas baixas densidades, sendo comparáveis aos aerogéis de sílica e celulose amplamente estudados na literatura. A morfologia dos criogéis é heterogênea o que faz com que haja um desvio padrão considerável nos resultados de todos os ensaios realizados. Nas propriedades mecânicas, os criogéis de celulose/biochar apresentam resistência a compressão semelhante aos criogéis de celulose/NPG, além disso o aumento da resistência a compressão se dá pelo aumento da concentração de biochar/NPG nos criogéis (comportamento observado também no **Artigo II**). Ao serem estudados para duas aplicações, isolantes térmicos e adsorventes, os criogéis de celulose/biochar e celulose/NPG mostram resultados semelhantes entre si, o que se pode concluir que o tipo de partícula (biochar o NPG) não tem influência sobre essas aplicações. Devido a isso, mostrou-se que o biochar tem potencial para substituir as nanoplaquetas de grafeno, tornando-se uma matéria prima mais acessível devido ao baixo custo e simplicidade do processo de produção.

Considerando os resultados encontrados no **Artigo I**, nos **Artigo II e III** buscou-se encontrar a concentração ideal de biochar para os criogéis de celulose serem aplicados como isolantes térmicos e adsorventes, respectivamente.

No **Artigo II**, a concentração de biochar variou de 0-100% m/m (em relação a massa de celulose – 1,43%m/m). A adição do biochar aos criogéis de celulose não apresentou mudança significativa na densidade aparente e porosidade dos mesmos, mantendo a porosidade acima de 90% e densidade abaixo de 0,035 g cm^3, resultados também encontrados

no **Artigo III**. Estes materiais são considerados materiais muito interessantes para fins de isolamento térmico pois apresentam alto desempenho como resultado de sua condutividade térmica extremamente baixa (valores inferiores a 0,04 W m^{-1} K^{-1}), muito próxima a condutividade térmica do ar e de materiais comercialmente utilizados como as espumas de poliuretana e mantas de polipropileno.

Com o aumento da concentração de biochar, há uma diminuição da estabilidade térmica dos criogéis, isso ocorre devido ao aumento da área superficial específica obtida após o processo mecânico, o que facilita o processo de degradação quando comparado ao material de origem, a celulose. Porém há um aumento da resistência mecânica de aproximadamente 60% com a adição de 40%m/m de biochar. Os criogéis de celulose/biochar sofreram uma deformação plástica de forma irreversível e após esta região, devido a estrutura densamente comprimida, os criogéis tornam-se resistentes. Nos resultados obtidos de condutividade térmica (valores inferiores a 0,027 W m^{-1} K^{-1}), os criogéis de celulose/biochar não apresentam diferenças significativas entre si, isso porque a mudança na condutividade térmica se dá pelas mudanças na fase sólida do material. Nos criogéis produzidos no presente trabalho, não houve mudanças na estrutura dos mesmo pela a adição do biochar.

Tendo como base a concentração de 40%m/m de biochar encontrada como melhor resultado no **Artigo II**, no **Artigo III**, avaliou-se a influência da concentração de celulose e biochar na capacidade de adsorção de óleos, utilizando a concentração de 0-20%m/m de biochar em relação a concentração de celulose (1,43-0,715%m/m). Diferentemente dos **Artigos I e II**, no Artigo 3, houve mudanças na porosidade e densidade aparente, mas devido a concentração de celulose utilizada, onde os criogéis com menor concentração apresentaram maior porosidade (>95%) e menor densidade (<0,020 g cm^{-3}). Essa diferença na concentração de celulose também influenciou a capacidade de adsorção de óleos dos criogéis. Os criogéis com menor concentração de celulose apresentaram maior capacidade de adsorção, cerca de 50% a mais. Em relação a concentração de biochar, há um aumento de 76% da capacidade de adsorção do criogel de celulose/biochar com a adição de 5%m/m de biochar em relação ao criogel de celulose. A adsorção dos óleos ocorre em curto período de tempo, o sistema atinge o equilíbrio em menos de 5 minutos, e assim o criogel atinge sua capacidade máxima de adsorção de óleo.

A realização dos estudos de cinética de adsorção revelaram que a adsorção de óleo ocorre por difusao intra partícula, apresentando duas etapas no processo de adsorção: inicialmente ocorre a adsorção na superfície externa do criogel, tendo uma taxa maior de

remçao de óleo; e próximo ao equilíbrio a taxa de adsorção é mais lenta e constante. revelaram que a adsorção de petróleo ocorre por difusao intra partícula, apresentando duas etapas no processo de adsorção. No estudo das isotermas de adsorção, foi possível afirmar que o modelo de Freundlich é o que melhor se ajusta aos dados experimentais, indicando que o processo ocorre através da formação de multicamadas e que os sítios de adsorção do criogel são energicamente heterogêneos.

8 CONCLUSÃO

Os resultados obtidos mostraram que a substituição das nanoplaquetas de grafeno pelo biochar mostrou-se eficaz, pois os criogéis apresentaram propriedades físicas e mecânicas semelhantes independentemente da estrutura utilizada, biochar ou nanoplaquetas de grafeno. Portanto é possível utilizar uma matéria-prima produzida a partir de resíduo agrícola e de baixo custo, como o biochar, na substituição de estruturas de carbono comercialmente utilizadas.

Com a adição de biochar aos criogéis de celulose, os mesmos apresentaram estruturas heterogêneas com porosidade superior a 90% e densidade aparente interior 0,035 g cm^{-3}. Houve uma diminuição da estabilidade térmica dos mesmos e um aumento na resistência a compressão de 60% em relação ao aerogel de celulose. Por outro lado, o biochar não apresentou influência na condutividade térmica dos aerogéis (cerca de 0,025 W m^{-1} K^{-1}), que mostrou-se próxima a das espumas de poliuretano (0,02 – 0,03 W m^{-1} K^{-1}).

Como adsorvente, os criogéis de celulose/biochar apresentaram capacidade de adsorção de óleo 70% maior que o criogel de celulose, com a adição de apenas 5%m/m de biochar. A partir dos estudos de cinética e isotermas de adsorção, pode-se concluir que o processo de adsorção de óleos ocorre em multicamadas e que os sítios de adsorção são energeticamente heterogêneos.

Assim, os resultados encontrados mostram que os criogéis de celulose/biochar são promissores materiais para serem aplicados como isolantes térmicos e adsorventes.

9 REFERÊNCIAS

ABDELMOULEH, M. et al. Modification of cellulosic fibres with functionalised silanes : development of surface properties. v. 24, p. 43–54, 2004.

AEGERTER, M. A.; LEVENTIS, N.; KOEBEL, M. M. **Aerogels Handbook**. [s.l: s.n.].

BAKIERSKA, M. et al. Functional starch based carbon aerogels for energy applications. **Procedia Engineering**, v. 98, p. 14–19, 2014.

BASSA, A. G. M. C. et al. Mixtures of Eucalyptus Grandis x Eucalyptus Urophylla and Pinus Taeda Woodchip for the Production of Kraft Pulping Using the Lo-Solids Process. **Scientia Florestalls**, v. 75, p. 19–29, 2007.

BASU, P. **Biomass Gasification and Pyrolysis: pratical design and theory**. [s.l.] Academic Press, 2010.

BHATNAGAR, A.; SILLANPÄÄ, M. Utilization of agro-industrial and municipal waste materials as potential adsorbents for water treatment-A review. **Chemical Engineering Journal**, v. 157, n. 2–3, p. 277–296, 2010.

BI, H. et al. Carbon Fiber Aerogel Made from Raw Cotton : A Novel , Effi cient and Recyclable Sorbent for Oils and Organic Solvents. p. 5916–5921, 2013.

BRIDGWATER, A. V. Review of fast pyrolysis of biomass and product upgrading. v. 8, 2011.

BRYNING, B. M. B. et al. Carbon Nanotube Aerogels **. **Advanced Materials**, v. 19, p. 661–664, 2007.

ÇENGEL, Y. A.; GHAJAR, A. J. **Transferência de Calor e Massa**. 4. ed. [s.l: s.n.].

CHANG, X.; CHEN, D.; JIAO, X. Starch-derived carbon aerogels with high-performance for sorption of cationic dyes. **Polymer**, v. 51, n. 16, p. 3801–3807, 2010.

CHEN, C. et al. Compressive, ultralight and fire-resistant lignin-modified graphene aerogels as recyclable absorbents for oil and organic solvents. **Chemical Engineering Journal**, v. 350, n. January, p. 173–180, 2018a.

CHEN, W. et al. Sorption of chlorinated hydrocarbons to biochars in aqueous environment: Effects of the amorphous carbon structure of biochars and the molecular properties of adsorbates. **Chemosphere**, v. 210, p. 753–761, 2018b.

CHENG, H. et al. Materials & Design Cotton aerogels and cotton-cellulose aerogels from environmental waste for oil spillage cleanup. **Materials & Design**, v. 130, n. May, p. 452–458, 2017.

COLLARD, F.; BLIN, J. A review on pyrolysis of biomass constituents : Mechanisms and composition of the products obtained from the conversion of cellulose , hemicelluloses and lignin. **Renewable and Sustainable Energy Reviews**, v. 38, p. 594–608, 2014.

CONG, L. et al. High-performance graphene oxide/carbon nanotubes aerogel-polystyrene composites: Preparation and mechanical properties. **Materials Letters**, v. 214, p. 190–193, 2018.

CRUZ, M. P. **Aplicaçao de resíduo industrial para isolamento térmico: uma proposta para utilizaçao do poliuretano de mamona com agregado de resíduo plástico**. [s.l.] Universidade Federal do Rio Grande do Norte, 2009.

CUCE, E. et al. Optimizing insulation thickness and analysing environmental impacts of aerogel-based thermal superinsulation in buildings. **Energy and Buildings**, v. 77, p. 28–39, 2014a.

CUCE, E. et al. Toward aerogel based thermal superinsulation in buildings : A comprehensive review. **Renewable and Sustainable Energy Reviews**, v. 34, p. 273–299, 2014b.

DEMILECAMPS, A. et al. Cellulose – silica aerogels. **Carbohydrate Polymers**, v. 122, p. 293–300, 2015.

DEMIRBAS, A. Biorefineries : Current activities and future developments. **Energy Conversion and Management**, v. 50, n. 11, p. 2782–2801, 2009.

DERVIN, S. et al. Graphene oxide reinforced high surface area silica aerogels. **Journal of Non-Crystalline Solids**, v. 465, p. 31–38, 2017.

DIMITRIEV, Y.; IVANOVA, Y.; IORDANOVA, R. HISTORY OF SOL-GEL SCIENCE AND TECHNOLOGY (REVIEW). p. 181–192, 2008.

DINIZ, J. Conversão térmica de casca de arroz à baixa temperatura: produção de bioóleo e resíduo sílico-carbonoso adsorvente. **… À Baixa Temperatura: Produção De Bioóleo E Resíduo …**, p. 156, 2005.

DU, A. et al. A special material or a new state of matter: A review and reconsideration of the aerogel. **Materials**, v. 6, n. 3, p. 941–968, 2013.

EBBESEN, T. W. et al. Eletrical conductivity of individual carbon nanotubes. **Nature**, v. 384, p. 54–56, 1996.

ESQUIVEL-CASTRO, T. A. et al. Porous aerogel and core/shell nanoparticles for controlled drug delivery: A review. **Materials Science and Engineering C**, v. 96, p. 915–940, 2019.

FENG, J. et al. Advanced fabrication and oil absorption properties of super-hydrophobic recycled cellulose aerogels. **Chemical Engineering Journal**, v. 270, p. 168–175, 2015.

FENG, J. et al. Colloids and Surfaces A : Physicochemical and Engineering Aspects Silica – cellulose hybrid aerogels for thermal and acoustic insulation applications. **Colloids and Surfaces A: Physicochemical and Engineering Aspects**, v. 506, p. 298–305, 2016.

FENG, J.; ZHANG, C.; FENG, J. Carbon fi ber reinforced carbon aerogel composites for thermal insulation prepared by soft reinforcement. **Materials Letters**, v. 67, n. 1, p. 266–268, 2012.

FISCHER, F. et al. Cellulose-based aerogels. **Polymer**, v. 47, n. 22, p. 7636–7645, 2006.

FOO, K. Y.; HAMEED, B. H. Insights into the modeling of adsorption isotherm systems. **Chemical Engineering Journal**, v. 156, p. 2–10, 2010.

FRICKE, J. NON-CRYSTALLINE Aerogels and their applications. v. 148, p. 356–362, 1992.

FU, J. et al. Facilitated fabrication of high strength silica aerogels using cellulose nanofibrils as scaffold. **Carbohydrate Polymers**, v. 147, p. 89–96, 2016.

FUN, S. et al. Fabrication of hydrophobic and magnetic cellulose aerogel with high oil absorption capacity. **Materials Letters**, v. 115, p. 241–243, 2014.

GANESAN, K. et al. Design of aerogels, cryogels and xerogels of cellulose with hierarchical porous structures. **Materials and Design**, v. 92, p. 345–355, 2016.

GAVILLON, R. **Preparation and characterization of ultra porous cellulosic materials**. [s.l.] Ecole Nationale Sup´erieure des Mines de Paris, 2007.

GE, X. et al. High-strength and morphology-controlled aerogel based on carboxymethyl cellulose and graphene oxide. **Carbohydrate Polymers**, v. 197, p. 277–283, 2018.

GUERRERO, M. et al. Pyrolysis of eucalyptus at different heating rates : studies of char characterization and oxidative reactivity. **Journal of Analytical and Applied Pyrolysis**, v. 74, p. 307–314, 2005.

GUPTA, P. et al. Low density and high strength nanofibrillated cellulose aerogel for thermal insulation application. **Materials and Design**, v. 158, p. 224–236, 2018.

HAN, S. et al. Green and facile fabrication of carbon aerogels from cellulose-based waste newspaper for solving organic pollution. **Carbohydrate Polymers**, v. 136, p. 95–100, 2016.

HOKKANEN, S.; BHATNAGAR, A.; SILLANPÄÄ, M. A review on modification methods to cellulose-based adsorbents to improve adsorption capacity. **Water Research**, v. 91, p. 156–173, 2016.

HU, H. et al. Ultralight and Highly Compressible Graphene Aerogels. **Advanced Materials**, v. 25, p. 2219–2223, 2013.

HU, H. et al. Polymer/Graphene Hybrid Aerogel with High Compressibility, Conductivity, and " Sticky " Superhydrophobicity. **ACS Applied Materials & Interfaces**, v. 6, p. 3242–3249, 2014.

HÜSING, N.; SCHUBERT, U. Aerogels—Airy Materials: Chemistry, Structure, and Properties. **Angewandte Chemie International Edition**, v. 37, n. 1/2, p. 22–45, 2002.

HWANG, H. C.; WOO, J. S.; PARK, S. Y. Flexible carbonized cellulose/single-walled carbon nanotube films with high conductivity. **Carbohydrate Polymers**, v. 196, p. 168–175, 2018.

INNERLOHINGER, J.; WEBER, H. K.; KRAFT, G. Aerocellulose : Aerogels and Aerogel-like Materials made from Cellulose. p. 126–135, 2006.

JAVADI, A. et al. Polyvinyl Alcohol-Cellulose Nano fi brils-Graphene Oxide Hybrid Organic Aerogels. 2013.

JIM, A. C.; BERNARD, B. S.; GROHENS, C. Y. Spray freeze-dried nanofibrillated cellulose aerogels with thermal superinsulating properties. **Carbohydrate Polymers**, 2016.

JIMÉNEZ-SAELICES, C. et al. Spray freeze-dried nanofibrillated cellulose aerogels with thermal superinsulating properties. **Carbohydrate Polymers**, v. 157, p. 105–113, 2017.

KLEMM, D. et al. Polymer Science Cellulose : Fascinating Biopolymer and Sustainable Raw Material Angewandte. p. 3358–3393, 2005.

KLOCK, U. et al. **Química Da Madeira**. [s.l: s.n.]. v. 3ª. Edição

KOEBEL, M.; RIGACCI, A.; ACHARD, P. Aerogel-based thermal superinsulation: An overview. **Journal of Sol-Gel Science and Technology**, v. 63, n. 3, p. 315–339, 2012.

KORHONEN, J. T. et al. Inorganic Hollow Nanotube Aerogels by Atomic Layer Deposition onto Native Nanocellulose Templates. n. 3, p. 1967–1974, 2011.

LAZZARI, L. K. et al. Sorption capacity of hydrophobic cellulose cryogels silanized by two different methods. **Cellulose**, v. 24, p. 3421–3431, 2017.

LAZZARI, L. K. et al. Cellulose / biochar aerogels with excellent mechanical and thermal insulation properties. **Cellulose**, v. 26, p. 9071–9083, 2019.

LEE, Y. et al. Comparison of biochar properties from biomass residues produced by slow pyrolysis at 500°C. **Bioresource Technology**, v. 148, p. 196–201, 2013.

LEI, E. et al. An ultra-lightweight recyclable carbon aerogel from bleached softwood kraft pulp for

efficient oil and organic absorption. **Materials Chemistry and Physics**, v. 214, p. 291–296, 2018.

LENGOWSKI, E. C. **Caracterização e predição da cristalinidade de celulose através de espectroscopia no infravermelho e análise multivariada**. [s.l.] Universidade Federal do Paraná, 2012.

LI, J. et al. Ultra-light, compressible and fire-resistant graphene aerogel as a highly efficient and recyclable absorbent for organic liquids. **Journal of Materials Chemistry A**, v. 2, n. 9, p. 2934–2941, 2014.

MADYAN, O. A.; FAN, M. Organic functionalization of clay aerogel and its composites through in-situ crosslinking. **Applied Clay Science**, v. 168, n. June 2018, p. 374–381, 2019.

MALEKI, H. Recent advances in aerogels for environmental remediation applications: A review. **Chemical Engineering Journal**, v. 300, p. 98–118, 2016.

MI, H. Y. et al. Highly compressible ultra-light anisotropic cellulose/graphene aerogel fabricated by bidirectional freeze drying for selective oil absorption. **Carbon**, v. 132, p. 199–209, 2018.

NAKAGAITO, A.; KONDO, H.; TAKAGI, H. Cellulose nanofiber aerogel production and applications. **Journal of Reinforced Plastics and Composites**, v. 32, n. 20, p. 1547–1552, 2013.

NGUYEN, S. T. et al. Advanced thermal insulation and absorption properties of recycled cellulose aerogels. **Colloids and Surfaces A: Physicochemical and Engineering Aspects**, v. 445, p. 128–134, 2014.

O'SULLIVAN, A. Cellulose: the structure slowly unravels. **Cellulose**, v. 4, n. 3, p. 173–207, 1997.

PERONDI, D. et al. Steam gasification of poultry litter biochar for bio-syngas production. **Process safety and Environmental Protection**, v. 109, p. 478–488, 2017.

QIU, H. et al. Critical review in adsorption kinetic models *. **Journal of Zhejiang University SCIENCE A**, v. 10, n. 5, p. 716–724, 2009.

SILIGARDI, C. et al. Temperature-induced microstructural changes of fiber-reinforced silica aerogel (FRAB) and rock wool thermal insulation materials: A comparative study. **Energy and Buildings**, v. 138, p. 80–87, 2017.

SILVA, F. M. F. **Estudo de materiais de isolamento térmico inovadores**. [s.l.] Universidade do Porto, 2013.

SKOUTERIS, G. et al. The effect of activated carbon addition on membrane bioreactor processes for wastewater treatment and reclamation - A critical review. **Bioresource Technology**, v. 185, p. 399–410, 2015.

SUN, T. et al. Hydrophobic silica aerogel reinforced with carbon nanotube for oils removal. p. 967–973, 2014.

WAHI, R. et al. Oil removal from aqueous state by natural fibrous sorbent : An overview. **Separation and Purification Technology**, v. 113, p. 51–63, 2013.

WAN, C.; LI, J. Graphene oxide/cellulose aerogels nanocomposite: Preparation, pyrolysis, and application for electromagnetic interference shielding. **Carbohydrate Polymers**, v. 150, p. 172–179, 2016.

WANG, J.; ELLSWORTH, M. W. Graphene Aerogels. **ECS Transactions**, v. 19, n. 5, p. 241–247, 2009.

WANG, J.; WANG, S. Preparation, modification and environmental application of biochar: A review. **Journal of Cleaner Production**, v. 227, p. 1002–1022, 2019.

XIANG, C. et al. Synthesis of carboxymethyl cellulose-reduced graphene oxide aerogel for efficient removal of organic liquids and dyes. **Journal of Materials Science**, v. 54, n. 2, p. 1872–1883, 2019.

XIAO, S. et al. Fabrication and characterization of nanofibrillated cellulose and its aerogels from natural pine needles. **Carbohydrate Polymers**, v. 119, p. 202–209, 2015.

YU, S. et al. Characterization of biochar and byproducts from slow pyrolysis of hinoki cypress. **Bioresource Technology Reports**, v. 6, n. March, p. 217–222, 2019.

ZANINI, M. et al. Producing aerogels from silanized cellulose nanofiber suspension. **Cellulose**, v. 24, p. 769–779, 2017.

ZARBIN, A. J. G.; OLIVEIRA, M. M. Nanoestruturas de carbono (nanotubos, grafeno): Quo Vadis? **Química Nova**, v. 36, n. 10, p. 1533–1539, 2013.

ZHANG, Z. et al. Insights into biochar and hydrochar production and applications: A review. **Energy**, v. 171, p. 581–598, 2019.

ZHAO, Y.; LI, Y.; ZHANG, R. Silica aerogels having high flexibility and hydrophobicity prepared by sol-gel method. **Ceramics International**, v. 44, n. 17, p. 21262–21268, 2018.

ZHU, C.; LI, Z. International Journal of Heat and Mass Transfer Modeling of the apparent solid thermal conductivity of aerogel. **International Journal of Heat and Mass Transfer**, v. 120, p. 724–730, 2018.